Neutrinos and co. - Multi-messenger analyses with neutrinos

Damien Dornic

Aix-Marseille Université

Habilitation à diriger les recherches

Damien Dornic

Neutrinos and co.

"Multi-messenger analyses with neutrinos"

Soutenue le 14/12/2020 devant le jury composé de :

Nelson Christensen	OCA	Rapporteur
Alain Klotz	IRAP	Rapporteur
Nicolas Leroy	IJCLab	Rapporteur
Frederic Piron	LUPM	Examinateur
Cristinel Diaconu	CPPM	Examinateur
Jose Busto	CPPM	Tuteur

"Un jour, dit la légende, il y eut un immense incendie de forêt. Tous les animaux terrifiés, atterrés, observaient impuissants le désastre. Seul le petit colibri s'activait, allant chercher quelques gouttes avec son bec pour les jeter sur le feu. Après un moment, le tatou, agacé par cette agitation dérisoire, lui dit : "Colibri ! Tu n'es pas fou ? Ce n'est pas avec ces gouttes d'eau que tu vas éteindre le feu ! Et le colibri lui répondit : "Je le sais, mais je fais ma part."

Extrait de "La Part du Colibri" Pierre Rabhi.

Table des matières

1 Introduction

Ever since I was in University, I have been fascinated by cosmic rays (CRs). I studied them directly during my thesis with the Pierre Auger Observatory and then indirectly with the search for the sources of high-energy neutrinos, a smoking gun for the identification of the cosmic-ray sources with the ANTARES and KM3NeT experiments. CRs have been discovered more than 100 years ago, but their origins are still unknown. The CR energy spectrum follows more or less a single power-law with an index of -2.7 over more than 12 orders of magnitude in energy and 32 in flux. The studies of the few breaks (solar modulation, knees, ankle) have provided crucial elements of the composition and on the origin. Macroscopic energies, up to 3 10^{20} eV, have been measured for a few of them, dubbed at ultra-high-energy cosmic rays (UHECRs). Which are the sources of these UHECRs ? How they are accelerated to such energy ? How these sources are distributed in the Universe ? These questions are still a hot topic nowadays. Moreover, CRs are key elements in the Universe, having large impacts on the ionisation, the astro-chemistry, heating, turbulent magnetic field, galactic winds, regulation of the star formation, etc. The formation of the light elements (Li, Be, B) in the Universe is directly linked to the cosmic ray interactions by spallation of stable elements. CRs are also at the heart of the non-thermal Universe.

Unfortunately, as CRs are charged particles, their propagation is directly affected by the magnetic fields present in the Universe. Except maybe at UHE, it is not possible to look in their direction to find the sources. The only way is to use the secondary products of the CR interactions with the radiation or matter fields. The resulting meson decays will produce high-energy gamma-rays and neutrinos. This intimate relationship between these three messages is one of the basis of the so-called multi-messenger analysis. Measuring high-energy to very high energy (VHE) gamma-rays is now a completely mature technique and hundreds of sources have already been identified. However, the gamma-rays can be originated from either leptonic or hadronic mechanisms. Only very detailed studies of the spatial profile of the sources and on the shape of the high-energy spectrum can be used to hint the hadronic emission. This requires a large statistic which is quite difficult to obtain at VHE. On the contrary, high-energy neutrinos are a unique signature of these hadronic processes. Neutrinos present the advantage to point directly to their sources (neutral particle). However, neutrinos are incredibly difficult to detect, 1/10000000 neutrinos interact in or close to the detector. It requires gigantic detection volumes, probably larger than 1 km^3. The context of the time-domain

astronomy and the multi-messenger analysis is described in Chapter 2.

My works in this field was from the beginning to look for these neutrino sources with the maximal sensitivity possible, concentrating on the detection of transient sources. By design, neutrino telescopes constantly monitor at least one complete hemisphere of the sky and are thus well suited to detect neutrinos produced in transient astrophysical sources. The flux of high-energy neutrinos from transient sources is in general lower than the one expected from steady sources. But, the background originating from atmospheric neutrinos can be drastically reduced by requiring a directional and temporal coincidence with the direction and time of the astrophysical phenomena detected by a satellite or a telescope. For a typical duration of a flare (1-100 days), we can gain at least a factor $\sim$2-3 in the discovery potential compared to a steady point-like source analysis. We have applied this time-dependent analysis to different catalogues of blazars, X-ray binaries, gamma-ray bursts and fast-radio bursts. The results of these searches are summarized in Chapter 3. Pushing this method at the maximum, ie detecting one source with only one neutrino, is at the basis of the TAToO project, started mid 2008. It consists of the online follow-up by external telescopes of a selected sample of "potential" cosmic neutrinos. The results of these searches with ANTARES are summarized in Chapter 4. Recently, we have upgraded the online analysis platform to be able to process in real-time any potential electromagnetic transient triggers and multi-messenger alerts. We have been following all gamma-ray burst triggers detected by Fermi and Swift, the IceCube high-energy neutrino alerts, the LIGO/VIRGO gravitational waves candidates and other transients. The results of these online follow-ups are presented in Chapter 5.

ANTARES is already running smoothly since 2007 without major interruption. Even if its detector size is quite small (1/100 of a cubic kilometer), we have performed a lot of multi-messenger analyses, plenty of them with competitive results than IceCube. Since a few years, we are building the second generation neutrino telescope in the Mediterranean Sea, which consists of two detectors : the low-energy site, ORCA, in France and the high-energy one, ARCA, in Italy. In this manuscript, I will only concentrate on the physics potential related to astronomy. What I like about this kind of detector is that there are a very versatile scientific case with the same data in particle physics (neutrino oscillation, standard model physics), astronomy or marine sciences. The KM3NeT detector is described in Chapter 6. In KM3NeT, we have started the implementation of the real-time analysis framework that would allow to pursue the real-time multi-messenger analyses started in ANTARES with the upgraded detector sensitivities and improved analysis methods. In 2015, I have also joined the SVOM Collaboration to go further on the analysis of the extreme sources in the Universe, in particular the detailed studies of the gamma-ray bursts. It will also permit to secure the link between KM3NeT and SVOM, providing simultaneous X-ray/γ-ray observations to the neutrino emission, so important for

the understanding of the micro-physics of the jets. In this project, I am working on the ground segment of SVOM, mainly on the COLIBRI telescope, one of the SVOM ground facilities. On this telescope, I am working on the analysis software and on the link between the different ground and space instruments. SVOM activities are described in Chapter 7.

Finally, a conclusion and some perspectives are given in Chapter 8. To finish this introduction, I would like to thank all my collaborators and in particular all the PhD students, I have been working with (Aurore, Salvatore, Imen, Aurore, Agustin, Damien and Massimiliano). All this would have not been possible without their invaluable works. A special thanks to Michel, who has been my closest collaborator in the last thirteen years on ANTARES and SVOM.

2 Time domain astronomy and multi-messenger analyses

2.1 Context

Time-domain astronomy has received a considerable boost in recent years due to its ability to study extreme physics, to track cataclysmic phenomena like the birth of stellar mass black holes or the mergers of neutron stars, to probe distant regions of the Universe, and to identify candidate sources for multi-messenger astrophysics. These explosive events can release enormous amounts of energy both in electromagnetic radiation and in non-electromagnetic forms such as neutrinos and gravitational waves. They lie at the frontier of our understanding of the laws of physics under the most extreme conditions.

The opening of the temporal domain is transforming our knowledge of how the Universe evolves, particularly for objects which are undergoing explosive change, such as a supernova, blazar or gamma-ray burst (GRB) [1, 2]. Despite many years of observations, the knowledge on how these sources are working is still quite poor. Many of the previously developed theories have come under intense constrain from new observational results : launching jets turn to be notably difficult in magneto-hydro-dynamic simulations and the link between accretion and ejection is still difficult to be modeled. Due to their extreme properties, the physical understanding is especially challenging, but with more data and more advanced modeling, this would offer the possibility to improve our knowledge of the final fate of massive stars, to understand astrophysical relativistic jets and to study an extreme case of cosmic accelerators.

Multi-messenger astronomy – the observation of astrophysical objects and processes using combinations of different messengers such as electromagnetic radiation, neutrinos, cosmic rays and gravitational waves – has emerged as a major new field in astronomy during the last years. The first example is the detection of an enormous amount of neutrinos from the Sun in the 60's. The precise measurements of the flux of each type of neutrinos (electron, muon and tau) yields to the discovery of the fundamental neutrino oscillation properties : only 1/3 of the predicted electron neutrinos were detected. As neutrinos are directly produced in the fusion nuclear reaction in the core of the Sun, these detections have permitted to build the Standard Solar Model. Later, a neutrino signal coming from the supernova

SN1987a was recorded by the Kamiokande II (Japan) [3], IMB (USA) [4] and Baksan (Russia) [5] shortly before the measurement of the optical radiation. Even if the supernova explosion occurs at a very short distance of 50 kpc in the Large Magellanic Cloud, only 25 neutrinos were recorded over the 10^{16} neutrinos that have crossed the detectors. However, this has allowed to set stringent limits on the mass of the $\bar{\nu}_e$, its lifetime, its magnetic moment and the number of leptonic flavors could be derived [6]. Although the optical detection of supernova explosions is nowadays common, detailed features of the gravitational collapse can only be studied with neutrinos, which carry away nearly about 99 % of the gravitational binding energy soon after the collapse.

In the last five years, with the operation of very sensitive instruments, multi-messenger activities have undergone a second revolution. Major breakthroughs were the first observed coincidence of gravitational waves detected by LIGO/VIRGO and electromagnetic signals over a huge wavelength regime originated from a merger of two neutron stars [7, 8] and the detection of high-energy neutrinos by IceCube and gamma rays from the flaring blazar TXS0506+056 [9, 10]. Also, the identification of a PeV accelerator ("PeVatron") in the centre of our Galaxy by the H.E.S.S. gamma-ray telescope [11] is remarkable in this context since it represents a major step forward in linking gamma-ray observations to Galactic cosmic rays.

In 2017, LIGO and VIRGO have detected the gravitational wave signal of the merger of a binary neutron star system at a distance of 40 Mpc in the galaxy NGC 4993 [7] (Figure 2.1). The detection of the gamma-ray burst GRB170817 by Fermi and INTEGRAL 1.7s after the detection of the GW170817 [8] and the following optical detection of the kilonova AT2017gfo [12] represents nowadays the most studied transient phenomena in the Universe. It has involved more than 70 observatories on 7 continents and in space. The paper describing the multi-messenger observations [13] is co-authored by almost 4,000 astronomers (about one-third of the worldwide astronomy community) from more than 900 institutions.

Multi-messenger astronomy employs both spatial and time correlations between different observations and therefore particularly targets transient phenomena ; it thus belongs also to the field of time-domain astronomy. The crucial requirement for multi-messenger studies is the quasi-online communication of potentially interesting observations to partner instruments ("alerts"), with a very short latency of a few minutes, at most. Such alerts are the only way to achieve simultaneous observations of transient phenomena by pointing instruments. The recent observations of sub-TeV gamma-rays from three gamma-ray bursts by MAGIC [14] and H.E.S.S. [15] continue to enrich the harvest of results and illustrate the far-reaching potential of coordinated observations for time-domain astronomy.

Current observing facilities enable the sky to be monitored fairly continuously in

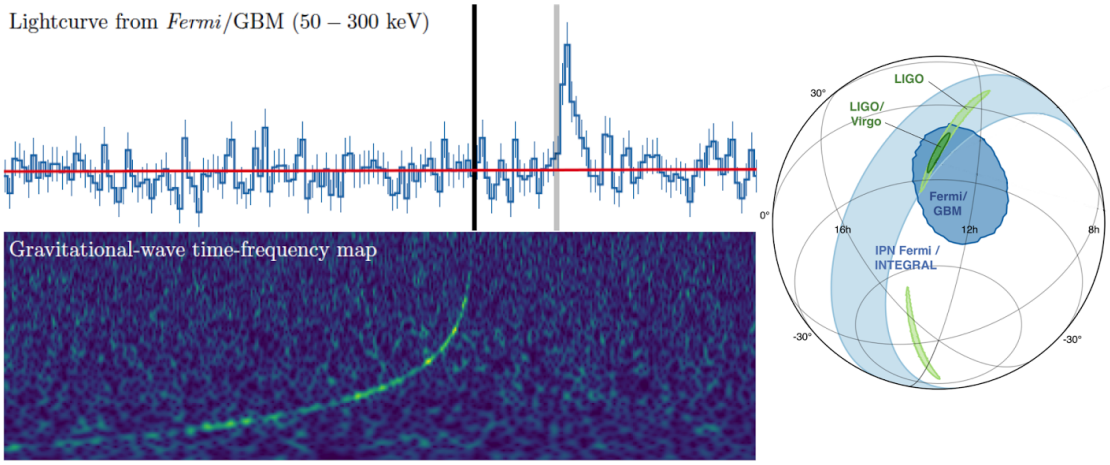

FIGURE 2.1 – Multi-messenger results of GW170817 : gravitational wave signal (bottom left), GRB170817 light-curve measured by Fermi-GBM (top left) and sky localisation (right).

real-time over large areas in electromagnetic radiations, gravitational waves, and neutrinos, capturing the temporal behavior of the Universe in a way previously unattainable. Example electromagnetic facilities include the LOFAR, MWA, Parkes radio telescopes, the MASTER, Pan-STARRs and ZTF optical facilities, and the Swift, INTEGRAL and Fermi high-energy satellites. Non-electromagnetic facilities are also now observing, particularly the Advanced LIGO and Virgo gravitational-wave observatories, and the ANTARES and IceCube neutrino experiments. The data from all these facilities and their immediate predecessors have already opened the temporal domain, but are just a foretaste of what is to come. With the arrival of new facilities in the next decade, in particular the Large Synoptic Survey Telescope (LSST), the Square Kilometer Array (SKA), the Space-based multi-band astronomical Variable Objects Monitor (SVOM) in the electromagnetic domain and the rapid progress of the multi-messenger facilities (IceCube/KM3NeT and advanced LIGO/VIRGO), the number of detected transients and the quality of the follow-ups will increase significantly.

2.2 Neutrino astronomy

Neutrino astronomy allows us to study the most energetic non-thermal sources in the Universe. Despite the observations of cosmic rays up to ultra-high energies and observations of γ-rays and astrophysical neutrinos, we do not yet know where or how these particles are accelerated. Neutrino astronomy is clearly a key to directly answer this question. Astrophysical neutrinos provide insight into source characteristics not accessible through the observation of other messengers. Due to

their low cross sections, neutrinos can escape dense astrophysical environments that are opaque to photons. In contrast to γ-rays, neutrinos travel through the Universe almost without interactions, allowing direct observation of their sources at high redshift with sub-degree-scale pointing. Unlike cosmic rays, neutrinos are not deflected by magnetic fields and can be observed in spatial and temporal coincidence with photons and gravitational waves, which is a key prerequisite to reap the scientific rewards of multi-messenger astronomy. In addition, neutrinos come in different flavors : electron, muon, and tau neutrinos (ν_e, ν_μ, ν_τ), and the flavor ratios observed at Earth give insight into the environment of cosmic-ray sources.

Doing astronomy with neutrinos is a long-standing dream for neutrino telescopes around the world. Up to now, IceCube at the South Pole [16] and ANTARES in the Mediterranean Sea [17] are the key players for neutrino astronomy analyses. The last decade is marked by the IceCube results in high-energy neutrino astronomy, with the discovery of an astrophysical neutrino flux in the 10 TeV – 10 PeV energy range in 2012 using high-energy starting track (HESE) events [18]. Between May 2010 and May 2012, IceCube has recorded 28 neutrino events with an expectation from the atmospheric muon and neutrino background of $10.6^{+5.0}_{-3.6}$. These events have been selected by asking that only those neutrino candidates that are first observed in the detector interior rather than on the detector boundary. This search is primarily sensitive to neutrinos from all directions above 60 TeV. This first result has been later confirmed by updated analysis using more data [19] and with others neutrino-event selections including shower-like events [20] and through-going events from the Northern hemisphere [21, 22]. Figure 2.2 shows the diffuse flux analysis results for IceCube using 7.5-year HESE sample. The diffuse fluxes can be fitted assuming a power-law :

$$\frac{d\phi_{\nu+\bar{\nu}}}{dE} = \phi_0 (\frac{E}{100TeV})^{-\gamma} \times 10^{-18} GeV^{-1} cm^{-2} s^{-1} sr^{-1} \tag{2.1}$$

Figure 2.3 shows the best fit flux normalization ϕ_0 and spectral index γ for the through-going track sample, the starting event sample, and also the sample of contained cascades [23]. The three measurements have distinctly different best-fit points, but appear to be compatible with each other within their 95.4 % regions. This mild effect may underline a two-components diffuse emission with a softer diffuse component of Galactic origin and a harder one originating from extra-galactic sources or different sources in the Northern and Southern hemispheres [24]. Only much larger statistics will tell us the origin of this disagreement. ANTARES has also detected a mild excess (1.8 σ) of both track and cascade events at high energies using data collected from January 2007 to June 2018 for a total life time of 3350 days [25, 26]. The analysis has selected 50 events (27 track-like events and 23 shower-like events) as cosmic neutrino candidates to be compared with the atmospheric background expectation of 36.1±8.7 events. In Figure 2.4, the

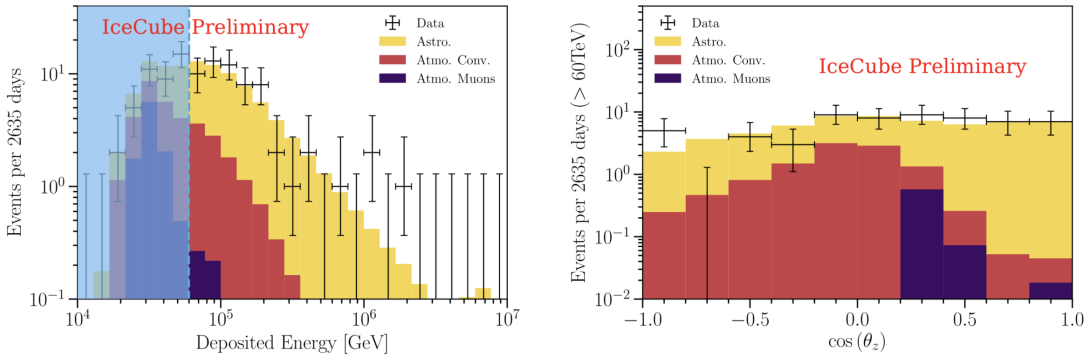

FIGURE 2.2 – Deposited energy (left) and reconstructed cosθ (right) distributions for the IceCube HESE event sample. Data are shown as black crosses and the best-fit expectation as a stacked histogram with each color specifying a flux component : astrophysical (golden), conventional atmospheric as mentioned above (red), and penetrating muons (purple) ; the best fit normalization for the prompt component is zero and is not shown [23].

distribution of the energy estimator for track like events (left) and the shower-like events (right) are reported. The best fit parameters obtained are : $\gamma = 2.3 \pm 0.4$ and $\phi_0(100\ \text{TeV}) = 1.5 \pm 1.0$. Both results are compatible.

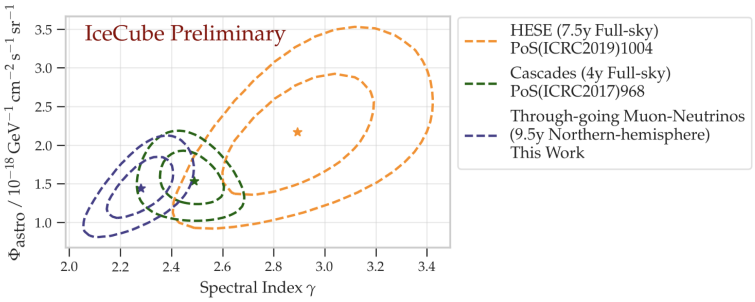

FIGURE 2.3 – Best fit flux normalization and spectral index for a single power law fit to through-going tracks (blue), contained cascades (green) and starting tracks + cascades (yellow) detected by IceCube. Inner/outer contours are 68 % and 99 % uncertainties respectively [23].

One interesting property of the diffuse neutrino flux [27] is when we compare the energy densities (proportional to the flux times E^2) of the isotropic gamma-ray background (IGRB) measured by Fermi-LAT and of the ultra-high-energy cosmic rays, they all lie at the same level (Figure 2.5). This correspondence suggests a strong multi-messenger relationship, may be common sources.

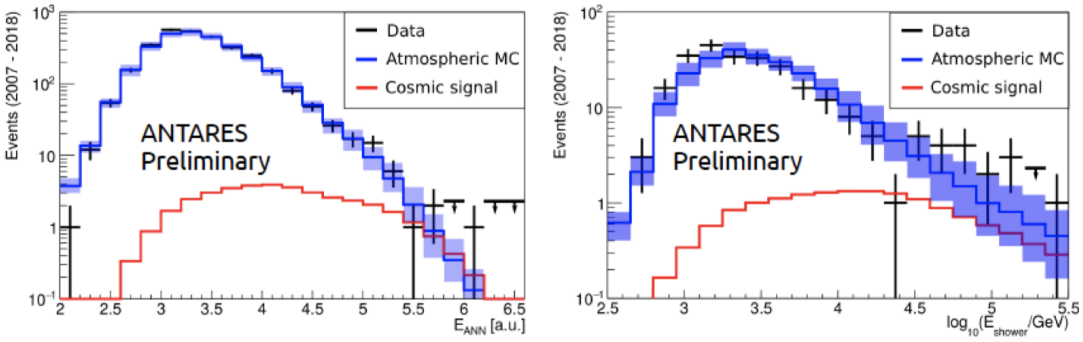

FIGURE 2.4 – Energy estimator distributions for track-like events (left) and shower-like events (right) for the ANTARES 11-year sample. The red line shows the cosmic flux as estimated in this analysis and the blue line represents the background contribution [26].

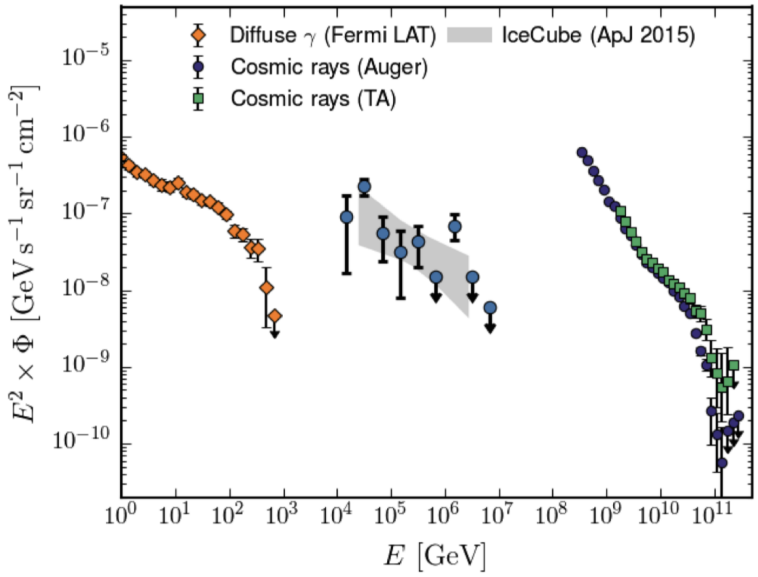

FIGURE 2.5 – Spectral energy distribution of the isotropic gamma-ray background, the IceCube cosmic neutrino, and the UHECR flux [27].

Up to now, the arrival directions of the most energetic neutrinos seem to be consistent with a uniform distribution across the sky. The isotropic distribution of high-energy neutrinos indicates that at least part of the flux is extra-galactic in origin and that the galactic component of the diffuse flux is largely sub-dominant. The region around the Galactic Plane is an interesting region accessible with high visibility by a neutrino telescope located in the Mediterranean Sea. No excess has been found using the latest ANTARES data set and the upper limits have

excluded a neutrino flux with a normalization factor of about 1.1 × ϕ_{KRA} at 90 % confidence level. The KRA model [28] is used for the estimation of the neutrino diffuse emission from the Galactic plane region, assuming a non-uniform cosmic-ray transport scenario with a radially dependent diffusion coefficient. The normalisation of this model is adjusted to the γ-ray diffuse flux measured by the Fermi-LAT instrument. Others searches have been performed in the Fermi Bubble region [29, 30], in the Loop1 super bubble [31] without finding any significant excess.

The second challenge is to determine the origins of the cosmic neutrinos. The principle of the analysis is to look for clusters of high-energy neutrino events in the top of the isotropic medium-energy atmospheric neutrino background. The point source search uses a maximum likelihood ratio to compare the hypothesis of point-like signal plus isotropic background to an isotropic background-only null hypothesis. Scanning all the sky position with a grid of 1 degree represents the most universal search as no assumption is made on the nature of the sources. However, trial factors (look-else-where effect) are larger and therefore a large number of events in the clusters are required, decreasing the sensitivity of the search. Figure 2.6 shows the results of the all-sky point source search using 11 years of ANTARES data [32].

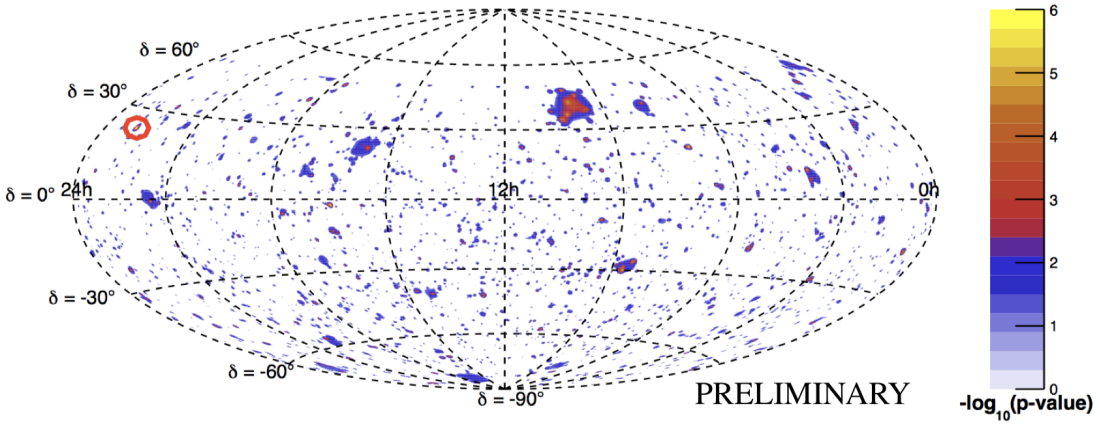

FIGURE 2.6 – Sky map in equatorial coordinates of pre-trial p-values for a point-like source search performed by ANTARES. The red contour indicates the location of the most significant cluster of the full-sky search.

Additionally, using a catalog of promising source directions helps to improve this sensitivity. The catalog contains promising sources such as galactic γ-ray sources (supernova remnants, pulsar-wind nebulae, micro-quasars, etc.) and energetic extra-galactic sources (blazars, starburst galaxies) detected in gamma-rays at high energies. The size of the catalog contains typically about one hundred objects so as to limit trial factors applied to the most significant source in the catalog.

No sources have been detected so far above a 5σ threshold. The brightest hotspot detected by IceCube in the Northern Hemisphere sky coincides with the brightest catalog source, NGC 1068 (M77), a Seyfert II galaxy located at a distance of 14.4 Mpc accounting for a 2.9σ post-trial [33]. Three additional point-like sources are a bit below a 3σ threshold : TXS 0506+056, PKS 1424+240 and GB6 J1542+6129, all of them are blazars [33]. The warmest cluster detected by ANTARES is associated with HESS J0632+057 with a post-trial value of 1.4σ [34]. Another interesting source is the blazar MG3 J225517+2409 classified as BL-Lac and LSP (Low Synchrotron Peak) and with unknown redshift [35]. Five ANTARES events were found within 1 degree from the location of this source and one IceCube EHE (ID3) at a distance of 1.1°. The combined IceCube+ANTARES pre-trial p-value is estimated to be $\sim 2.2 \times 10^{-7}$.

The only solution to increase the significance is to use the time variation of the source fluxes directly in the analysis. This time-dependent approach will be described in more details in the following chapters. On September 22, 2017, IceCube has emitted an alert to the GCN for the HESE event IC-170922A. This event is an up-going, through-going track event with a most likely energy of 290 TeV and a 55.6 % probability of being of astrophysical origin [9]. Following the alert, Fermi-LAT and MAGIC detected an increased of gamma ray flux from the known blazar, TXS 0506+056 [10]. The multi-wavelength campaign has permitted to measure the redshift to be 0.3365 ± 0.0010 [36]. The probability of such an association is on the 3σ level. Later, IceCube has searched additional events in the region of IC-170922A in their archival data : an excess of high-energy neutrino events with respect to atmospheric backgrounds was observed between September 2014 and March 2015 [9]. The best fit Gaussian time window to the excess is centered on December 13, 2014, with a duration of around 110 days. The observed excess is 13 ± 5 events above the expected atmospheric neutrino background. The excess is inconsistent with the background-only hypothesis at the 3.5σ level. Figure 2.7 shows the archival data from this region in IceCube, and the best fit Gaussian time window to the neutrino excess, along with results from a complementary box-shaped time window analysis. Despite the quite sparse EM data, it can be noted that there seems to be no significant gamma-ray activity at the time of the flare. The TXS 0506+056 direction was also investigated by ANTARES in steady mode with 11 years of data and time-dependent search [37]. No excess of events was found in both analyses.

This association may yield to the first high-energy source detection. However, many opened questions are still present. Blazars, being radio-loud active galactic nuclei with their jets pointing toward the Earth, dominate the extragalactic γ-ray sky [38, 39] and are particularly attractive potential neutrino point sources since they are among the most likely sources of the very high-energy cosmic rays. Their spectral energy distribution (SED) can be described by two components : a low-energy one from radio to X-rays and a high-energy one from X-rays to

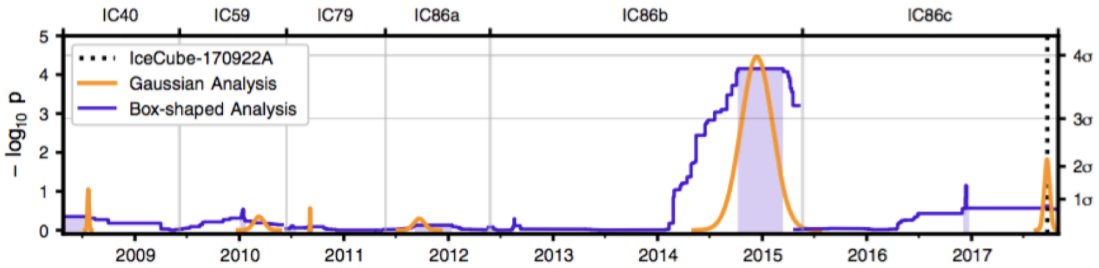

FIGURE 2.7 – IceCube archival data search from the region of IC-170922A [9].

very high-energy gamma rays. The low-energy component is generally attributed to synchrotron radiation in the relativistic jet by a non-thermal population of accelerated electrons and positrons ; the origin of the second component is still under discussion. In leptonic models [40, 41, 42], it is ascribed to an inverse Compton process between the electrons and a low-energy photon field (their own synchrotron radiation, or external photons), while in hadronic models it originates from synchrotron emission by protons and secondary particles coming from p-γ or p-p interactions [43, 44, 45, 46]. Associated with these very high-energy gamma rays from π_0 decays, the decay of the charged pions may give rise to a correlated neutrino emission. In both cases, primary cosmic rays (mainly protons) need to be accelerated to PeV energies and then interact with radiation or gas. Despite a wealth of electromagnetic data over the whole energy range, blazar radiation mechanism(s) remain unclear, with leptonic and (lepto)hadronic [47, 48, 49, 50] scenarios providing viable explanations. Concomitant X-ray and very-high energy gamma-ray data are crucial for constraining the hadronic contribution, although the latter may be absorbed in the extra-galactic background light (EBL) for high-redshift sources [51]. PeV protons will interact mainly with keV photons, therefore the X-ray flux determines the neutrino production efficiency. A second reason is that proton interaction may lead to a significant secondary gamma-rays either directly or after re-processing in these energy ranges [52]. In a general p-γ model, the neutrino production rate can be computed from the product of the proton density with the radiation density. The proton density depends on the proton injection and the confinement time (maximum energy of the cosmic rays). The radiation density is given by source luminosity, its size and geometry. Figure 2.8 right shows the SED of TXS 0506+056 in the quiescent and flaring states together with the fit of the 2017 single flare [45]. Simple one-zone photo-hadronic models may describe the 2017 neutrino event of TXS 0506+056 but stringent assumptions have to be made on the proton injection, the luminosity and the magnetic field [45]. Figure 2.8 left shows the time response of the flare. This highlights the importance of having simultaneous X-ray and γ-ray data together with the neutrino. Alternative more complex approaches have been developed : formation of a compact core [45], adding external radiation fields [50], adding several emission zones with different

properties [53, 54]. But the addition of more free parameters leads that these models difficult to constrain with actual data. For the interpretation of the 2014-15 neutrino flare, a common approach is difficult since one needs to "hide" the EM radiation from the hadronic interaction not observed by the EM detectors [55, 56, 57, 58].

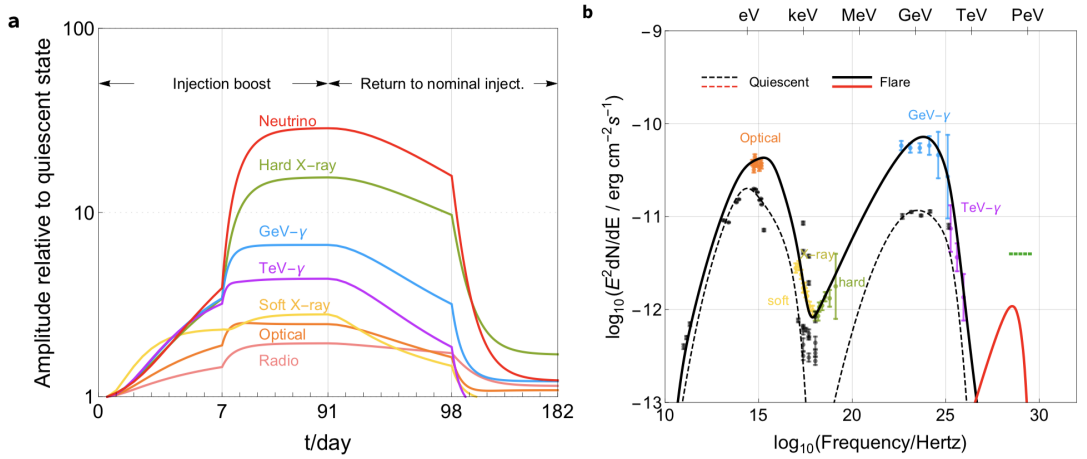

FIGURE 2.8 – Time response of the neutrino and electromagnetic fluxes (left panel) and the SED (right panel) during the electromagnetic flare of TXS 0506+056 for a one zone model (2017 neutrino event). Figure taken from Reference [45].

Blazars seem to be the natural candidates for the high-energy neutrino sources, but this is not the end of the story. Model-independent analyses (stacking and auto-correlation analyses) have disfavored the blazar population as the dominant origin of IceCube's neutrinos. The most recent results limits their contribution to less than ∼3 % to 30 % of the diffuse neutrino intensity in the 0.1–1 PeV range [58, 59].

We are just at the beginning to understand this puzzle. There are other potential sources that may contribute to the diffuse neutrino flux : starburst galaxies, low-luminosity gamma-ray bursts, fast-radio bursts (FRB), tidal-disruption events (TDE), etc. For the TDE, it can be noted that IceCube has measured a mild coincidence between one high-energy muon neutrino event IC191001A (with an energy of ∼0.2 PeV) and one TDE AT2019dsg identified by Zwicky Transient Facility (ZTF) at a redshift of 0.051 with an association probability of 0.5 % [60].

With the impressive results of the last few years, many new questions arise :
— Identify the high-energy astrophysical neutrino sources
— Measure features in the diffuse spectrum and extend it to higher energies. Connection UHECR ?
— Identify the sources of the highest energy cosmic rays

— Neutrino flavour ratio and its indication of the source properties
— Constrain the production mechanisms of high-energy cosmic particles
— Obtain a unique multi-messenger view into the explosion of stars and the evolution of stellar remnants
— Study of galactic and extra galactic propagation of CR with neutrinos as tracers

In the next decade, the main challenge will be to identify and characterize the population of sources of high-energy neutrinos. To solve this challenge, we will need to work on two main axes : obtaining high statistics to be able to perform precision measurements of the diffuse neutrino spectrum and having high-resolution neutrino data from observatories with deep exposure and wide sky coverage.

2.3 ANTARES neutrino telescope

Completed in 2008, ANTARES (*Astronomy with a Neutrino Telescope and Abyss Environmental Research*) is the first neutrino telescope installed in the Mediterranean Sea [17]. It is composed of 12 detection lines of about 500 m height anchored by 2500 m depth offshore Toulon (42° 48' N, 6° 10' E). The mean distance between lines is about 60-70 m. Each line is formed by a chain of 25 storeys with an inter-storey distance of 14.5 m. Every storey holds three optical modules housing a single 10-inch photo-multiplier tube (PMT) looking downward at an angle of 45°. In total, an instrumented volume of about 0.01 km^3 is instrumented with 885 optical modules. Each line is connected through an interlink electro-optical cable to a Junction Box, used as terminal distribution node of the main 40 km electro-optical cable connecting the detector to shore at La Seyne-sur-Mer (Figure 2.9).

High-energy neutrinos are detected through the Cherenkov light induced by relativistic secondary particles produced by deeply inelastic interactions. With the chosen detector dimensions, the ANTARES detector has a low energy threshold of about 10-20 GeV. The typical energy range is about 100 GeV - 10 TeV. Its location makes it sensitive to a large part of the southern sky, including the Galactic Centre region.

The data acquisition system of the ANTARES telescope is based on the "all-data-to shore" concept [61]. The time and charge amplitude of all the PMT signals above a threshold of 0.3 photo-electrons are sent to an onshore computing farm for the processing. The typical data output is about 0.5 GB/s and can increase to 5-10 GB/s during high bioluminescence periods. A filter is applied on shore to select the physics events among the raw data set structured in time slices of 104.85 ms and dominated by hits due to the optical background produced by bioluminescence and radioactive decay of ^{40}K. Two filtering algorithms look for a combination of local clusters of hits within a time window of 2.2 μs. The first one selects events made of five local causally connected clusters anywhere in the detector (3N), while

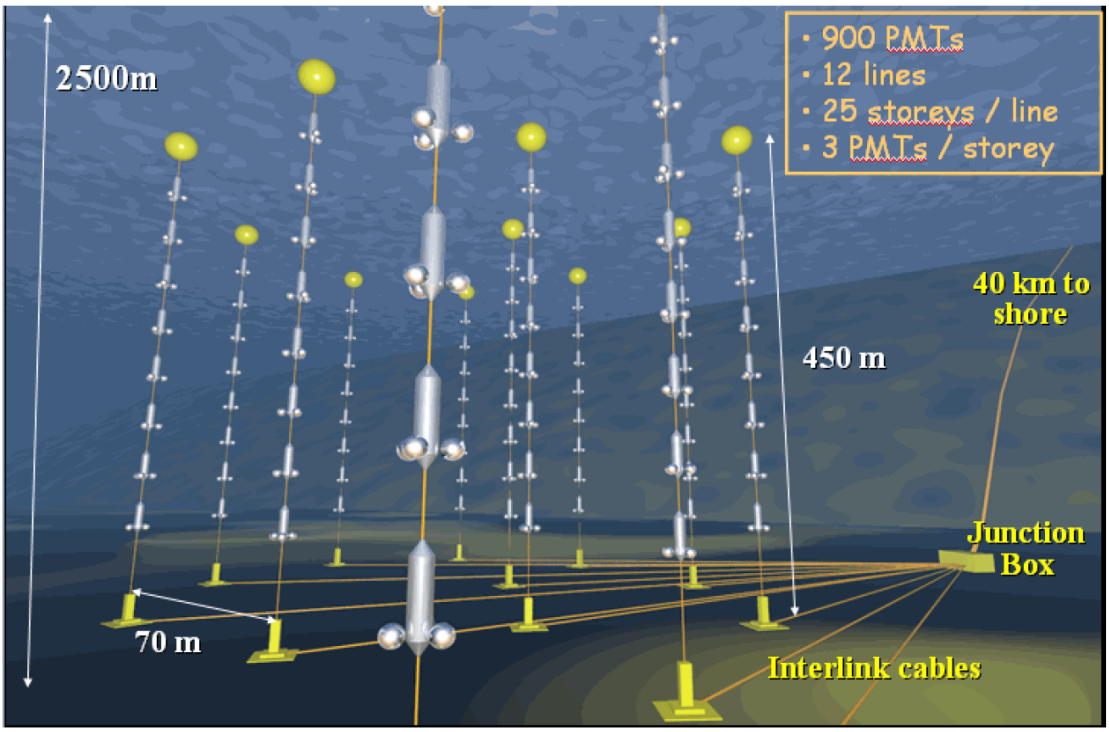

FIGURE 2.9 – Scheme of the ANTARES detector.

the second one requires at least two clusters on nearby PMT storeys (2T3). Two additional low-energy triggers (TQ and GC) are also in operation, based on a selection of only one local coincidence and 4 additional single hits. To have an acceptable rate, only specific directions are scanned in the causality search. The filtering removes typically about 99 % of the optical background. The rates of the selected events are about 3-10 Hz. The selected events are dumped in ROOT files and sent every night to the computing center CC-IN2P3 (Villerbanne) for the offline processing.

To achieve the optimal performances of the reconstruction, each PMT of the detector is calibrated in time, in charge and in position [62, 63]. The time calibration is performed using 4 LEDs installed along the line that illuminate few OMs above their positions. An independent cross check of the inter calibration between the OMs in the same storey is done with the Cherenkov light from a potassium decay. There are about 150 photons from each decay which can be simultaneously seen in both OMs. There are also two laser beacons which are used for the calibration of the time offsets between the lines. At the end of the calibration process, all PMT hits are relatively calibrated in time within less than 1 ns. The absolute time of the events is given by an external clock system coupled to a GPS, with a precision of around few microseconds. To have a homogeneous response of the detector, the high voltage of the PMTs is tuned, once per year, to have a uniform response (1

photo-electron peak). The lines move freely in the water due to the sea currents and the OMs change their absolute position and orientation. The position and orientation of each OM are determined using the compasses, tilt-meters and the piezoelectric sensors inside each OMs. Their position is monitored by a system of acoustic transponders and receivers distributed over the lines and on the sea bed. This allows to monitor relative positions of the optical modules with an accuracy better than 20 cm. There are two types of calibration sets - sets which are used in the online detector work (needed for the triggering and the online event reconstructions) and more precise offline calibrations are using the data already collected (used for the offline event reconstruction).

Based on the charge and the time of the hits, the reconstruction algorithms determine the position, the direction and the energy of the events. Depending on the flavor of the neutrino, different topologies of the events can be identified (Figure 2.10). Events induced by charged-current interactions of muon neutrinos produce a track-like signature in the detector corresponding to a long extension of the signal in the direction of the neutrino trajectory. All-flavor neutral-current and charged-current ν_e and ν_τ interactions produce electromagnetic and hadronic showers (so called cascades) in the instrumented volume. Dedicated algorithms have been developed by the ANTARES Collaboration [64, 65, 66]. From muon neutrino simulations, we expect a good angular resolution in the full energy range reaching 0.3° (median) at the highest energies, i.e., factors of about 2-3 better than IceCube. However, the energy resolution is quite poor and is determined with a factor 3 uncertainty. This is due to the limited size of the instrumented volume compared to the length of the muon track. This is clearly the main channel for neutrino astronomy since it is possible to point to the neutrino sources with an accuracy competitive with other messengers. The angular precision of the cascade events is about 3° at the highest energies, a factor 4-5 better than IceCube. As the cascade events are almost all the time contained in the instrumented volume, the energy is estimated with a very good accuracy, typically, less than 10 %. Figure 2.11 shows the point-spread function (PSF) for both channels assuming a E^{-2} neutrino spectrum. The PSF represents the probability to reconstruct one event at a given distance from a source. Owing to the lower atmospheric background contamination, the cascade channel is also a promising window to detect astrophysical sources. The discovery potential for a given source scales with the instrumented volume and is evolving with the square of the angular resolution.

The cosmic neutrino signal is largely dominated by the huge background coming from atmospheric muons and neutrinos. This background is produced in the atmospheric showers originated from the cosmic ray interaction with the atmosphere. In ANTARES, the rates of atmospheric muons and neutrinos are about 3 Hz and 3-5 events per day, respectively, while the expected cosmic neutrino signal is about 1-2 per year. That's explain the depth of the detector which is a compromise of the

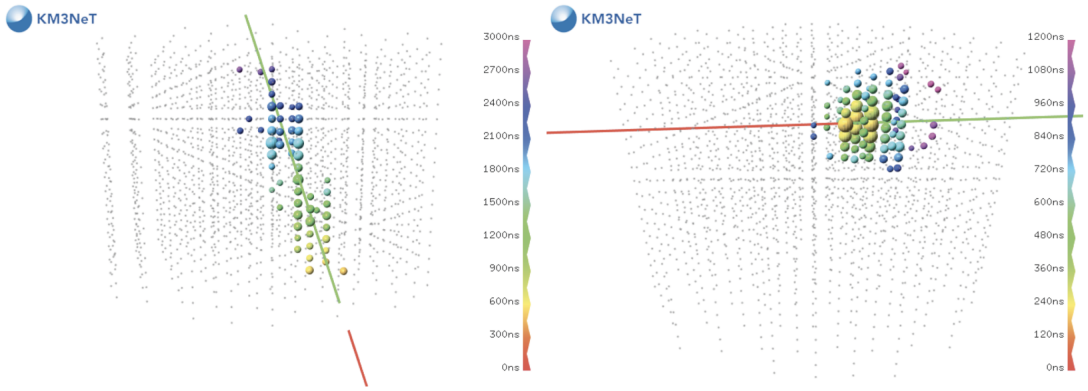

FIGURE 2.10 – Event displays of a simulated ν_μ CC event (left) and a contained ν_μ NC event (right) in the KM3NeT ARCA detector. The incoming neutrino is indicated by the red line, and the outgoing lepton (muon or neutrino) by the green line. The color scale gives the hit times with respect to the time of the neutrino interaction, while the size of the circles is proportional to the total charge of the hit PMTs [67].

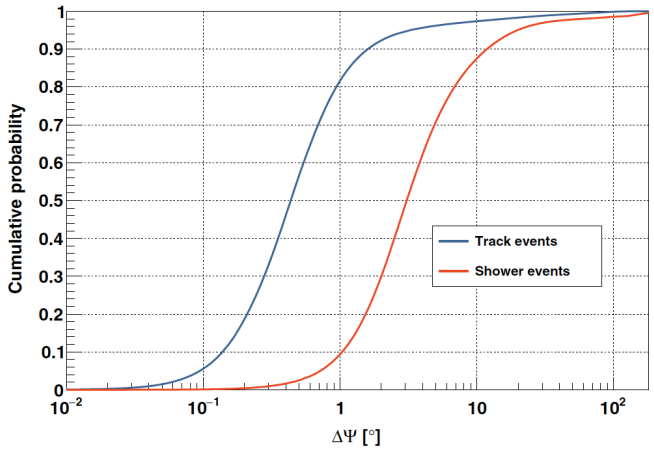

FIGURE 2.11 – Point Spread Function of ANTARES track (red) and cascade (blue) events assuming a E^{-2} neutrino spectrum.

muon absorption and the difficulty to work at such depth. Moreover, to further reduce the muon contamination, the search for cosmic signal concentrates on the up-going events, which corresponds to the events which have passed through the Earth.

Out of the installed 885 OMs, 550 OMs are still active and in permanent data taking today. ANTARES has clearly demonstrated that it is possible to operate a large neutrino telescope in the deep-sea with an average data taking efficiency larger than 94 % (Figure 2.12). The data losses can be due to the shutdowns of

the detection, calibration periods and too high bioluminescence activities. The operation of the ANTARES detector will be carried on until a similar sensitivity is reached with the operation of the first lines of the KM3NeT detector, in order to ensure continuity in the online survey of transient sources and in multi-messenger analyses of external alerts, in particular from gravitational wave detectors. The end of the operation of ANTARES and the decommissioning of the detector is today foreseen in 2021.

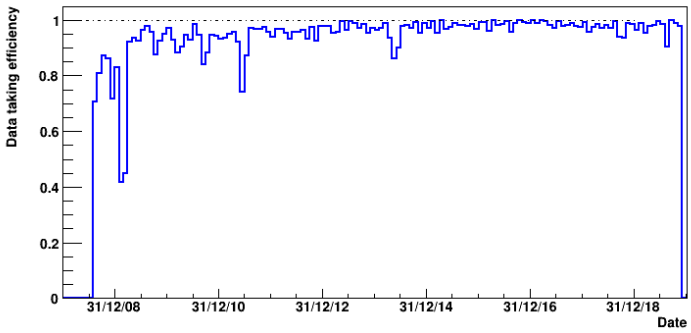

FIGURE 2.12 – Online data taking efficiency of the ANTARES data taking between 2008 and 2019.

Since 2008, about 13000 muon neutrinos have been identified online, most of them being atmospheric neutrinos (Figure 2.13). Figure 2.14 shows the time evolution of the average number of neutrinos per day and the number of reconstructed atmospheric muons. This loss has mainly two origins : the loss of active OMs and the loss of the efficiencies of the PMTs (ageing and bio-fouling). This effect has been studied in detail using ^{40}K decay [68]. Figure 2.15 shows the evolution of the average OM efficiencies over 9 years. A moderate degradation of about 20% can be observed attributed to the combined effect of bio-fouling and gain loss of the photo multipliers. The latter could partly be recovered by high voltage tunings (blue arrows).

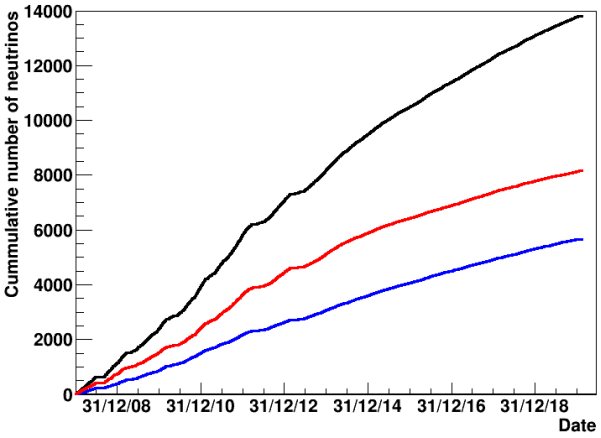

FIGURE 2.13 – Cumulative number of muon neutrino events detected in online by ANTARES between 2008 and 2019. The red, blue and black curves correspond to the single and multi-line events and the total online detected events.

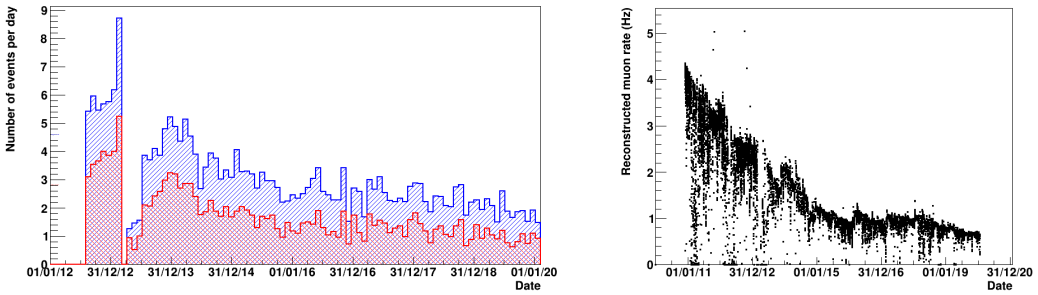

FIGURE 2.14 – (Left) Evolution of the average number of neutrinos per day between 2012 and 2019 detected in online by ANTARES : red and blue histograms shows these numbers for the events reconstructed on one single line and on multi-line, respectively. (Right) Evolution of the muon reconstruction rate between 2010 and 2019.

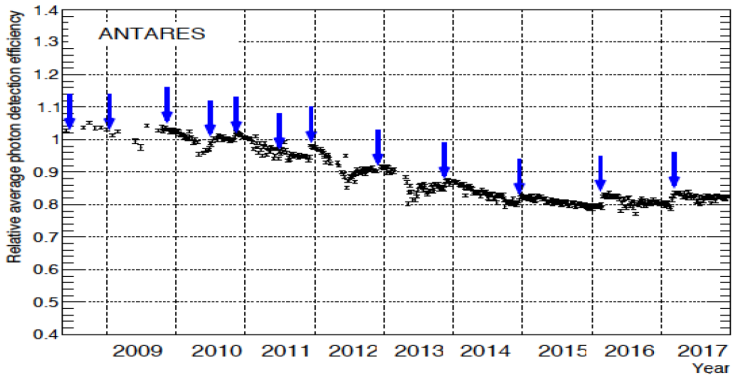

FIGURE 2.15 – Average PMT efficiency of ANTARES Optical Modules between 2008 and 2017 obtained by the ^{40}K decays analysis. Blue arrows indicated the high voltage tunings of the PMTs. Reference [68].

3 Offline time-dependent analysis for electromagnetic variable events

As described in Chapter 2, looking for a point like neutrino source consists in evaluating the statistical significance of a cluster of high-energy events with similar directions over the isotropic low-energy background of the atmospheric neutrino and muons. As the number of events is in general small, this statistical evaluation is performed using an unbinned method based on the extended maximum likelihood ratio test statistic to discriminate the two hypotheses : background only and signal+background. The likelihood is built factorising the contributions of the direction, the energy and the time. To reduce significantly the atmospheric background, adding the time information help a lot. For example, looking only during an AGN flare of 30 days yields a gain in discovery potential larger than a factor 2-3 compared to a steady point-source search for the full data-taking period. Flaring sources are interesting from a physics point of view since processes required for flare production would imply high magnetic fields and high photon densities which, in the presence of protons, may give rise to hadronic processes and neutrino production. Therefore, time correlations between X-ray/gamma-ray and neutrino fluxes can be expected for these variable sources.

The likelihood, $\mathcal{L}$, is defined as :

$$\ln \mathcal{L}(\mathcal{N}_{\mathrm{S}}) = \left(\sum_{i=1}^{N} \ln[\mathcal{N}_{\mathrm{S}}\mathcal{S}_i + \mathcal{N}_{\mathrm{B}}\mathcal{B}_i] \right) - [\mathcal{N}_{\mathrm{S}} + \mathcal{N}_{\mathrm{B}}] \tag{3.1}$$

where $\mathcal{S}_i$ and $\mathcal{B}_i$ are the probabilities for signal and background for an event i, respectively, and $\mathcal{N}_{\mathrm{S}}$ (not known) and $\mathcal{N}_{\mathrm{B}}$ (known) are the number of expected signal and background events in the data sample. N is the total number of events in the considered data sample. To discriminate the signal-like events from the background, these probabilities are described by the product of three components related to the direction, energy, and timing of each event. For an event i, the signal probability is :

$$\mathcal{S}_i = \mathcal{S}^{space}(\Psi_i) \cdot \mathcal{S}^{energy}(dE/dX_i) \cdot \mathcal{S}^{time}(t_i + t_{lag}) \tag{3.2}$$

Here, $\mathcal{S}^{space}$ is a parametrization of the point spread function, i.e., $\mathcal{S}^{space}(\Psi_i)$ is the probability to reconstruct an event i at an angular distance Ψ_i from the true source location. The energy PDF, $\mathcal{S}^{energy}$, is the normalised distribution of the muon energy estimator, dE/dX, of an event according to the studied energy spectrum. The typical energy spectrum follows a power law with an index varying between 1 and 3 depending on the type of sources. The shape of the time PDF, $\mathcal{S}^{time}$, for the signal event is extracted directly from the EM light curve assuming proportionality between EM and neutrino fluxes. A possible lag of up to ± 5 days has been introduced in the likelihood to allow for small lags in the proportionality. This corresponds to a possible shift of the entire time PDF. The lag parameter is fitted in the likelihood maximisation together with the number of fitted signal events in the data. The background probability for an event i is :

$$\mathcal{B}_i = \mathcal{B}^{space}(\delta_i) \cdot \mathcal{B}^{energy}(dE/dX_i) \cdot \mathcal{B}^{time}(t_i) \tag{3.3}$$

where the directional PDF, $\mathcal{B}^{\text{space}}$, the energy PDF, $\mathcal{B}^{\text{energy}}$, and the time PDF, $\mathcal{B}^{\text{time}}$, for the background. They are derived from data using, respectively, the observed declination, δ_i, distribution of selected events in the sample, the measured distribution of the energy estimator, and the observed time distribution of all the reconstructed muons.

The goal of the unbinned search is to determine, in a given direction in the sky and at a given time, the relative contribution of each component, and to calculate the probability to have a signal above a given background model. This is done via the test statistic, λ, defined as the ratio of the probability of the hypothesis of background plus signal over the probability of only background :

$$\lambda = \sum_{i=1}^{N} \ln \frac{\mathcal{L}(\mathcal{N}_{\text{S}})}{\mathcal{L}(\mathcal{N}_{\text{S}} = 0)} \tag{3.4}$$

The evaluation of the test statistic is performed by generating pseudo-experiments simulating background and signal in a 30° cone around the considered source according to the background-only and background plus signal hypotheses. The performance of the time-dependent analysis is computed using toy experiments. For time ranges characteristic of flaring activity, the time-dependent search presented here improves the discovery potential by on-average a factor 2-3 with respect to a standard time-integrated point-source search (Figure 3.1), under the assumption that the neutrino emission correlates with the EM flaring activity.

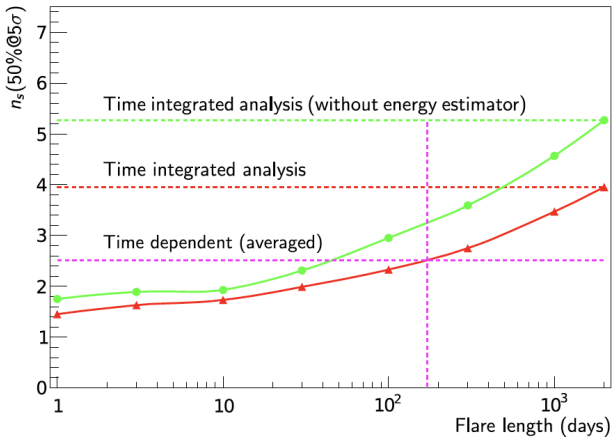

FIGURE 3.1 – The number of signal events required for a 5σ discovery 50% of the time as a function of the flare length. A sample period of 2000 days has been used. The cases where the energy information is included in the analysis (red) or not (green) are shown.

3.1 X-ray binaries and microquasars

X-ray binaries are binary systems composed of a compact object (neutron star (NS) or stellar mass black hole (BH) candidate) and a companion non-degenerate star. Due to the strong gravitational attraction, matter expelled from the companion is accreted by the compact object. Depending on the mass of the companion star and the process of matter accretion, X-ray binaries are separated into two classes :

— Low-Mass X-ray Binaries (LMXB) which contain an evolved companion star of spectral class later than B-star transferring matter to the compact object through Roche lobe overflows.

— High-Mass X-ray Binaries (HMXB) consisting of a massive O or B star developing intense stellar winds, a fraction of which is accreted by the compact object. While some of these objects are seen as persistent sources, most of them exhibit occasional outbursts, making them transient sources, in particular in the radio and X-ray domains.

The detections of GeV–TeV gamma-ray signals from some X-ray binaries confirm that they can produce outflows containing particles accelerated away from the compact object up to relativistic speeds [69]. At the moment, it is not clear whether the high-energy particle acceleration is a common process occurring in X-ray binaries, but observed only in some systems with preferred (geometrical) characteristics with respect to the line of sight, or whether it is powered by a different mechanism at work only in some specific systems.

The theoretical mechanisms of gamma-ray production from X-ray binaries ge-

nerally assume (very-) high-energy photon emission from the interaction of a relativistic outflow from the compact object with the wind and radiation emitted by the companion star. The outflow can take different shapes. In microquasars [70] the high-energy emission is due to accretion energy released in the form of collimated relativistic jets, detected in the radio domain through synchrotron emission. On the contrary, in other binary systems, high-energy emission can occur in a wide-angle shocked region, at the interface between the pulsar and the stellar winds [71]. They are probably the sites of effective acceleration of particles (electrons and/or protons) to multi-TeV energies, but the nature of the high-energy emission is still unknown, and leptonic or hadronic origin is still debated nowadays [72, 73, 74].

Even if a rich variety of binary systems seem to be cosmic accelerators, some major issues are still open : are jets a common feature of X-ray binary systems ? What is the particle acceleration mechanism at work in these systems ? Is it unique ? Constraining the jet composition and its baryonic content will help answer these questions. Indeed, the jet composition should be affected by the outflow-launching processes. For instance, jets powered by an accretion disk are likely to contain baryons [75] while jets, which get their power from black hole spin, are expected to be purely leptonic [76]. Up to now, a hadronic component has been identified in only two X-ray binaries (SS 433 and 4U 1630-472) [77, 76] while a population of cold baryons present in the relativistic jet of Cyg X−1 has been proposed [78].

Hadronic models of jet interactions with the winds of massive stars were developed these last decades. The dominant hadronic contributions are expected from the photo-hadronic (p-γ) interactions between relativistic protons and synchrotron photons in the jet or coming from external sources [79, 80], and from the hadronic (p-p) interactions between relativistic protons from the jet and thermal protons from the stellar wind [81, 82, 83, 84]. In the absence of a jet, neutrinos can be produced through p-p processes between the accelerated protons in the rotation-driven relativistic wind from the young neutron star and the circumstellar disk in the case of Be type stars [85, 86]. The detection of high-energy neutrinos from an X-ray binary system would definitively confirm the presence of relativistic protons in the outflow, and thus further constrain the particle acceleration mechanism.

3.1.1 Source and outburst period selections

The time-dependent analysis described in the following sections is applied to a list of X-ray binaries exhibiting outburst periods in their light curves. In the following, particle acceleration is assumed to take place in the XRB and neutrino emission is assumed to be correlated with hard X-ray outbursts. This is generally the case for microquasars exhibiting relativistic jets. Indeed, a correlation is expected between hard X-ray outbursts (usually produced by both synchrotron

and inverse Compton mechanisms) and compact jet emission where cosmic ray acceleration may occur [87]. It can be noticed that larger Lorentz factors and potentially larger neutrino emission might be expected during transition states, when transient outbursts are observed.

However, most of the X-ray binaries included in our sample are not classified as microquasars. This might not prevent a neutrino emission, in particular during hard X-ray outburst phases. For instance, the LMXB GRO J0422+32 does not present any clear evidence of a relativistic jet although hard X-ray flares are observed [88]. During these outbursts, cosmic rays might be accelerated through magnetic reconnection in the corona (where hard X-ray photons are produced) surrounding the black hole, as suggested by [84]. X-ray binaries containing a magnetized NS do not usually exhibit relativistic ejection of matter. However, as observed in systems such as Cir X-1 [89], transient jets can be produced upon a sufficiently low ($\lesssim 10^8$ G) magnetic field magnitude at the surface of the NS [90], based on a similar accretion/ejection mechanism as microquasars. In supergiant fast X-ray transients (HMXB composed of a NS and exhibiting rapid hard X-ray flux evolution) magnetic field decay could also allow for relativistic particle injection when large clumps of matter are accreted by the NS [91], producing again a potential correlation between hard X-ray flares and particle acceleration. Finally, when the magnetosphere of an accreting NS penetrates the decretion disk of the companion star (as observed in HMXB composed of a Be type companion star), intense hard X-ray emission is expected [92]. Meanwhile, in the case of magnetized NS, the magnetosphere may develop electrostatic gaps where protons could be accelerated along the magnetic field lines, thus allowing for neutrino production [93].

The source and outburst selections are based on the list of XRB detected by swift/BAT telescope[1]. These data are complemented by those of other instruments : RXTE/ASM[2] and MAXI[3]. A maximum likelihood block (MLB) algorithm [94, 95] is used to remove noise from the light curve by iterating over the data points and selecting periods during which data are consistent with a constant flux within statistical errors. This algorithm is applied independently to all the light curves from all the satellites. Depending on the time period and the availability of the different instruments, outbursts are better observed in one apparatus compared to others. As the energy range and the sensitivity of these telescopes are different, it is not easy to combine measurements into a single time-dependent function to describe the light curve. Figure 3.2 displays the light curves of the source 4U 1705-440.

The flaring periods are defined from the blocks of the light curve characterised by the MLB algorithm in three main steps. Firstly, seeds are identified by searching

1. http ://swift.gsfc.nasa.gov/results/transients
2. http ://xte.mit.edu/ASM_lc.html
3. http ://maxi.riken.jp

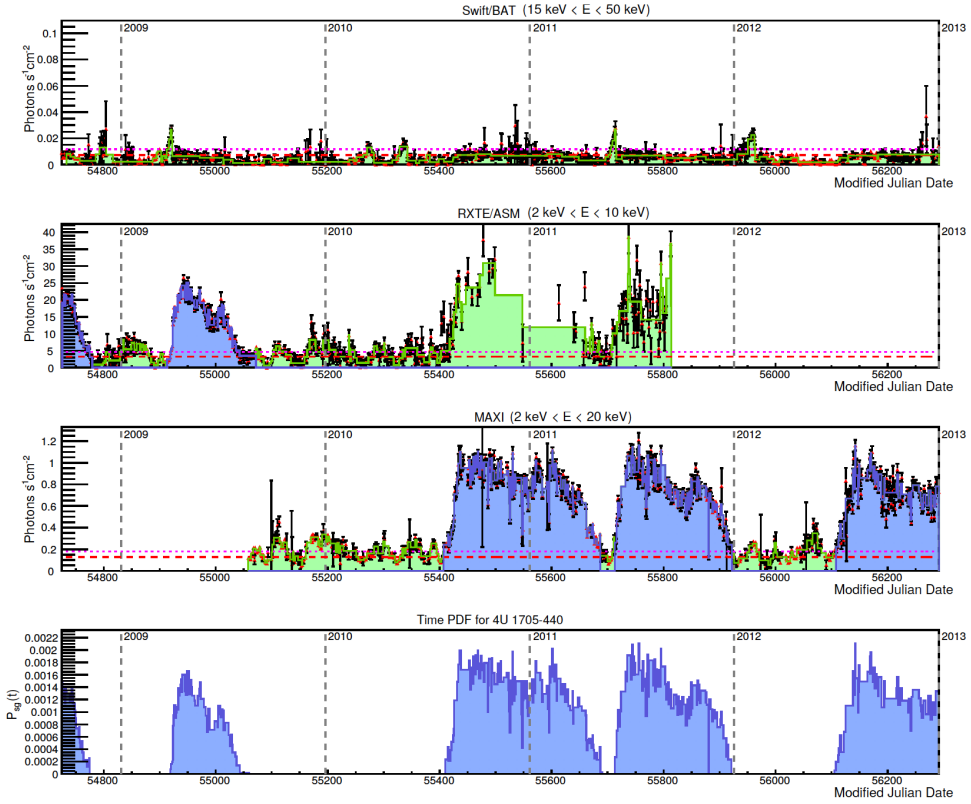

FIGURE 3.2 – Light curves for 4U 1705-440 as seen by Swift/BAT, RXTE/ASM and MAXI during the studied period. The estimated baseline emissions, BL, (red lines) and $BL + 1\sigma_{BL}$ (magenta lines) are also shown. Histograms correspond to the light curves treated with the MLB algorithm. The blue histograms represent the selected flaring periods of each light curve, merged to produce the time PDF (bottom). Green histograms show periods of each light curve not selected for this analysis.

for blocks with an amplitude above $BL + 8\sigma_{BL}$. Then, each period is extended forward and backward up to an emission compatible with $BL + 1\sigma_{BL}$. A delay of 0.5 days is added before and after the flare in order to take into account that the precise time of the flare is not known (one-day binned light curve) and the potential delay between the X-ray and neutrino emissions. Finally, spurious flares are discarded if they are not visible by at least one other instrument. The final list includes 33 X-ray binaries : 1 HMXB (BH), 11 HMXB (NS), 8 HMXB (BH candidate), 10 LMXB (NS) and 3 XRB (BH candidate), as reported in Table 3.1.

Spectral transition states of XRB are difficult to define : there are no regular observations with X-ray satellites, and statistics are very low due to the inaccurate measurement of the hardness ratio, defined as the ratio of counts in different

X-ray wavelength bands. Considering the difficulties of an extensive coverage of the transition states of XRB, the selection of the these transition periods relies on the alerts reported in Astronomer's Telegram.

TABLE 3.1 – List of 33 X-ray binaries with significant flares selected for this analysis.

Name	Class	RA [°]	Dec [°]
Cyg X−1	HMXB (BH)	230.170	-57.167
1A 0535+262	HMXB (NS)	84.727	26.316
1A 1118−61	HMXB (NS)	170.238	-61.917
Ginga 1843+00	HMXB (NS)	281.404	0.863
GS 0834−430	HMXB (NS)	128.979	-43.185
GX 304−1	HMXB (NS)	195.321	-61.602
H 1417−624	HMXB (NS)	215.303	-62.698
MXB 0656−072	HMXB (NS)	104.572	-7.210
XTE J1946+274	HMXB (NS)	296.414	27.365
GX 1+4	HMXB (NS)	263.009	-24.746
MAXI J1409−619	HMXB (NS)	212.011	-61.984
GRO J1008−57	HMXB (NS)	152.433	-58.295
GX 339−4	LMXB (BHC)	255.706	-48.784
4U 1630−472	LMXB (BHC)	248.504	-47.393
IGR J17091−3624	LMXB (BHC)	257.282	-36.407
IGR J17464−3213	LMXB (BHC)	266.565	-32.234
MAXI J1659−152	LMXB (BHC)	254.757	-15.258
SWIFT J1910.2−0546	LMXB (BHC)	287.595	-5.799
XTE J1752−223	LMXB (BHC)	268.063	-22.342
SWIFT J1539.2−6227	LMXB (BHC)	234.800	-62.467
4U 1954+31	LMXB (NS)	298.926	32.097
Aql X−1	LMXB (NS)	287.817	0.585
Cir X−1	LMXB (NS)	230.170	-57.167
EX O1745−248	LMXB (NS)	267.022	-24.780
H 1608−522	LMXB (NS)	243.179	-52.423
SAX J1808.4−3658	LMXB (NS)	272.115	-36.977
XTE J1810−189	LMXB (NS)	272.586	-19.070
4U 1636−536	LMXB (NS)	250.231	-53.751
4U 1705−440	LMXB (NS)	257.225	-44.102
IGR J17473−2721	LMXB (NS)	266.825	-27.344
MAXI J1836−194	XRB (BHC)	278.931	-19.320
XTE J1652−453	XRB (BHC)	253.085	-45.344
SWIFT J1842.5−1124	XRB (BHC)	280.573	-11.418

3.1.2 Main results and discussions

Only one source exhibited a significant signal excess during an X-ray flare : GX 1+4, with 287 days of flare duration included in the analysis, shows a p-value of 4.1% with a fitted signal of 0.7 events and a lag of −4 days, which is obtained with the 100 TeV cutoff energy spectrum. This result is due to one (three) events in a cone of 1 (3) degrees in coincidence with X-ray outbursts detected by RXTE/ASM and Swift/BAT (Figure 3.3). The post-trial probability, computed by taking into account the 33 searches, is 72%, and is thus compatible with background fluctuations. In the hardness transition state analysis, no significant excess has been found, with a 77% post-trial probability for the full analysis.

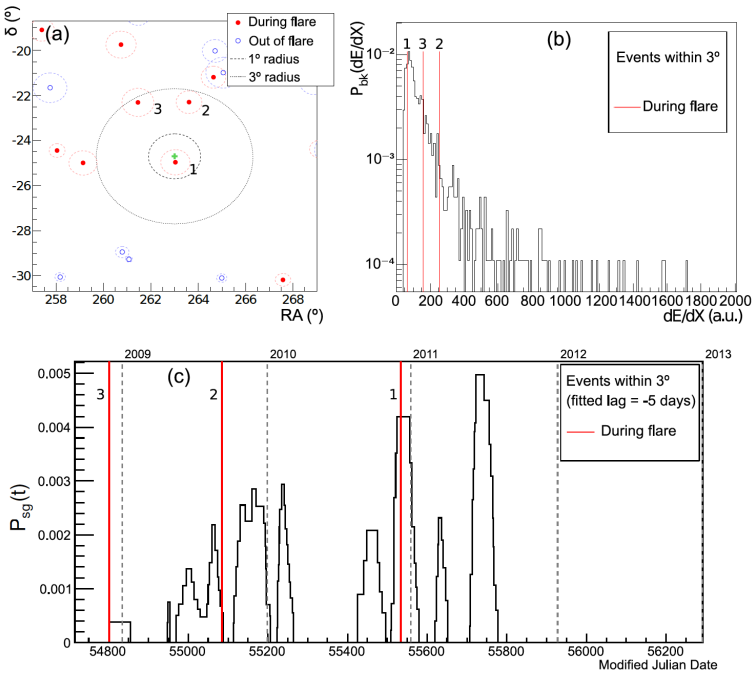

FIGURE 3.3 – The results of this analysis for GX 1+4. (a) Event map around the direction of GX 1+4 indicated by the green cross. The full red (hollow blue) dots indicate the events (not) in time coincidence with the selected flares. The size of the circle around the dots is proportional to the estimated angular uncertainty for each event. The three closest events from the source direction are labeled 1, 2 and 3. (b) Distribution of the estimated energy dE/dX in a ±10° declination band around the source direction. The red line displays the values of the three most significant events. (c) Time distribution of $\mathcal{B}^{\text{time}}$. The red line displays the times of the 3 ANTARES events indicated in panel (a).

In the absence of a discovery, upper limits on the neutrino fluence, $\mathcal{F}_\nu$, the energy

flux, F, and the differential flux normalisation, ϕ_0, at 90% confidence level are computed using 5-95% of the energy range as :

$$\mathcal{F}_\nu = \Delta t \cdot F = \Delta t \int_{E_{min}}^{E_{max}} \mathrm{d}E \cdot E \cdot \phi_0 \cdot \mathcal{S}(E) = \Delta t \cdot \phi_0 \cdot \mathrm{I}(E) \tag{3.5}$$

where $\mathcal{S}(E)$ is the dimensionless neutrino spectrum, e.g. for the E^{-2} spectrum, $\mathrm{d}N/\mathrm{d}E = \phi_0 \cdot \mathcal{S}(E) = \phi_0 \cdot (E/\mathrm{GeV})^{-2}$. The limits are calculated according to the classical (frequentist approach) method for upper limits [96]. Figure 3.4 displays these upper limits. Systematic uncertainties of 15% on the angular resolution and 15% on the detector acceptance have been included in the upper limit calculations [34].

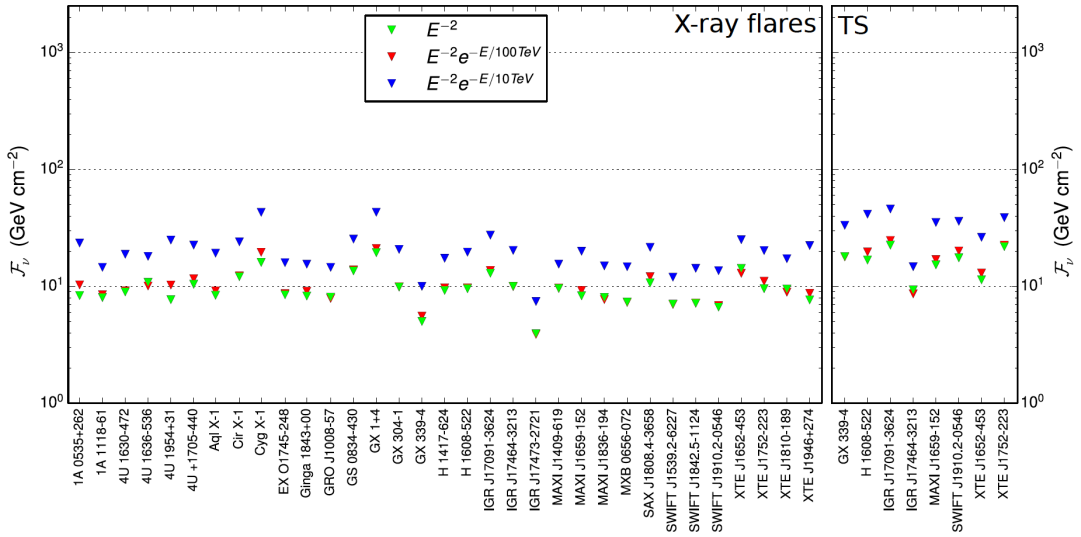

FIGURE 3.4 – Upper limits at 90% C.L. on the neutrino fluence for the 33 XRB with outburst periods (left) and for the 8 XRB with transition state periods (right) in the case of E^{-2} (green triangles), $E^{-2}\exp(-E/100$ TeV) (red triangles) and $E^{-2}\exp(-E/10$ TeV) (blue triangles) neutrino energy spectra.

Upper limits imposed by ANTARES allow to constrain the most favorable hadronic models for microquasars. Hereafter, the neutrino energy flux predictions, F_{pred}, has been computed for seven microquasars according to the photohadronic model [80], based on a previous work Levinson & Waxman [79]. Since they are less stringent, the energy flux upper limits of the transition states are not discussed in the following. Thus, in the following, only the neutrino energy flux upper limits related to the hard state periods are considered. Using the latest measurements of their distance and of the jet parameters, the model predicts the neutrino energy flux based on the radio luminosity of the jets observed in radio during flares. The derived

neutrino energy flux depends on the fraction of jet kinetic energy, $L_{\rm jet}$, converted respectively to relativistic electrons and magnetic field, $\eta_{\rm e}$, and protons $\eta_{\rm p}$, and the fraction of proton energy converted into pions, f_π, which depends in turn on the energy to which protons are accelerated. Resolved and unresolved sources are considered separately. In the following, resolved sources refer to microquasar jets resolved by radio interferometry, which enables the physical parameters of the jet to be probed.

For resolved sources, the neutrino energy flux is estimated from the radio flux density, S_f, at frequency f, the distance of the source, d, the size of the emitting region, l, the jet Lorentz factor, Γ, the jet velocity, β, the angle, θ, between the line of sight and the jet, and the jet opening angle, ψ. The ratio of the minimum and maximum electron Lorentz factors, respectively $\gamma_{\rm min}$ and $\gamma_{\rm max}$, is assumed to be equal to 100, while ψ is taken equal to a conservative value of 20° except in the case of Cyg X-1 [97]. When θ is not constrained by observation, all the values between 0 and 90° are considered. Similarly, if the bulk Lorentz factor, Γ, of the jet is poorly known, all the potential values are tested. These uncertainties, together with the error on the other jet parameters, are taken into account to derive the range of neutrino energy fluxes $F_{\rm pred}$ satisfying the model which is linearly dependent on $\eta_{\rm e}/\eta_{\rm p}$.

The resulting predictions are compared with the upper limits obtained with ANTARES data under the hypothesis of a cutoff at 100 TeV in the neutrino flux, to account for limits in the acceleration process included in the model [80]. As an example, Figure 3.5 shows how the predicted flux is compared with this result as a function of the jet parameter β for resolved microquasars Cyg X-1, Cir X-1 and MAXI J1659-152 [5]. Comparing the predicted flux and the ANTARES neutrino energy flux upper limits, upper limits at 90% C.L. on $\eta_{\rm p}/\eta_{\rm e}$ are set. These limits have been derived taking into account the discrepancy between Lorentz factors reported in radio observations, and uncertainties on the opening angle of the jet, the distance of the source, and on the inclination angle between the line of sight and the jet.

However, the potential variability of the Lorentz factor during a burst and between the periods of activity of the source is not taken into account in this calculation. Thus, constraints on baryon loading may have different implications : the proton component in the jet can be negligible in comparison with the electromagnetic component, the proton energy fraction converted to pions can be less significant than the values considered [80], and/or the jet Lorentz factor is lower than the constraints set by radio observations.

For unresolved sources, the jet kinetic power is evaluated from the jet synchrotron luminosity derived from the flux density, $S_{f_{\rm break}}$, at the frequency break, $f_{\rm break}$,

5. The energy flux upper limit obtained for H 1743-322 is around 2 orders of magnitude higher than the expectations [80]. Thus, this source is not included in Figure 3.5.

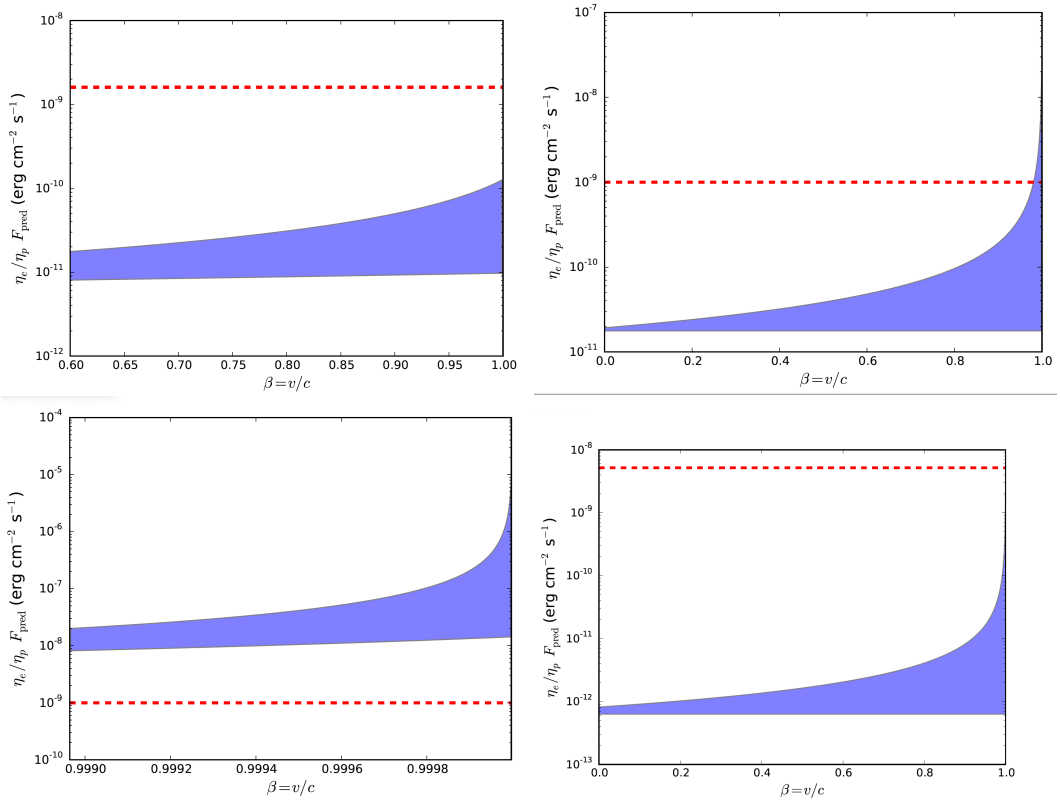

FIGURE 3.5 – Comparison of the energy flux upper limit at 90% C.L. provided by ANTARES (red dashed line) with the predictions [80] as a function of the jet velocity, β : Cyg X-1 (top left), Cir X-1 with jet parameters [89] (top right), Cir X-1 with jet parameters [78] (bottom left) and MAXI J1659-152 (bottom right).

between optically thick and optically thin radio emission, and the spectral index, α_R [80]. When no spectral index value is provided in the literature, $\alpha_R = 0$ is assumed as given by the standard jet radio emission theory [98]. Again, the neutrino energy flux is linearly dependent on f_π and η_e/η_p. The results from both resolved and unresolved sources are summarised in Figure 3.6.

3.1.3 Perspectives

This analysis has been performed using a limited dataset of ANTARES (5 years). No significant neutrino signal has been detected in coincidence with the selected sample of X-ray binaries. This analysis has been extended to 4 more years without finding clear association. In the near future, we plan to further extend this analysis with a new PhD student end 2020 using the full ANTARES dataset (∼15 years) and the first KM3NeT data. In particular, KM3NeT will bring an increase sensitivities

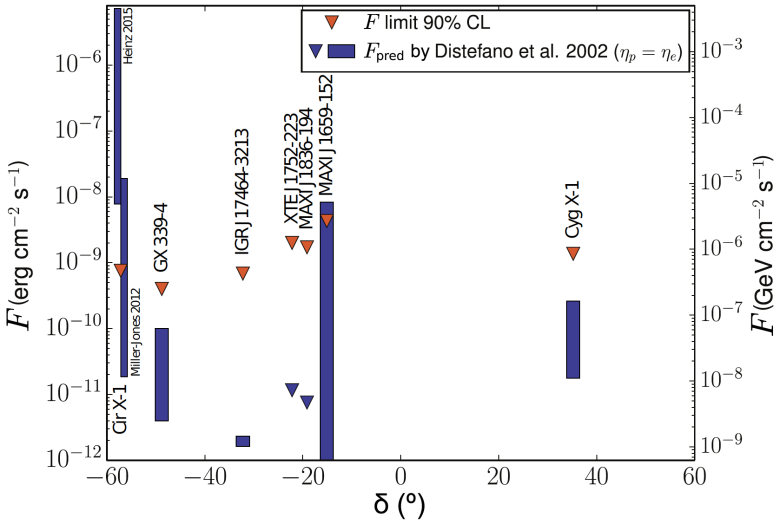

FIGURE 3.6 – Upper limits at 90% C.L. on the neutrino energy flux obtained in this analysis considering a $E^{-2}\exp(-\sqrt{(E/100\text{ TeV})})$ spectra, compared with the expectations [80] assuming energy equipartition between electrons and protons. The blue rectangles show the expectations from [80] taking into account the uncertainty on the jet velocity. For the unresolved microquasars XTE J1752-223 and MAXI J1836-194, a single energy flux prediction value is given, since no detail on the jet velocity is available in the literature.

at the low energies (< 500 GeV) with ORCA, a window quite interesting to test the acceleration of cosmic rays in the winds of the binaries and at the basis of the jets in case of micro-quasars. The new analysis will also include the cascade contribution together with the track one. We will mainly concentrate on the transient jet phases, the most promising periods to look for high-energy emissions. This requires a detailed study of the X-ray light-curves to identify the changes in the hardness ratio and the increases of the X-ray flux.

The time-dependent analysis has the best discovery potential if we know where and when to look for neutrinos. For typical out-bursting periods, the gain in sensitivity and in discovery power can be larger than a factor 2 compared to a steady point-like source analysis. We have also applied this type of algorithm to blazar flares. These sources are extremely energetic events in the Universe for which the fluxes in electromagnetic radiations are transient or variable with typical variations of days to months. We were using the time variations to select only the most probable time periods to look for neutrino emissions, which allow to drastically reduce the atmospheric background contributions. In hadronic models, we can expect a direct link between the gamma-ray flux and the neutrino flux. The search for correlation between neutrino and γ-ray flaring periods was performed using 5

years of ANTARES data [99]. This has yielded to no significant neutrino source detection. With the possible neutrino association with the blazar TXS 0506+056, there have been intense discussion on the time correlation between neutrino and γ-ray emissions. The neutrino emission detected in 2014-2015 seems to not correlate with a flaring period in γ-ray while for IC170922 there is a clear correlation. If the neutrino production happens close to the basis of the jet, then p-γ interactions dominate with the intense EM radiations, the decays of the mesons will produce high-energy γ-ray and neutrinos in the same energy range. However, the presence of strong magnetic fields and strong radiation/matter fields will transfer most of the energies down to the lower energy range. In this kind of lepto-hadronic models, γ-rays are produced in a different zone further away in the jet where the jet is not opaque. In this zone, the neutrino production efficiency is quite low. Therefore, it is more natural to look for a correlation between bright X-ray sources, and even during X-ray flares with high-energy neutrinos. Since the end of RXTE and Rosat, only Swift provided a quite complete X-ray sample, but since it is done with the BAT instrument, the sensitivity is quite low. In the future, eRosita will provide a deeper sample that could be used to look for these correlations. In [100], a correlation between high-energy neutrinos and intense radio flares detected during VLBI campaigns in the central region of blazars. This correlation is quite elegant since the radio observations are good tracer of the activity of the jets. However, it is complicated to obtain a complete sample.

Finally, the time-dependant analysis framework, we have implemented for ANTARES analyses, is being moved to the KM3NeT analysis framework. It is currently adapted to the data format of the KM3NeT simulation and data.

3.2 Fast Radio Bursts

In 2007, Duncan Lorimer and his colleagues reported the discovery of a mysterious radio burst signal detected on 2001, August 24 and located close to the Large Magellanic Cloud [101]. The discovery of the so-called "Lorimer" burst was made using the Parkes Observatory in Australia. This was the starting point of new exciting field of investigation into the world of the transient objects. Fast Radio Bursts (FRBs) are characterised by a short duration (t $\sim$ a few ms) of intense radio emission (> 1 Jy $\cdot$ ms) measured so far in the 800 MHz and 1.4 GHz bands by various radio telescopes. The astrophysical origin of FRBs is largely unknown. However, their high dispersion measures (DM), due to the scattering of the radio wave propagating through an ionised column of matter, suggest an extra-galactic/cosmological origin [102].

From the FRBs already detected and reported in the FRB catalog [1] [103], the observed DM can be used to derive upper limits on their cosmological redshift, $z_{DM} \in [0.08\,;2.3]$. This translates into an upper limit on the isotropic radio energy release of $E_{rad} \in [10^{37}\,;10^{41}]$ erg. Up to now, the FRB progenitors are thought to originate from a large variety of astrophysical sources [104] usually split into two classes : the repeating ones and the single cataclysmic events. Indeed, such a large amount of energy, released in a millisecond time scale, may favor an FRB origin from violent cataclysmic events. Those are powered by compact objects where the progenitor does not survive afterwards (single burst model). Several models have been proposed such as neutron star mergers [105, 106, 107, 108, 109] possibly associated with short Gamma-Ray Bursts (GRBs) [110, 111, 112] or supramassive neutron star collapses [113, 114, 115]. Non-destructive flaring models including giant pulses from young and rapidly rotating neutron stars [116, 117], magnetar giant flares [118, 119], hyper-flares from soft gamma-repeaters [120], a young neutron star embedded in a wind bubble [121] or maybe from the interior of young supernovae [122] are however good astrophysical candidates to explain both types of repeating and non repeating FRBs. More exotic models have also been proposed such as radio burst radiation of superconducting cosmic strings [123, 124, 125, 126].

The discovery of the repeating behavior of FRB 121102 [127, 128] has brought new insights into the nature of the FRB progenitors. In addition, radio interferometric observations of FRB 121102 [129, 130] made possible, for the first time, to unambiguously determine the redshift of the FRB source at $z \sim 0.19$ [131], confirming the tremendous amount of radio energy that can be released during an FRB event. Few others repeating FRBs have been recently discovered, FRB 180814 [132], FRB180916 [133, 134, 135] and FRB 200428. With the upgraded radio telescope, more and more repeating bursts have been identified [136, 137]. FRB200428 is the first FRB detected inside the Milky-Way and it has been associated to the magnetar SGR 1935+2154 where an intense X-ray emission has been observed [138, 139, 140, 141, 142].

The spatial distribution and the all-sky rate of FRBs, $\mathrm{R_{FRB}}$, can provide additional constraints on the nature of the FRB progenitors when it is compared to those of known astrophysical sources. The all-sky rate $\mathrm{R_{FRB}} \sim 10^3$ day^{-1} has been estimated for radio pulses with $\mathrm{F} > 1$ Jy $\cdot$ ms [143]. This high event rate would already rule out a short GRB-dominated population of FRBs since $\mathrm{R_{FRB}}/\mathrm{R_{short\ GRB}} \sim 10^3$ assuming that $\mathrm{R_{short\ GRB}} = \frac{\mathrm{N_{short\ GRB}}}{\mathrm{N_{all\ GRB}}} \times \mathrm{R_{GRB}}$ where $\mathrm{R_{all\ GRB}} = 1000$ yr^{-1} in the entire sky and the detected GRB population is composed of 1/3 of short GRBs according to the CGRO-BATSE observations [144]. Alternatively, $\mathrm{R_{FRB}}$ corresponds to only 10% of the observed CCSNe rate [102]. Therefore, the CCSNe reservoir may account for the high event rate of FRBs. For instance, [113] claimed that only

1. see the FRB catalog : http://frbcat.org/

3% of the core collapse supernovae (CCSNe) producing supramassive neutron stars are needed to explain the FRB rate. The various models proposed are difficult to discriminate because of lack of additional information on the broadband FRB spectra. Many multi-wavelength follow-ups have been organised recently [145, 146, 147, 128, 148, 149], but counterparts (optical/x-rays/gamma-rays/VHE gamma-rays) have been identified only for very few FRBs with very good localisation precision. However, in 2016, [150] reported the detection of a gamma-ray GRB-like counterpart in association with FRB 131104 but with a small significance (3.2 σ). For FRB 131104, [150] determined that the radio to gamma-ray energy output ratio would be $E_{rad}/E_{\gamma} > 10^{-9}$ assuming the source is at the redshift inferred by the DM measurement. This may show that a large fraction of the total energy radiated during these radio bursting events may be emitted at high energy while being still undetected or marginally detected. If the radio emission is likely produced by the coherent emission of leptons [151], hadronic processes may be the source of the most energetic photons in the gamma-ray energy domain. In this case, TeV-PeV neutrinos can be produced by photohadronic interactions. These hadronic processes may occur in the energetic outflow released during a cataclysmic FRB event [113] or in the vicinity of the FRB progenitor through the interaction of the outflow with the surrounding environment [152, 115, 121, 153]. The detection of the high-energy component of the FRB is still to be done. It will be one key ingredient to determine if FRBs are efficient cosmic accelerators.

Based on their high rate, R_{FRB}, and under the assumption that a fraction of FRBs are indeed efficient accelerators of TeV-PeV hadrons, they may contribute significantly to the cosmic diffuse neutrino signal discovered by the IceCube Collaboration. Multi-messenger observations of FRBs are crucial to probe them as cosmic accelerators. Neutrino searches from FRBs by the IceCube [154, 155] and the ANTARES [156, 148, 147, 157] Collaborations have been performed by both Collaborations.

3.2.1 Analysis of the FRB samples detected in 2013-2017

In this section, the analysis focusing on the period from Jan. 2013 to Jan. 2017 during which 16 FRBs are reported. The FRBs were detected by the Parkes telescope, UTMOST and ASKAP. When active, the ANTARES telescope monitors the sky region with declinations $\delta < -48^{\circ}$ with almost 100% duty cycle; for $-48^{\circ} < \delta < +48^{\circ}$ the duty cycle decreases gradually because of the requirement that the neutrino candidates are upgoing. The first selection criterion is that the FRB position must be within the ANTARES field of view (FoV) within a chosen time window $\Delta T = [T_0 - 6h\ ; T_0 + 6h]$ where T_0 is the FRB trigger time. Three FRBs did not fulfill this first selection criterion and were then removed from the sample used in this analysis. In addition, the quality of the ANTARES data

TABLE 3.2 – Properties of the 12 FRBs visible by ANTARES in the period 2013-2017 according to the FRB catalogue [103]. z_{DM} corresponds to the upper limit on the cosmological redshift inferred from the DM measured in excess of the Galactic contribution.

FRB	z_{DM}	T_0 (UTC)	RA (°)	dec (°)	radio telescope
131104	0.59	18 :04 :11.20	101.04	-51.28	Parkes
140514	0.44	17 :14 :11.06	338.52	-12.31	Parkes
150215	0.55	20 :41 :41.71	274.36	-4.90	Parkes
150418	0.49	04 :29 :06.66	109.15	-19.01	Parkes
150807	0.59	17 :53 :55.83	340.10	-55.27	Parkes
151206	1.385	06 :17 :52.78	290.36	-4.13	Parkes
151230	0.76	16 :15 :46.53	145.21	-3.45	Parkes
160102	2.13	08 :28 :39.37	339.71	-30.18	Parkes
160317	0.70	09 :00 :36.53	118.45	-29.61	UTMOST
160410	0.18	08 :33 :39.68	130.35	6.08	UTMOST
160608	0.37	03 :53 :01.09	114.17	-40.78	UTMOST
170107	0.48	20 :05 :45.14	170.79	-5.02	ASKAP

acquired during the whole day around each FRB detection was verified to avoid any anomalous behavior of the detector. One more FRB (FRB 150610) was excluded since the detector was not active due to a power cut that happened 4 hours before the trigger time. At the end, the final sample is composed of 12 FRBs for which ANTARES data were considered. In Table 3.2, the main properties of the FRB sample are summarised and a sky map of the FRB positions superimposed with the ANTARES sky visibility is shown in Figure 3.7.

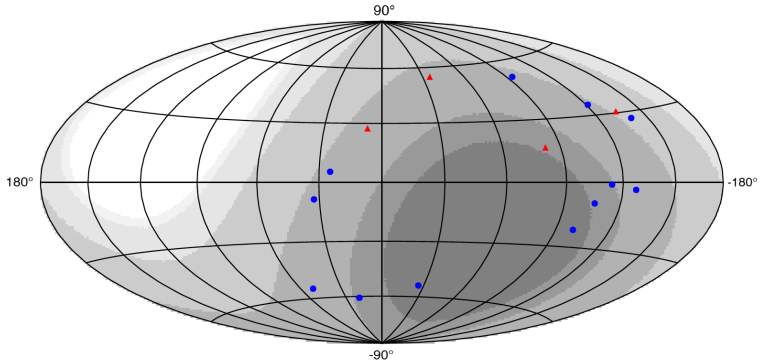

FIGURE 3.7 – Skymap in Galactic coordinates showing the positions of the 16 FRBs detected in the period 2013-2017. The 12 selected FRBs are shown with the blue dots while the 4 non-selected FRBs are displayed with the red triangles. The region of the sky observable by ANTARES (on average) is also displayed in greyscale from 100% of visibility for the darkest area to 0% for the white area when considering upgoing neutrino candidates in the detector.

For each selected FRB, the ANTARES data set is extracted within a time window $\Delta T = [T_0 - 6h\ ; T_0 + 6h]$. This time window is chosen to encompass various delay scenarios between the radio and the neutrino signals while keeping the background noise at a low level. Within ΔT, the event rates are checked to verify the detector stability. No significant time variability of the counting rates was found which ensures the quality of the extracted data. The search for a significant neutrino flux is then based on the detection of upgoing neutrino-induced muons coincident with the position of the FRB within ΔT.

To suppress the atmospheric muon background contamination in the neutrino sample, selection cuts are applied using the quality variables of the track reconstruction algorithm [64] : the reconstructed zenith angle, θ, the error estimate on the reconstructed direction, β, and the quality fit parameter, Λ. Each selected upgoing ($\cos\theta > 0$) event was required to have a direction error $\beta < 1°$. The final selection criterium is based on the quality fit parameter Λ. For ΔT centered on each FRB time, the optimal value, $\Lambda_{3\sigma}$, was chosen in such a way that the presence of one neutrino candidate in the time window would correspond to a positive signal with 3σ significance. Finally, a search cone of 2° is set around each FRB position. From radio information, the typical localization errors correspond to radii of 10 arcmin.

3.2.2 Main results

No upgoing events spatially and temporally correlated with the 12 selected FRBs were found. This null result is compatible with the background event rate

of ANTARES estimated to be $\sim 5 \cdot 10^{-8}$ event $\cdot$ s^{-1}. Since no neutrino signal is detected in coincidence with any of the selected FRBs, constraints on the fluence of neutrinos that would have been observed by the ANTARES detector are derived.

As the neutrino production mechanisms for FRBs are unknown, three spectral models have been tested in this analysis to conservatively cover a large range of possibilities : a hard spectrum with $\gamma = 1.0$ usually considered in some stages of pγ acceleration processes, an intermediate spectrum with $\gamma = 2.0$ corresponding to the theoretical index for Fermi acceleration processes and a softer spectrum with $\gamma = 2.5$. The latter almost corresponds to the best fit value of the isotropic astrophysical neutrino signal measured by IceCube. The upper limits on the neutrino fluence, $F_\nu^{90\%}$, for each individual FRB and for the three test spectral indexes are drawn in Figure 3.8.

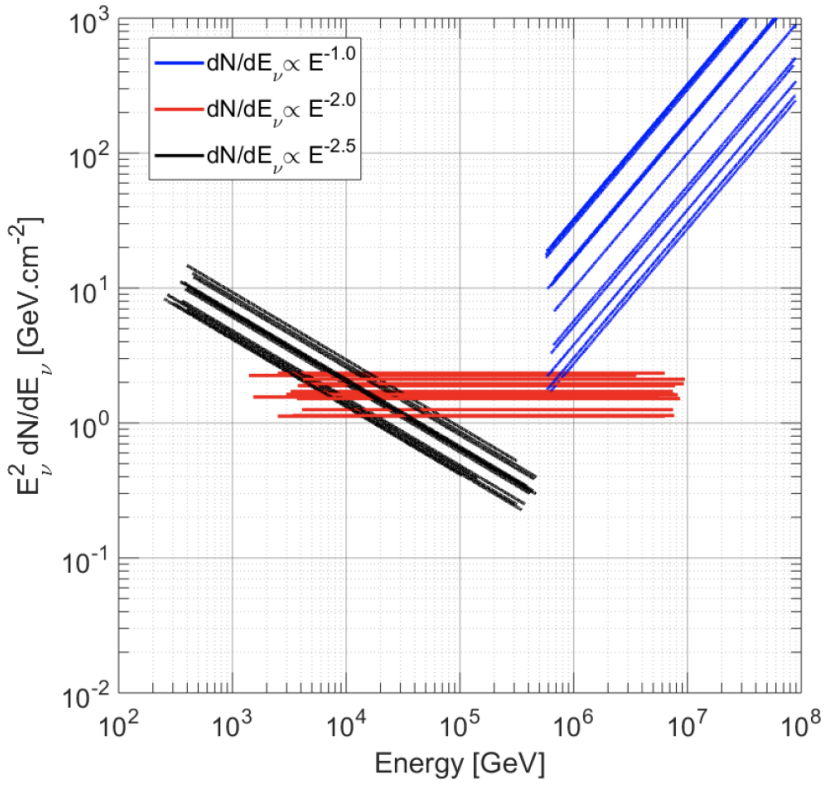

FIGURE 3.8 – The 90% confidence level ANTARES upper limits on the neutrino fluence for the power law spectral models with $\gamma = 1.0$ (blue), 2.0 (red), 2.5 (black), for each FRB. The limits are computed in the energy range $[E_{min}\ ; E_{max}]$ where 5-95% of the neutrino signal is expected.

The isotropic neutrino energy, $E_{\nu,iso}$, possibly released during an FRB event is an important physical property of the bursting source. It may give information on the baryonic load within the ejected outflow as well as the efficiency of the hadronic processes at work on the acceleration site nearby the progenitor source. It can be expressed as :

$$E_{\nu,iso} = \frac{4\pi D(z)^2}{1+z} \cdot F_\nu \tag{3.6}$$

where z is the redshift of the source and $D(z)$ is the distance traveled by the neutrinos depending on the assumed cosmological model :

$$D(z) = \frac{c}{H_0} \int_0^z \frac{(1+z')dz'}{\sqrt{\Omega_m(1+z'^3)+\Omega_\Lambda}} \tag{3.7}$$

where c is the velocity of light in vacuum and the cosmological parameters are $H_0 = 67.8$ km s^{-1} Mpc^{-1}, $\Omega_m = 0.308$ and $\Omega_\Lambda = 1 - \Omega_m$ [158]. For distances in the range d $\in [1kpc\,; D(z_{DM})]$, the 90% C.L. upper limits on $E_{\nu,iso}$ have been computed and the results are shown in figure 3.9 for each FRB. The excluded region in the $E_{\nu,iso}$-$D(z)$ plane for the hardest considered spectrum ($\gamma = 1.0$) and the softest spectrum ($\gamma = 2.5$) are also indicated. The constraints on $E_{\nu,iso}$ obtained with the power law spectrum $\gamma = 2.0$ are similar to that obtained with $\gamma = 2.5$ as the two corresponding $F_\nu^{90\%}$ are similar.

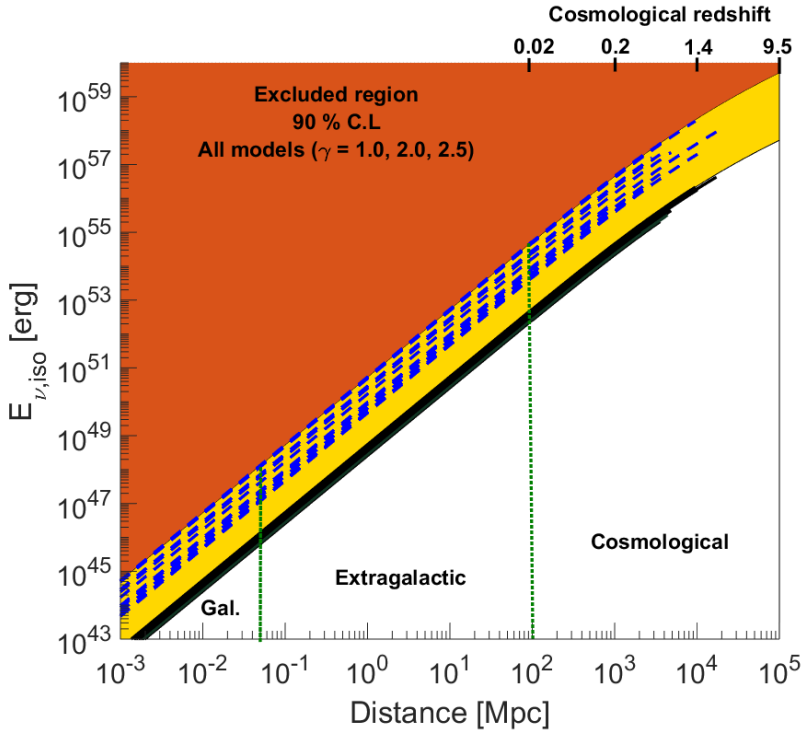

FIGURE 3.9 – The 90% confidence level upper limits on the neutrino energy released by the FRB sources. The per burst limits, assuming different neutrino power law spectra, are shown by the dashed blue lines ($\gamma = 1.0$) and the black solid lines ($\gamma = 2.5$). These limits are computed in the distance range d $\in [1kpc\,; D(z_{DM})]$. The red area indicates the region that is already excluded by ANTARES at the 90% C.L. for any considered hadronic model ($\gamma = 1.0, 2.0, 2.5$). The yellow area is only excluded by the soft spectral models ($\gamma = 2.0, 2.5$). The white area, divided in 3 distance scenarios, is still allowed according to the ANTARES sensitivity.

Since the distances of these FRBs are unknown, three distance scenarios can be assumed :

— the sources are galactic or very close to our Galaxy, typically up to the distance to the Magellanic Clouds d $\leq$ 50 kpc ;
— Extragalactic but non-cosmological d $\in$ [50 kpc ; 100 Mpc] ;
— Cosmological d $\geq$ 100 Mpc.

For these three ranges of distance, the upper limits on the neutrino fluence, see Figure 3.9, for a $E_\nu^{-2.5}$ model, can be converted in the source rest frame by $E^{90\%}_{\nu,iso} \leq [10^{43}\,; 10^{46}]$, $[10^{46}\,; 10^{52}]$ and $[10^{52}\,; 10^{57}]$ erg, respectively.

3.2.3 Neutrino constrains on the origin of the FRB

The upper limits on the neutrino energy released by both the individual FRB sources and the whole population must be compared to the expectations of some FRB hadronic models.

3.2.3.1 Short GRB progenitor

In the merger scenario, collapsing neutron stars may power an FRB at the merger time and then produce a short γ-ray burst few seconds to hundreds of seconds after [159]. In the standard framework of GRBs, particles are accelerated by internal shocks within the relativistic jetted outflow and photo-hadronic processes may give rise to a burst of high-energy neutrinos [160, 161, 110]. The neutrino flux can be roughly scaled to the γ-ray flux and to the baryonic load in the outflow according to [110, 107] :

$$E_{\nu,iso} \approx \frac{f_p}{8} \cdot (1 - (1 - < \chi_{p/\gamma} >)^{\tau_{p\gamma}}) \cdot E_{\gamma,iso} \tag{3.8}$$

with f_p the baryonic loading factor assumed to be preferentially in the range $f_p \in [1\,;100]$, $\langle \chi_{p/\gamma} \rangle \sim 20\%$ the fraction of the proton energy transferred to the pions, and $\tau_{p\gamma}$ the optical depth of photohadronic interactions. For short GRBs, the isotropic γ-ray energy released is usually in the range $E_{\gamma,iso} \in [10^{47}\,;10^{50}]$ erg. The short GRB 170817A associated with the binary neutron star merger event of august 2017 [7] was sub-luminous with $E_{\gamma,iso} = 3.1 \pm 0.7 \cdot 10^{46}$ erg integrated over an observed duration $T = (2 \pm 0.5)\ s$ [8]. Typically, for a so-called standard short GRB [2], the optical depth is $\sim 5 \cdot 10^{-2}$. Based on these rough estimates, the neutrino expectations are in the range $10^{-3} \cdot E_{\gamma,iso} \lesssim E_{\nu,iso} \lesssim 0.1 \cdot E_{\gamma,iso}$. As shown in Figure 3.10, the derived limits on the neutrino flux can rule out short GRB models in a very nearby environment (d $<$ 1 kpc) assuming that the neutrinos are produced with an unbroken power law spectrum. Our limits can not constrain any model associating FRBs to short GRBs if the astrophysical sources are located at a distance d $>$ 100 Mpc. Recent advanced hadronic models imply a broken power law spectrum for the neutrino emission in short GRB events. Also the predictions of those models are weakly constrained by our exclusion regions. For instance, [162] have computed the expected neutrino spectrum from the short GRB GRB170817A using the NeuCosmA model [52, 163] for different configurations of the jetted outflow. Considering the low luminosity jet scenario ($\Gamma = 30$, $f_p \in [1\,;1000]$), see figure 2 given by [162], the corresponding neutrino fluences integrated over 100 TeV-100 PeV are $F_\nu \in [4.3 \cdot 10^{-5}\,;0.07]$ GeV $\cdot$ cm^{-2}. At a distance of 40 Mpc and a redshift z = 0.008, this translates into $E_{\nu,iso} \in [10^{46}\,;10^{49}]$ erg which is still below the ANTARES sensitivity as shown in Figure 3.10.

2. with the following parameters : the Lorentz factor $\Gamma = 300$, the gamma-ray energy $E_{\gamma,iso} \approx 10^{50}$ erg, the minimum variability time scale of the gamma-ray emission t_{var}= 0.01 s, the radius at which the pγ interactions occur $R_{p\gamma} \approx 10^{13}$ cm and the redshift z = 0.5.

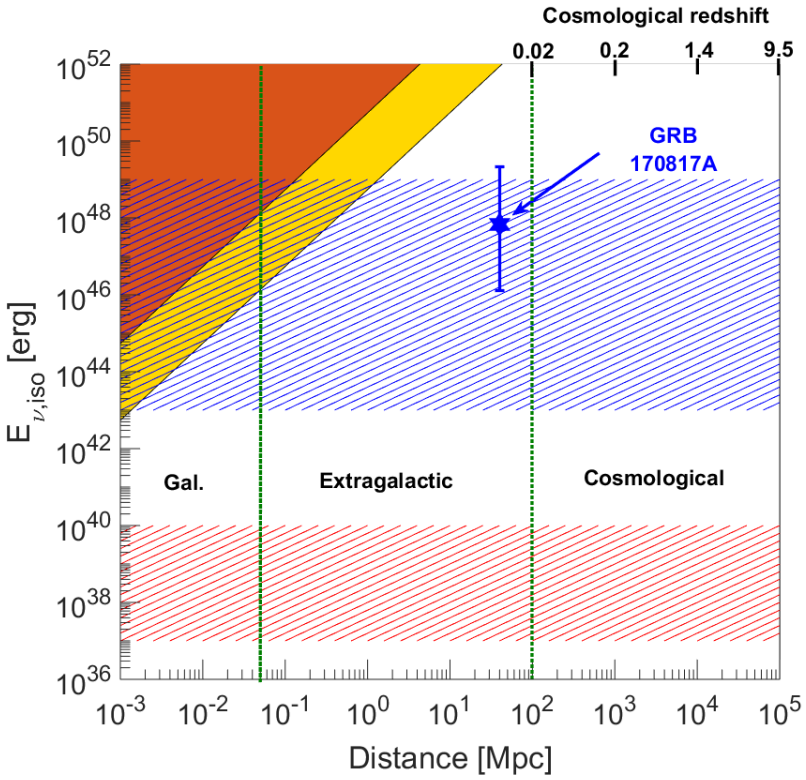

FIGURE 3.10 – The $E_{\nu,iso}-$distance plane with the region already excluded by ANTARES for different neutrino models (red : $\gamma \geq 1.0$, yellow : $\gamma \geq 2.5$). The neutrino predictions from short GRBs (standard internal shock model) are represented by the blue hatched region while the magnetar/young neutron star neutrino flare expectations are shown with the red hatched area. The neutrino expectations for the short GRB GRB 170817A given by [162] are also shown. The errors are due to the possible range for $f_p \in [1\ ; 1000]$.

3.2.3.2 Magnetar giant flare / Soft Gamma Repeater (SGR)

In these two scenarios, the FRB event is produced by a sudden release of energy in the magnetosphere of the magnetar either driven by magnetic instabilities or high rotational loss (spin-down power). Protons may be accelerated into the polar cap regions and interact with the x-ray photon field emitted in the neutron star environment to produce high-energy neutrinos and secondary particles [152]. In the first scenario, the extremely strong magnetic field ($B > 10^{15}$ G) is the source of the x-ray photon field and of the particle acceleration. It corresponds to the giant flares from magnetars or the SGR models. The second scenario is related to some highly magnetised ($B \sim 10^{14}$ G) neutron stars which are born with a millisecond timescale period of rotation, making them able to power the particle

acceleration and the subsequent high-energy neutrino emission [153]. In both neutron star scenarios, a very high magnetic field is required with at least $B > 10^{14}$ G. For a magnetar, the typical values for the stellar radius and the magnetic field used here are $B = 10^{15}$ G, $R = 10$ km. The rotational period, P, can vary from hundreds of milliseconds for a very young neutron star to few seconds for slow rotating magnetars (with P $>$ 2 s). Based on these magnetar properties, the models of [152, 153] predict a high-energy neutrino luminosity in the range $L_{\nu,\text{quiescent}} \in [10^{32}\,; 10^{35}]$ erg s^{-1} when the magnetar is in the quiescent state. For a giant flare like the one observed from SGR 1806-20 [164], the luminosity of the x-ray/γ-ray background (with $E_\gamma = 20 - 30$ keV [165]) can increase by at least a factor 10^6 in less than a second compared to the quiescent periods of the magnetar [166]. This kind of bursting event may also produce an FRB. By scaling the typical neutrino luminosity expected from quiescent magnetars to the SGR bursting events (with a typical duration for the main spike $t_{\text{spike}} \sim 0.1$ s [166, 164]), one can obtain a rough estimation of the total energy released in neutrinos during giant flares from magnetars $E_{\nu,iso} \leq 10^6 \cdot L_{\nu,\text{quiescent}} \cdot t_{\text{spike}} \leq [10^{37}; 10^{40}]$ erg.

These estimates are also compared, in Figure 3.10, to the ANTARES neutrino upper limits. Magnetar/SGR sources are very likely weak sources of high-energy neutrino according to the models depicted above. Hence the magnetar flare origin of FRBs can not be significantly constrained on a per burst basis with the neutrino analysis presented here.

3.2.3.3 Core-collapse supernova environment

Core collapse supernovae are known to produce a compact object such as a neutron star or a black hole surrounded by the material ejected from the progenitor star during the explosion, the so-called supernova remnant. [161, 113, 114, 115] mention the possibility that cosmic-rays and high energy neutrinos may be produced by the interaction of an energetic outflow ejected by the newly born compact object with the surrounding pulsar nebula or supernova remnant at a distance R$\sim 10^{15-16}$ cm. A FRB could be also produced during this interaction or directly inside the ejected outflow. The resulting neutrino flux may be low since at such distance from the progenitor the density of the target medium for the photo-hadronic interaction is quite small. In addition, the delay between the production of the radio and the neutrino signal is not clear yet.

For all the hadronic models listed in this discussion, it seems that detecting a neutrino signal from single FRB sources may be difficult as most of the FRB hadronic model predictions remain orders of magnitude below the ANTARES neutrino detection threshold. However, the expected large number of FRBs over the entire sky may contribute to a diffuse flux that can be tested by a large scale

neutrino telescope. This possibility is discussed in the following section.

3.2.3.4 Contribution to the neutrino diffuse flux

So far, the sources responsible for this cosmic isotropic signal detected by IceCube and seen by ANTARES have not been clearly identified. Even if the first compelling evidence of a cosmic high-energy neutrino, it is still not clear how important is the contribution of the blazars to the neutrino diffuse flux. On the contrary, the GRB contribution to this diffuse flux has already been constrained to be less than 1% [167]. The population of fast radio bursts may also contribute significantly since their expected rate is high, $R_{FRB} \sim 10^3$ day^{-1} [143]. This hypothesis is tested here by computing the 90% C.L. upper limit on the diffuse neutrino flux associated with FRBs. As before, the neutrino flux associated with FRB sources is assumed with a power law energy distribution with spectral indexes γ= 1.0, 2.0, 2.5. The derived diffuse upper limits depend on the assumed neutrino spectrum. Hence,

$$E_\nu^2 \Phi_\nu^{90\%} = \frac{1}{4\pi} \cdot \phi_{FRB}^{90\%} \cdot \frac{R_{FRB}}{N_{FRB}} \quad \text{GeV} \cdot \text{cm}^{-2} \cdot \text{s}^{-1} \cdot \text{sr}^{-1} \tag{3.9}$$

where N_{FRB} are the number of FRBs considered in this analysis and $\phi_{FRB}^{90\%}$ is the characteristic neutrino fluence normalised to 100 TeV as defined in equation of the combined neutrino spectrum from the 12 FRBs. The neutrino fluence limit has been computed at the 90% confidence level by estimating the average ANTARES effective area over the 12 FRB events for the different spectral models :

$$\phi_{FRB}^{90\%} = \frac{2.3 \cdot E_0^{-\gamma+2}}{\int \langle A_{eff}(E_\nu) \rangle \cdot E_\nu^{-\gamma} \cdot dE_\nu} \quad \text{GeV} \cdot \text{cm}^{-2} \tag{3.10}$$

According to the ANTARES upper limit on the individual neutrino fluxes from the 12 selected FRBs and assuming the last updated estimate on the all-sky FRB rate $R_{FRB} \sim 1.7 \cdot 10^3$ day^{-1} [148], one can obtain the upper limits on the quasi diffuse flux normalised to $E_0 = 100$ TeV, $E_\nu^2 \phi_0^{90\%} < 0.9$, 2.0 and $0.7 \cdot 10^{-4}$ GeV $\cdot$ cm^{-2} $\cdot$ s^{-1} $\cdot$ sr^{-1} for $E^{-1.0}$, $E^{-2.0}$ and $E^{-2.5}$ neutrino spectra respectively.

The neutrino diffuse flux observed by the IceCube Collaboration for $E_\nu > 60$ TeV is at the level of $E_\nu^2 \Phi_0 \sim 10^{-8}$ GeV $\cdot$ cm^{-2} $\cdot$ s^{-1} $\cdot$ sr^{-1} normalised to $E_0 = 100$ TeV and with $\gamma = 2.46$ [18, 23]. In the present analysis, the derived upper limit on the diffuse flux for FRBs with $\gamma = 2.5$ is above the signal measured by IceCube by a factor $\sim$ 7300. This result is in agreement with the possibility that FRBs may originate from a wide variety of astrophysical progenitors with a few of them leading to hadronic processes in their environment. In addition, according to the FRB rate mentioned above and the fact that on average one cosmic neutrino with $E_\nu > 60$ TeV is detected every 20 days by IceCube [18, 23], it appears that finally less than 1 over $\sim$ 20000 FRB could be a detectable neutrino emitter. Nevertheless,

according to the IceCube analysis, the number of cosmic neutrinos at lower energy is one or two orders of magnitude larger than those with $E_\nu > 60$ TeV, depending on the spectral index of the cosmic signal and the low-energy cutoff. These cosmic neutrinos at energies below 60 TeV are hidden in the IceCube data set in the much larger sample of atmospheric neutrinos. The possibility to observe a temporal and spatial coincidence allows for a significant suppression of this background. In this paper, a selection method is presented and guarantees the 3σ significance based on the observation of one coincident event. If the IceCube cosmic neutrino diffuse flux is totally produced by the mechanism that induces FRBs, accounting for the neutrinos below 60 TeV, the number of neutrinos per FRB can increase by to two orders of magnitude. This means that searches for neutrinos with IceCube or ANTARES in coincidence with hundreds of FRBs could significantly constrain such a scenario. Alternatively, the non detection of a neutrino signal from FRBs could be also due to non-hadronic production mechanisms in the FRB environment, or to the presence of a beamed jet of neutrinos.

3.2.4 Perspectives

Since this analysis, the number of detected fast radio bursts has increased drastically, a few hundred of bursts have been observed by the most recent radio telescopes : UTMOST [168], ASKAP [169], CHIME [170], FAST [171], DSA [172]. The FRB catalogue includes 116 bursts [103], but many more have been detected and are not yet published. Using the dispersion measurements, it indicates that the bursts occur at cosmological distance [135, 172, 173]. Only a for few of them, the properties of the host galaxy have been estimated. The galaxy colors and star formation rates of the host galaxies show a great diversity of properties [120, 174]. The studies of their properties are a key element to infer the origin of the FRB population.

Before the discovery of FRB 200428, all localized FRBs were from cosmological distances. Even with the very precise localizations of the few events in their host galaxies, the origin of the progenitors of FRBs and by what process the powerful radio emission is generated are still not understood. They fall into two general categories : emission within the magnetosphere of a neutron star, and emission from a relativistic outflow which interacts with the surrounding medium at large distances from the NS or black hole. The detection of the FRB 200428 in radio and X-ray is therefore an unexpected and very interesting burst with a clear association with the magnetar SGR 1935+2154 [138, 139, 140, 141, 142]. But this FRB has very peculiar properties, such as a factor ~ 10 less energetic than the weakest FRB previously detected [141, 142].

Using the online ANTARES data, we have searched for a neutrino counterpart

to this FRB 200428 (ATel # 13721) : no up-going muon neutrino has been found in a time window of ± 1 h around the time of the trigger from the CHIME/FRB observed radio burst (14 :34 :33 UTC). At this time, the source was located 19 degrees below the horizon for ANTARES, and remained visible over the whole ± 1 h time window. A search over an extended time window of ± 1 day has also yielded no detection (38 % visibility). IceCube has also quickly searched in ± 1 day without finding coincidence (ATel # 13699).

No neutrino model from FRBs has been developed in the community. However, applying model already implemented for specific sources, we have seen that the expected number of neutrinos is quite small for an individual standard burst. But, because of their high rate in the Universe, the signal from the whole population may still be detectable as a diffuse neutrino flux. With the increased statistic these last two years, this will allow to further constrain the FRB population as a significant neutrino sources. This analysis needs at least few hundred of bursts to put relevant constrain. We are planing to update the ANTARES stacking analysis in the near future. Even better with KM3NeT, we should get much better performances and sensitivities together with a very large FRB statistic.

3.3 Analysis group and publications

Most of these analyses have been performed with the help of two PhD students Agustin Sanchez-Losa [2012-2015] and D. Turpin [2014-2016].

Up to now, there are 9 main publications (2 of them outside the ANTARES Collaboration) :

— Search for high-energy neutrinos from bright GRBs with ANTARES, A. Albert et al., ANTARES Collaboration, MNRAS 469 (2017) 906-915
— Investigating the impact of optical selection effects on observed rest frame prompt GRB properties, D. Turpin et al., Astrophys. J 831 (2016) 1-28
— The SUrvey for Pulsars and Extragalactic Radio Bursts II : New FRB discoveries and their follow-up, S. Bhandari et al., ANTARES Collaboration, MNRAS 475 (2018) 1427–1446
— Search for high-energy neutrinos in coincidence with Fast Radio Bursts with the ANTARES neutrino telescope, A. Albert et al., ANTARES Collaboration, MNRAS 482 (2018) 184–193
— A polarized fast radio burst at low Galactic latitude, E. Petroff et al., ANTARES Collaboration, MNRAS 469 (4) (2017) 4465
— Search for Neutrino Emission from Gamma-Ray Flaring Blazars with the ANTARES Telescope, S. Adrián-Martinez et al., ANTARES Collaboration, Astropart. Phys. 36 (2012) 204-210.

— Search for muon neutrino emission from GeV and TeV gamma-ray flaring blazars using five years of data of the ANTARES telescope, S. Adrian-Martinez et al., ANTARES Collaboration, J. Cosmol. Astropart. P 1512 (2015) 014
— Time-dependent search for neutrino emission from x-ray binaries with the ANTARES telescope, A. Albert et al., ANTARES Collaboration, J. Cosmol. Astropart. P 1704 (2017) 019
— A jet model for the fast IR variability of the black hole X-ray binary GX 339-4, Julien Malzac et al, MNRAS 48 (2018) 2054-2071.

4 TAToO : real-time follow-up of ANTARES neutrino alerts

In this context, multi-messenger approaches consisting in simultaneously looking for the same sources with both neutrino telescopes, gravitational wave interferometers and/or multi-wavelength facilities constitute a privileged way of locating high-energy neutrino and cosmic ray sources and thus further understanding the acceleration mechanisms at play in these sources. An alert system, dubbed TAToO (Telescopes-Antares Target of Opportunity), has been operating since 2009 [175], sending regular alerts to our electromagnetic partners. This approach has the advantage that it does not require an *a priori* hypothesis on the nature of the underlying neutrino source. It particularly targets transient sources such as GRBs, core-collapse SNe, flares of AGNs. It relies on the hypothesis that these astrophysics phenomena produce high-energy neutrino and electromagnetic radiations over the whole energy range. The search for the EM counterpart is versatile enough to include very short transients such as the GRB afterglow and more extended emission as in supernova or flares of AGNs. It is particularly interesting to note that during the flare of TXS0506, MASTER has also detected significant variations in the optical light-curve of this blazar [176]. A similar program is also in operation in IceCube [177, 178].

The project started only with the follow-up by small robotic telescopes of TAROT [179] and ROTSE [180]. The follow-up network has been regularly complete with additional robotic telescopes of ZADKO [181], MASTER [182] and the SVOM Chinese ground telescopes [183]. In 2013, ANTARES has signed a Memorandum of Understanding (MoU) with the X-ray telescopes of the Neil Gehrels Swift Observatory [184, 185] and later to INTEGRAL [186], the radio telescope Murchison Wide-field Array [187, 188] and the very high energy H.E.S.S. gamma-ray facility [189]. As its data are private, the ANTARES Collaboration has signed a MoU with each partner to fix the rules of data exchanges and the publication and communication of the joint results. During more than ten years of operations, we have built a very strong collaboration with our partners who followed a larger number of ANTARES neutrino alerts. This program is clearly a proof of the mutual benefits to look for the same sources at the same time with different messengers. The rapid provision of alerts for interesting neutrino events will enable both ground and space based observatories to quickly point at the direction of the alert. This fast follow-up is vital to catch and characterise any multi-messenger and multi-wavelength

counterparts of these cataclysmic and short-lived phenomena. By combining the information provided by the ANTARES neutrino telescope with information coming from other observatories, the probability of detecting a source is enhanced, allowing the possibility of identifying a neutrino progenitor from a single detected event. The gain can be as large as a factor 5 compared to a steady point-like source analysis.

4.1 Alert sending system

In parallel of the standard acquisition chain, a fast and robust online algorithm reconstructs all incoming events in nearly real time [190]. This algorithm is fast enough to reconstruct all the events without delay. A pre-selection is made based on the results of this fast reconstruction (zenith and quality cuts) to reduce the rate of events (from ~ 3 Hz to ~ 0.01 Hz). The remaining sample of events is then sent to a more accurate reconstruction algorithm [64], which improves the angular resolution of each event in less than 5 s. In the online framework, both algorithms use an idealised geometry of the detector that does not take into account the dynamical positioning of the optical modules due to sea current variations. For high-energy tracks, this leads to a median angular resolution of $\sim 0.4°$. However, if the sea current is too important, the line deformations are such that the reconstruction algorithm is not working properly and therefore the reconstructed direction can not be used anymore for the alert sending. This happens typically when the sea-current is above 10 cm/s. The on-line data taking conditions are very stable with a high duty cycle around 94 % since 2012 (Figure 2.12).

From the remaining atmospheric neutrino sample, the selection of the neutrino candidates with an increased probability to be of cosmic origin is performed using the zenith direction (only up-going events), the track reconstruction quality and the number of hits and its total amplitudes selected by the reconstruction. These two last parameters are used as an energy estimator. Currently, four online neutrino trigger criteria are implemented in the TAToO alert system [175, 191] :

- High energy (HE) trigger : the detection of a single high energy neutrino with a rate of ~ 1 per month. The typical energy of the events is > 5 TeV.
- Very high energy (VHE) trigger : the detection of a single very high energy neutrino with a mean energy > 30 TeV. This sub-sample of the HE trigger has a typical rate of 3-5 events per year.
- Directional : the detection of a single neutrino for which the direction points toward ($< 0.4°$) a local galaxy (< 20 Mpc) in the GWGC catalogue [192]. This trigger was mainly introduced to enhance the chance to detect a local CCSN. The typical rate is about 1 per month.
- Doublet trigger : the detection of at least two neutrinos coming from similar directions ($< 3°$) within a predefined time window (15 min).

Until now, no doublet trigger has been sent to the network. Figure 4.1 shows the distribution of the number of hits and the total amplitude of these hits for the 3 first trigger types. Based on these two variables, a p-value to be a very high energy event is built. The trigger conditions are inspired by the features expected from astrophysical sources and are tuned to comply with the alert rate to be sent to the telescope network. An agreement between ANTARES and the optical telescope collaborations allows a rate of around 25 alerts per year to be sent to each optical telescope, while an agreement to send 6 alerts per year to the Swift satellite have been accepted. Due to this reduced rate, only the VHE sample is sent to MWA, Swift, INTEGRAL and H.E.S.S. observatories.

The TAToO alert system is able to send alerts within a few seconds (6-7 s) after the neutrino detection with an angular resolution at around $\sim 0.5°$. Figure 4.2 displays the distribution of the delays between the time of the neutrinos and the time of the associated alert message. Figure 4.3 shows the estimate of the point spread function for a typical high-energy neutrino alert, compared to the fields of view of TAROT/ROTSE and Swift/XRT telescopes.

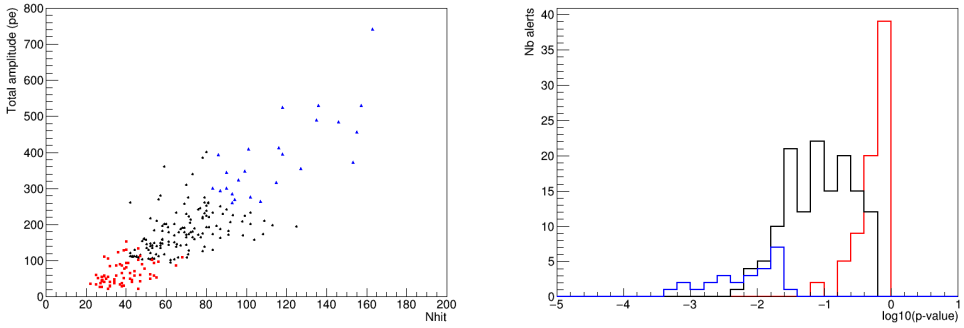

FIGURE 4.1 – (Left) Distribution of the number of hits and the associated total amplitude of these hits for 2011-2018 alerts. The 3 colors correspond to the selection of events for each trigger : red points for Directional, black and blue points for the HE and VHE sample, respectively. (Right) Distribution of the p-values to be a VHE neutrino event for the types of triggers for 2011-2018 alerts.

The TAToO Run Control (RC) is a stand-alone Qt control application developed at CPPM by M. Ageron, which channels the triggers generated by the alert application to the EM telescope network [175]. Figure 4.4 shows the control window of the TAToO RC. The connections to this network are checked periodically and automatic reconnection is performed, resulting in a fully autonomous and stable system. A veto prevents an alert to be sent if the ANTARES event counting rate exceeds a given threshold. In addition, if the alert criteria are fulfilled soon after a previous alert has already been issued, the new alert is stored in a FIFO and sent only after a certain period of time. This time lag, currently set at one hour, is used

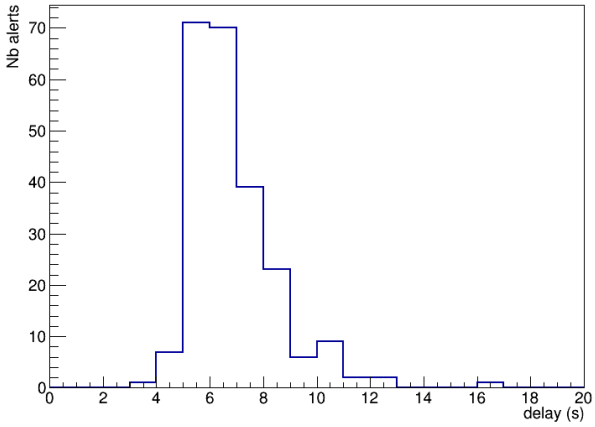

FIGURE 4.2 – Distribution of the delays for 2011-2019 alerts between the time of the neutrino and the corresponding alert sending.

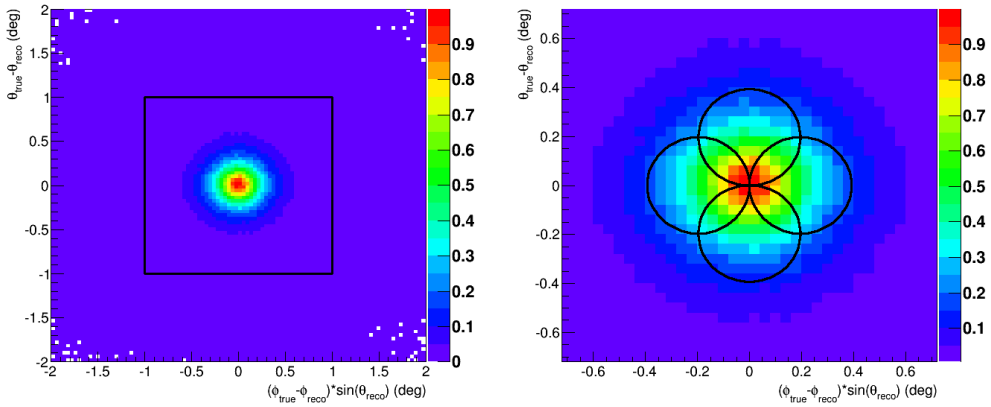

FIGURE 4.3 – Bi-dimensional angular resolution for a typical high-energy neutrino alert (right : zoom of the center). The black square and circle correspond to the TAROT/ROTSE telescope and Swift/XRT fields of view, respectively.

to avoid alert pileup in the optical telescope network. Manual alerts can also be generated and sent. All alerts are sent using the Gamma-ray bursts Coordinates Network (GCN) [193] normalized format and using the standard VO Event format (XML file [194]). Information about the event that triggered the alert, i.e. a unique identifier, the time and the celestial coordinates, the event p-value are sent to our partners at the time of the alert.

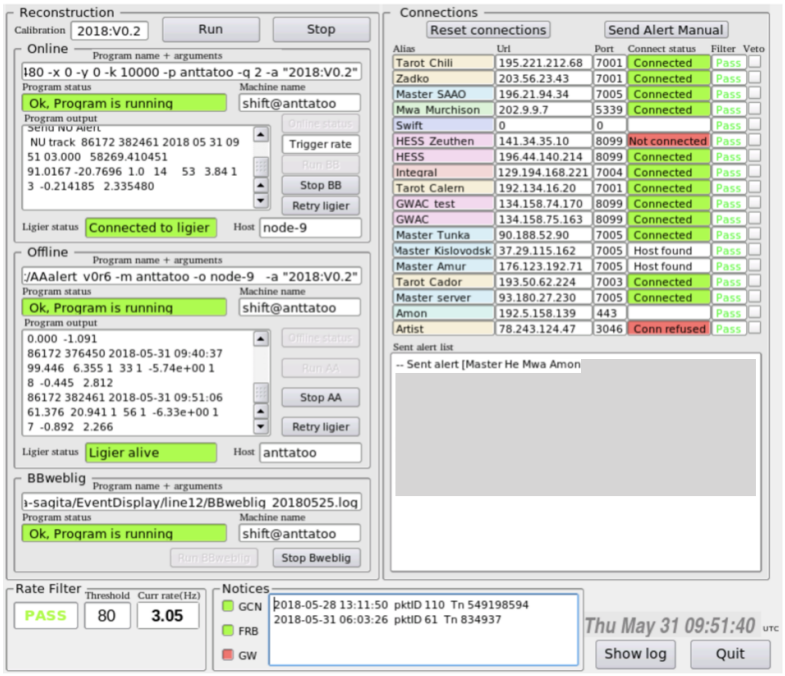

FIGURE 4.4 – Run control application of TAToO.

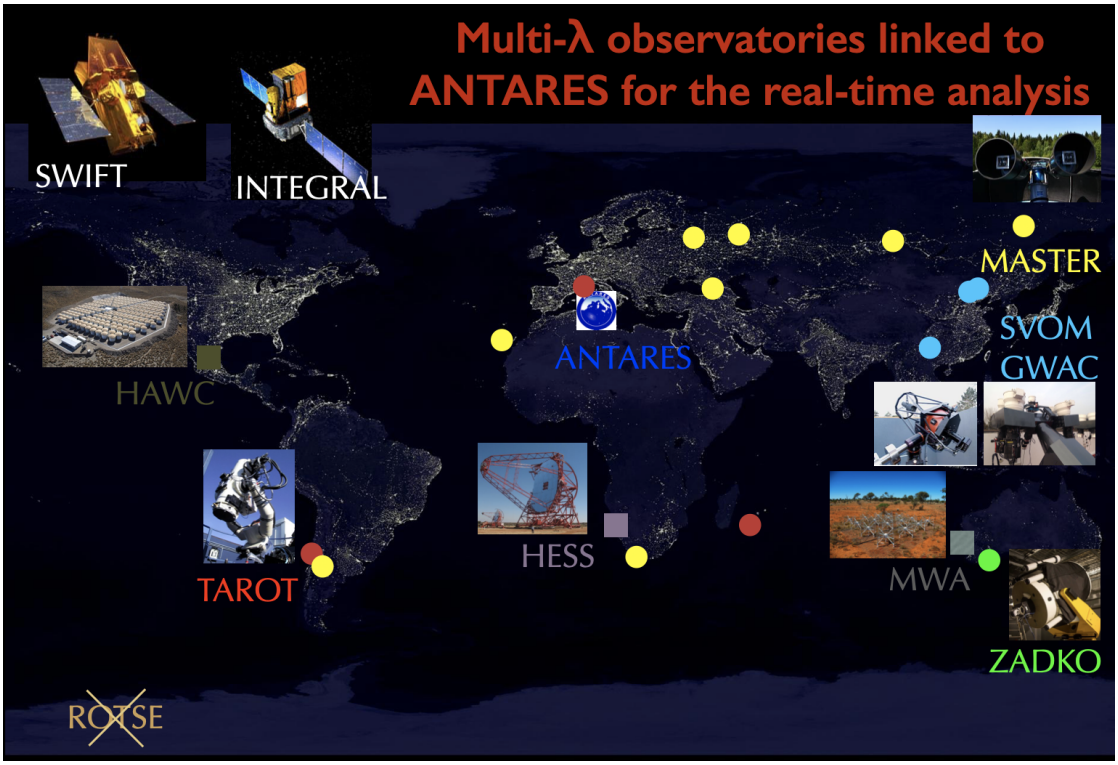

FIGURE 4.5 – Skymap illustrating the different EM partners.

4.2 EM follow-up of neutrino alerts

The multi-wavelength follow-up of ANTARES neutrino alerts is performed by the different partners illustrated in Figure 4.5. The follow-up of the ANTARES alerts has started with the robotic telescopes of TAROT and ROTSE in 2009. Their wide fields of view and their fast responses (images can be taken within less than 20 s after the neutrino detection) are well suited to the search for transient sources. TAROT [179] is a network of two identical 0.25 m telescopes with a field of view (FoV) of about 1.86°×1.86°, located in Calern (France) and La Silla (Chile). Zadko is a 1 meter telescope located at the Gingin observatory in Western Australia [181]. As its FoV is about 0.15 square degrees, seven tiles are needed to cover the ANTARES point spread function. The MASTER network [182] is composed of 7 telescopes located in Russia, Canary Islands (IAC), Argentina (OAFA) and in South Africa (SAAO), and consist on each site of one pair of tubes with a diameter of 0.40 m covering a field of view of up to 8 square degrees. Until the end of 2014, the network also comprises the four optical telescopes ROTSE [180], which have progressively stopped their activity. ROTSE telescopes had similar properties as TAROT ones. These telescopes reach a limiting magnitude of about 19-20.5 mag depending on their diameters. In 2017, the follow-up has been extended to the SVOM/GWAC [183] telescopes located in China, providing a very large FoV (about 40°) but with a not very deep sensitivity (about 15 mag). Figure 4.6 shows the probability to follow promptly an ANTARES alert as a function of the location of a given telescope in the world. This probability takes into account the field of view of ANTARES alerts, the observing conditions of the telescopes (night with no bright moon and elevation greater than 7°). Of course, we see that the antipode of ANTARES location has the best efficiency, but even telescopes in the Northern hemisphere have a significant chance to observe promptly the directions of the alerts. For each alert, the optical observation strategy is composed of an early follow-up (within 24 hours after the neutrino detection), to search for fast transient sources such as GRB afterglows, complemented by several observations during the two following months, to detect for example the rising light curves of CCSN or a flare of AGNs. Each observation is composed of series of optical images (with clear filter). Optical images are analyzed with dedicated pipelines based on the image subtraction method to look for new transient sources. This analysis strategy has been implemented by us for ROTSE and TAROT images.

The Swift satellite with its X-ray Telescope (XRT [185]) provides a unique opportunity to observe X-ray counterparts to neutrino triggers [191]. As explained in the Section 2, X-ray data are very important to identify neutrino sources. The detection sensitivity of the XRT is about 5×10^{-13} erg cm^{-2}s^{-1} in 1 ks exposure in an energy band from 0.3 to 10 keV [195]. Due to the small FoV of the XRT (radius of ∼0.2°) and the typical error radius of an ANTARES alert (∼0.4°), each observation of a neutrino trigger is composed of 4 tiles of 2 ks each. This mapping covers about 50%

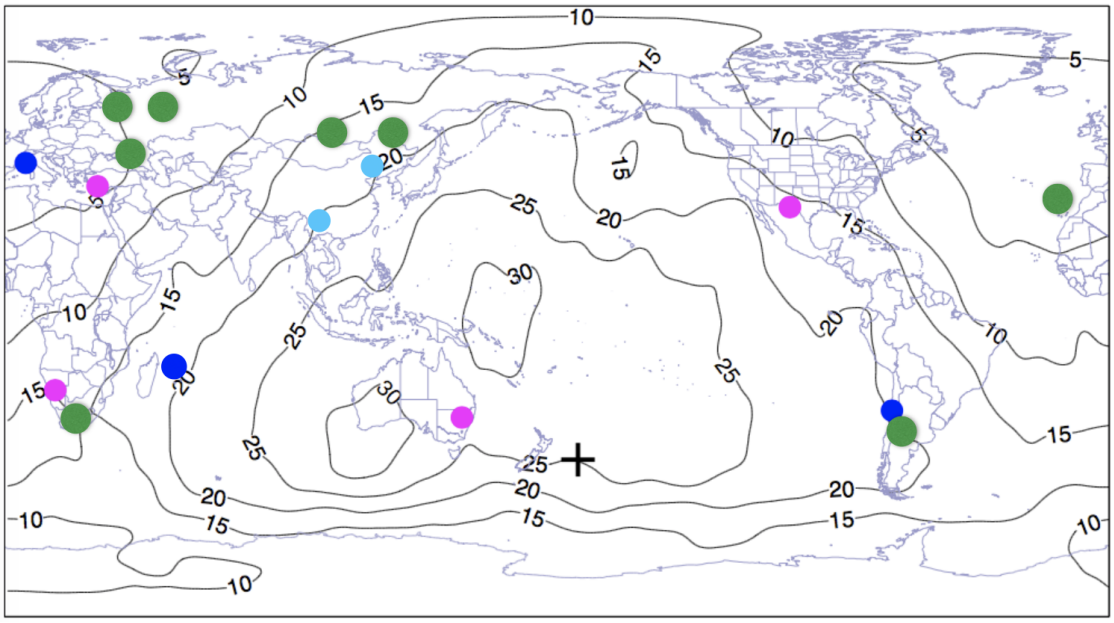

FIGURE 4.6 – Follow-up efficiency of the ANTARES alerts as a function of the location of a given telescope. The dots represent the positions of MASTER (green), ROTSE (pink), TAROT (blue) and SVOM ground telescopes (cyan). (A. Klotz)

of the ANTARES point spread function for a high-energy neutrino. This choice was a compromise between the size of the covered region and the sensitivity of the search. The observation strategy is composed of an automatic response to the neutrino trigger with observations starting as soon as possible. There is an online analysis of the data [195, 196] and in the case where an interesting candidate to be the counterpart is found, further observations are scheduled.

In the recent years, INTEGRAL [186] has been added to the follow-up network. The follow-up will be performed by the four on-board instruments SPI, IBIS, JEM-X and OMC telescopes with a very wide field of view (30°×30°). On receipt of the neutrino alert by INTEGRAL, the following observing strategy is applied :

— If the event is in the main telescopes (SPI and IBIS) FOV, a direct search for a possible counterpart will be done with the telescope images. If it is in their FOV, a search in images produced by JEM-X and OMC will also be done. If the event is sufficiently strong, the INTEGRAL/ANTARES follow-up team will propose a follow-up ToO.

— If the event is detected off-axis and sufficiently strong, then a member of the INTEGRAL/ANTARES follow-up team will propose a ToO requesting an INTEGRAL repointing to make a follow-up of this source. Then, the direct search and spectral analysis of the counterpart will be done by IBIS, SPI, JEM-X and OMC.

— In any case, if the event is not detected, upper limits will be produced from IBIS, SPI and JEM-X data.

In the last few years, follow-up observations of a sub-sample of neutrino alerts are also performed by the Murchinson Wide Field Array (MWA [187, 188]) which is the low frequency (80 - 300 MHz) precursor of the Square Kilometre Array. Its fast repointing and its huge field of view (700 square degrees at 150 MHz) is particularly valuable for follow-up of neutrino candidates, which have rather large position uncertainties. The MWA angular resolution is of order one arc minute, allowing good localisation of transient radio sources. At the low radio frequencies of the MWA, the dispersion delay means that the MWA can be repointed before the low frequency radio waves arrive at the telescope, making the MWA unique for the follow-up of prompt electromagnetic emission from ANTARES events.

A few alerts have also triggered observations by the H.E.S.S. imaging atmospheric Cherenkov telescope located in Namibia. H.E.S.S. has a typical energy threshold of 100 GeV and a large field of view of around 5° [189]. H.E.S.S. telescopes are located at an elevation of 1800 m above sea level on the Khomas Highland plateau of Namibia (23°16' S, 16°30' E). The original array, inaugurated in 2004, is composed of four 12 m-diameter telescopes. In 2012, a fifth telescope with a 28 m diameter mirror was commissioned.

4.3 Main results

High-energy neutrinos are thought to be produced in several kinds of astrophysical sources, such as the gamma-ray bursts, core-collapse supernovae or active galactic nuclei. Most of these sources are also transient events covering a large range in the time domain, from seconds for GRB to weeks for CCSN or AGN. Between mid 2009 and December 2019, a total of 322 alerts have been sent to robotic telescopes. Figure 4.7 shows the directions of the TAToO alerts. At the first order, the alerts are isotropically distributed, showing that the alerts are mainly coming from atmospheric origin. 26 targets of opportunity have been sent to Swift since mid-2013. The typical follow-up efficiency is around 70 % for the network of robotic telescopes and for the Swift satellite.

4.3.1 Results of the prompt follow-ups

From the 322 sent alerts, 218 triggers with early optical follow-up ($<$ 24 h after the neutrino time) have been analyzed (68% of the sent alerts). Among them, 55 have a delay lower than 1 min (18 %). Figure 4.8 shows the delay between the first image of the follow-up performed by the robotic telescopes of TAROT and MASTER and the time of the neutrino. The minimum delay is 17 s, this includes the time of the alert sending, the transmission of the alert, its reception at the

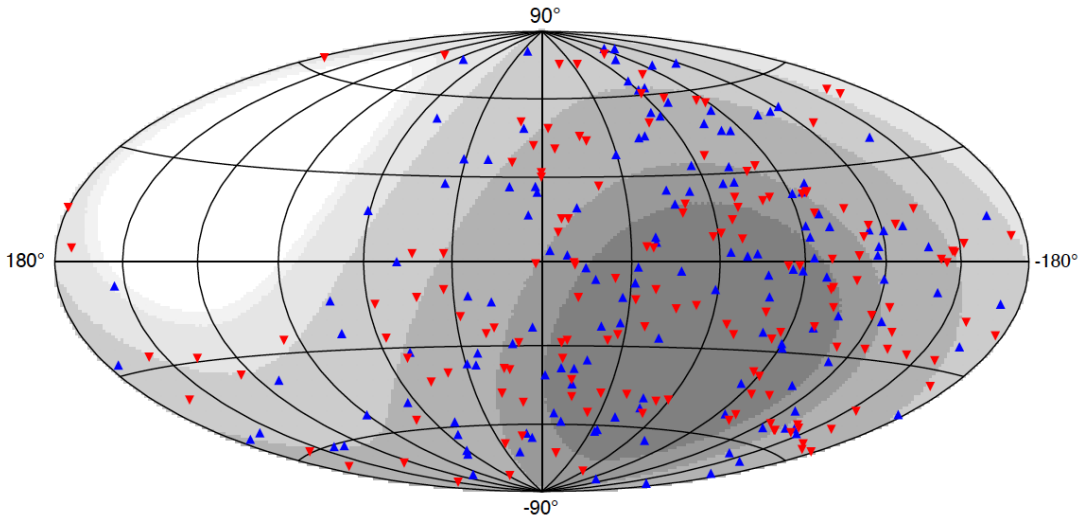

FIGURE 4.7 – Skymap in galactic coordinates showing the directions of all the TAToO alerts (red and blue dots correspond to alerts with early follow-up and with only late follow-up, respectively).

telescope site, the stop of the on-going acquisition, the pointing of the telescope and the start of a new image. The first bump at a few tens of seconds corresponds to the alerts immediately observable.

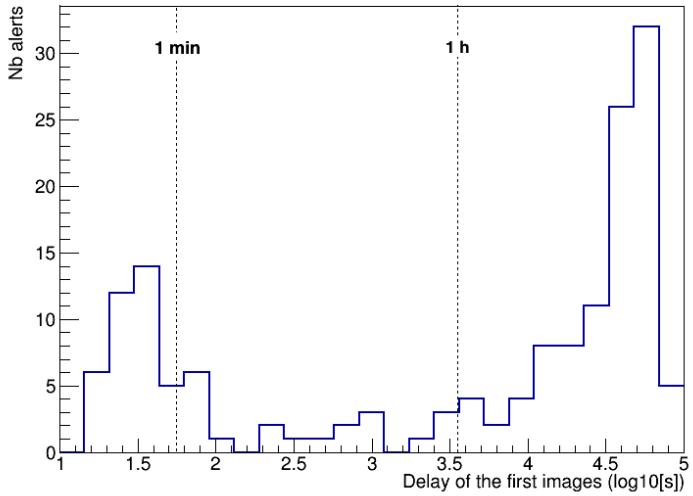

FIGURE 4.8 – Delay between the earliest images of the follow-up and the time of the neutrino for all the ANTARES alerts from 2011 and 2020.

No clear optical transient counterparts were found and upper limits on the R-band magnitude of a transient astrophysical source have been derived [191]. These

limits correspond to the limiting magnitude of images, which is the faintest signal that can be detected. As we are looking for rapidly-fading sources, the signal is supposed to be more important in the first image of the observation, so the upper limits are the limiting magnitude of each first image computed at 5 s and corrected for Galactic extinction [197]. For example, Table 4.1 summarises the characteristics of the optical follow-up with these telescopes for the VHE neutrino alerts. By comparing these upper limits with optical afterglow light curves of gamma-ray bursts (Figure 4.9), it becomes possible to reject a GRB association with each neutrino alert, in particular when the optical follow-up is performed within a few minutes after the neutrino trigger.

TABLE 4.1 – Main results of the optical follow-up by MASTER and TAROT telescopes for the VHE neutrino triggers.

Trigger Id	Telescope	Delay (s)	Exposure (ks)	M_{Lim}	Galactic extinction	Optical transient
ANT130915A	TAROT Chili	328893	180	18.1	0.09	0
ANT130927A	TAROT Chili	227552	180	17.8	0.36	0
ANT140123A	TAROT Calern	48025	180	17.8	1.35	0
ANT140311A	TAROT Calern	139294	180	18.8	0.07	0
ANT141220A	TAROT Chili	131438	180	18.8	0.03	0
ANT150109A	/	/	/	/	/	/
ANT150409A	Master SAAO	36	60	18.6	0.1	0
ANT150422A	Master Tunka	127871	60	17.3	1.3	0
ANT150809A	/	/	/	/	/	/
ANT150901A	Master SAAO	35217	60	20.1	1.9	0
ANT151027A	Master Tunka	120181	60	18.2	0.2	0
ANT151106A	Master SAAO	617926	60	19.4	0.2	0
ANT160227A	Master Bla	36	60	16.0	0.7	0
ANT160320A	Master SAAO	1840695	60	18.6	0.1	0
ANT160524A	Master SAAO	49446	60	18.7	0.3	0
ANT170401A	Master SAAO	31174	60	17.5	2.1	0
ANT170811A	Master OAFA	731191	60	18.4	1.5	0
ANT170902A	/	/	/	/	/	/
ANT180327A	Master SAAO	31584	60	16.6	1.0	0
ANT180725A	Master OAFA	10957	60	16.1	12.4	0
ANT180917A	Master OAFA	948	60	18.21	0.05	0
ANT190410A	Master OAFA	33269	60	15.5	0.03	0
ANT190428A	Master OAFA	42447	60	15.3	0.19	0
ANT191126A	Master Tunka	43	60	18.6	0.21	0
ANT191231A	Master SAAO	13598	60	17.6	0.07	0
ANT200108A	Master Amur	31	60	15.2	0.09	0

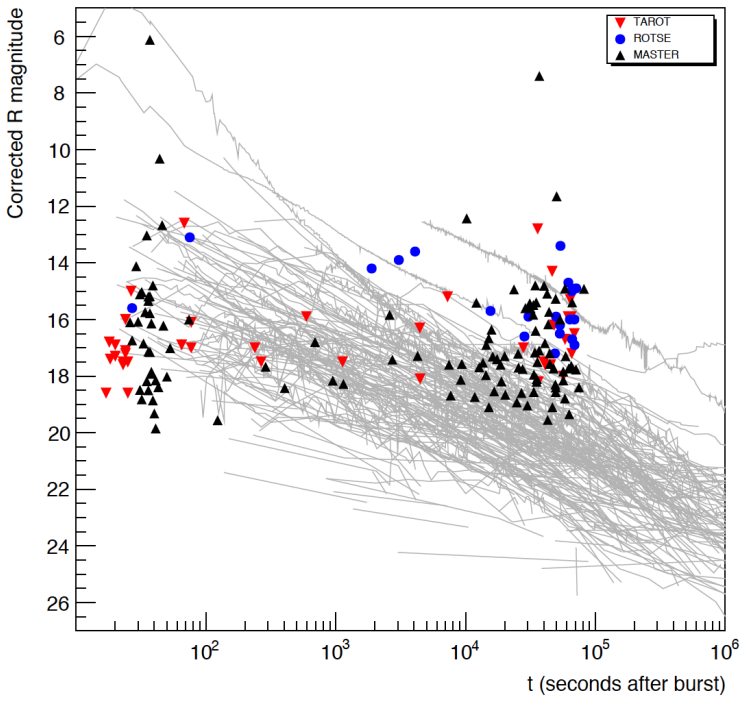

FIGURE 4.9 – Comparison between archived optical light-curves for 301 GRBs detected during the 1997-2014 period and the upper limits obtained for the 208 neutrino alerts during the 2009-2019 period. Red, blue and black markers indicate upper limits on GRB afterglow magnitudes for neutrino alerts observed by TAROT, ROTSE and MASTER respectively.

A similar analysis has been carried out with Swift-XRT follow-ups of 19 ANTARES alerts [191] (Figure 4.10). The average delay of the first Swift observation is around 8 h with a minimum delay of 1.1 h. The probability to reject the GRB hypothesis reaches more than about 50% if the X-ray follow-up occurs within few hours after the trigger (mainly dominated by the limited coverage of the ANTARES PSF with the 4 tiles). Table 4.2 summarises the observing conditions of the X-ray follow-up.

4.3.2 Multi-wavelength follow-up of ANT150901

In the X-ray follow-up, only for one alert, there is a bright and transient counterpart candidate. The neutrino ANT150901A has an energy of 87 TeV with 1 sigma range of 24 - 316 TeV. Assuming the IceCube cosmic diffuse flux as reference, the signalness is 0.08.

Observations with XRT started in September, 1st, 2015 at 16 :38 :42 UT (namely 9 hours after the neutrino trigger). In the first observations, 8 sources have been

TABLE 4.2 – Observing conditions of the XRT and results of the follow-up for the VHE alerts.

Trigger Id	Delay (ks)	Nfield	Exposure (ks)	New sources (Total sources)	Count. cand.	Flux limit ($erg.cm^{-2}.s^{-1}$)
ANT130722A	4117	4	7.3	4 (5)	0	2.74
ANT130915A	23418	4	5.45	2 (2)	0	3.67
ANT130927A	18416	4	7.1	3 (4)	0	2.82
ANT140123A	13267	4	3.5	1 (1)	0	5.73
ANT140311A	10142	3	5.5	3 (3)	0	2.73
ANT141220A	5260	4	7.6	2 (2)	0	2.63
ANT150129A	6244	4	7.5	3 (3)	0	2.74
ANT150409A	45882	4	7.3	5 (5)	0	2.74
ANT150809A	55636	4	7.0	2 (2)	0	2.86
ANT150901A	32411	5	7.1	4 (8)	1	2. 82
ANT160227A	6483	4	2.34	0 (0)	0	8.53
ANT170401A	8344	4	7.4	1 (1)	0	2.70
ANT170811A	67025	4	6.9	2 (3)	0	2.90
ANT180327A	10765	4	7.6	7 (9)	0	2.63
ANT180725A	22901	4	7.6	3 (5)	0	2.63
ANT180917A	15014	4	3.54	3 (3)	0	5.65
ANT190410A	15780	5	7.2	6 (7)	(1)	2.85
ANT191126A	32786	4	7.0	6 (6)	0	2.87
ANT191231A	15337	5	7.7	10 (10)	0	3.22
ANT200108A	48025	19	2.08	0 (0)	0	45.5
ANT200127A	73856	7	13.1	4 (4)	0	2.63

identified in the field of view, among them 5 are catalogued, 3 uncatalogued sources. From this list, one uncatalogued X-ray source has been detected above the Rosat All-Sky Survey (RASS) limit [199], with the flux varying between 5 10^{-13} and 1.4 10^{-12} erg cm^{-2} s^{-1} at 0.3 - 10 keV at location : RA = 16h26m2.12s and DEC = -27d26m14.8s with an uncertainty of 2.4 arcsec (radius, 90 % containment). This source is located at 6.8 arcmin from the neutrino direction. As the detected X-ray source seems to be variable, A GCN notice (GCN #18231) and an Astronomer's Telegram (Atel #7987) have been published on September 3rd, 2015 to encourage further multi-wavelength and multi-messenger observations to characterize the star identified by MASTER (USNO-B1.00626-0501169) and to test the association between the X-ray flare and this bright star. Further observations with XRT show finally a flare with a typical length of around 2 days (Fig 4.11). 19 multi-wavelength observatories have answered to this trigger covering the full EM spectrum : 1 radio telescope, 11 optical/IR telescopes, 4 X-ray satellites and 4 very high-energy gamma-ray observatories.

In parallel, the optical follow-up by the MASTER telescopes began 9h45 after

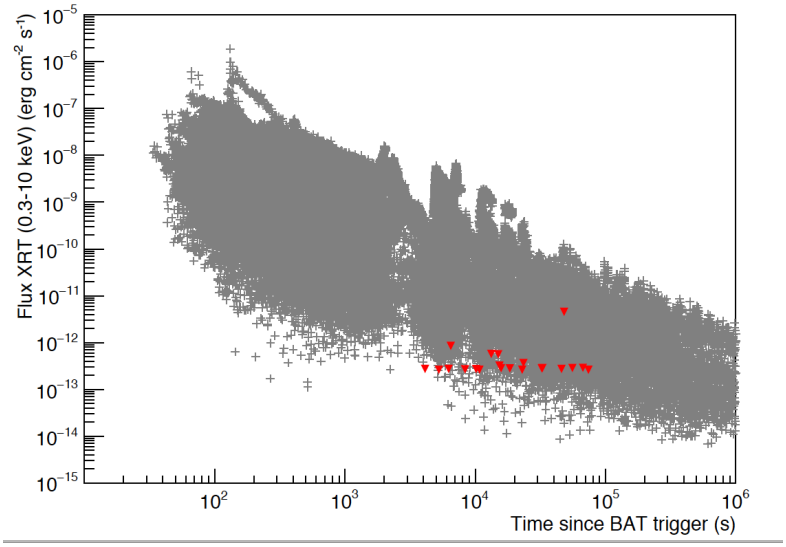

FIGURE 4.10 – Comparison between 979 X-ray light-curves detected in the period 1997-2017 by Swift [198] and the upper limits obtained for the 18 followed neutrino alerts during the 2013-2019 period (red markers).

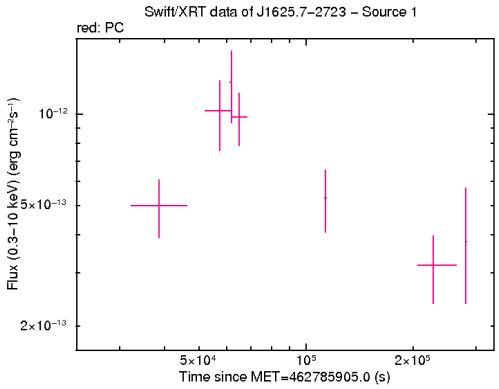

FIGURE 4.11 – Light curve measured by the XRT on board of Swift for the X-ray source identified in the follow-up of ANT150901A.

the neutrino detection while no data from TAROT and ZADKO had been collected. The field of view has been followed since the first day with two telescopes in South Africa and Canarias with the filter R, B, and V. This direction was regularly followed by one of the MASTER telescopes during the 8 successive days. Table 4.1 shows the observing conditions and the results of the follow-up. No obvious optical transient candidate was found in the observations down to a magnitude of 18.67 (60 s exposure). At the position of the X-ray source, MASTER has identified a bright star (USNO-B1.0 0626-0501169) of a magnitude 12.3 with a light curve showing no flux and no color variations just after the time of the alert [atel #8000].

Fig 4.12 illustrates the field of view of MASTER. Close by the ANT150901 neutrino direction, there are the globular cluster M4 at 0.97° and the Antares star (Alpha Scorpii) at 1.2°.

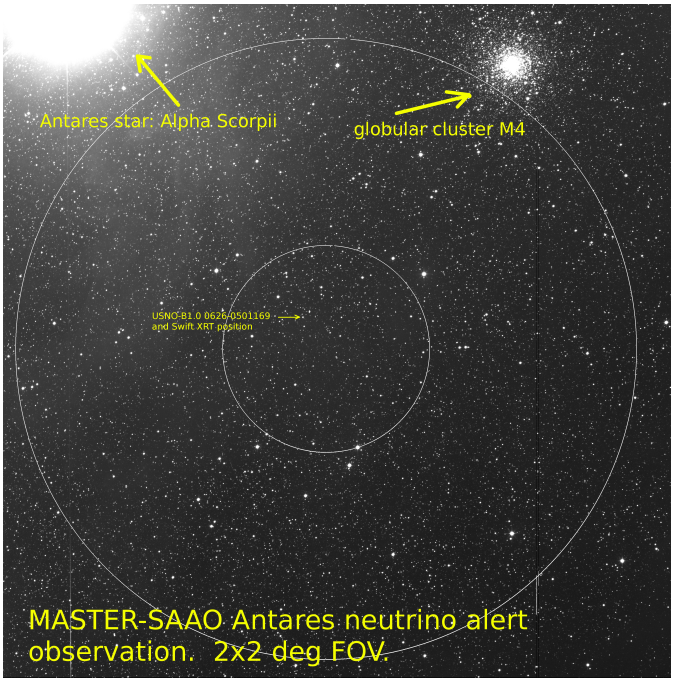

FIGURE 4.12 – Field of view of MASTER corresponding to ANT150901A.

Moreover, there are no detected galaxies within about 5 arc sec of the Swift X-ray source in the Pan-STARRS PS1 catalogue (ATel #8027). The bright star is saturated and there are several faint sources in the vicinity of the point spread function but none looks be extended galaxies. Follow-up data which allowed to constrain the nature of Swift J1625.7-2723 are described in the following sections.

The IceCube Collaboration performed a follow-up analysis and did not find any correlation above 10 TeV during a ±1 day time-window centered on the ANTARES event time (Atel #8097). Fermi/GBM (GCN #18352), INTEGRAL (ATel #7995) and MAXI/GSC (ATel #8003) have performed a high-energy follow-up quickly after the alert message that yielded no high-energy counterpart. A search for a gamma-ray counterpart was performed using the archive Fermi/LAT Pass8 data, applying a standard unbinned likelihood analysis using the LAT analysis tools (v10r0p5). All photons (event class `P8R2_SOURCE_V6`) within a region of interest of 15°-radius were selected within the energy range [100 MeV ; 500 GeV]. All the catalogues-source fluxes were fixed to their catalogued values while the normalization of the Galactic and diffuse isotropic background were left free in the likelihood maximization. Four different time windows were considered in the analysis from ± 6 hours to ± 6 days. No significant counterpart was detected and 95 % confidence-level upper limits on the energy flux have been computed assuming a point source with a fixed spectral

index of $\Gamma = -2.0$. Results are given in Table 4.3.

TABLE 4.3 – Fermi/LAT 95% C.L. upper limits on the energy flux in the 100 MeV to 500 GeV energy range.

Time window	95% C.L. upper limit MeV cm^{-2} s^{-1}
±6 h	2.2 10^{-4}
±12 h	1.5 10^{-4}
±24 h	5.0 10^{-5}
±6 d	7.0 10^{-6}

At very high energies (E>100 GeV), the MAGIC telescopes performed follow-up observations of a ∼3 degree-diameter sky region centered at the proposed X-ray counterpart of the ANTARES-detected neutrino event (ATel #8203). MAGIC observed the source under non-optimal conditions due to the large zenith angle (above 60 degrees), starting from September 3 at 20 :54 UT, 2.5 days after ANTARES detection. Observations were carried out for 6 nights, ending on Sep. 8, and collecting a total on-source exposure of 4 hours. No significant emission from the location of the X-ray source and no other gamma-ray source were detected. The H.E.S.S. telescope follow-up started on September 1st, 2015, at 18 :58 UT as soon as good observation conditions were reached [200]. No source was detected in the field-of-view. Consequently an upper limit on the gamma-ray flux has been derived as $\Phi(E > 320 \text{ GeV}) < 2.4\ 10^{-7}$ m^{-2} s^{-1} (99% C.L.).

Long-term near-infrared (NIR) Ks-band observations of USNO-B1.0 0626-0501169 were performed using the Infra-Red Imaging System (IRIS ; [201]) located at Cerro Armazones (Chile). The analysis was performed by A. Coleiro. The resulting light curve is shown in Figure 4.13 together with the Ks-band magnitude (red point) provided in ATel #8006. A NIR flux enhancement is observed at least until September 10, 2015, while a significant decrease of the flux is seen on September 06. This significant variation of ∼0.11 mag, followed by a decrease of ∼0.15 mag, could be interpreted as a succession of two NIR flares. Unfortunately, no later data prevents a precise constrain on the NIR flux evolution.

Optical and infrared archival data were used to build the spectral energy distribution (SED) of USNO-B1.0 0626-0501169. Although not contemporaneous of each other, those multi-wavelength data are considered as acquired during a similar persistent flux period and any flux variation due to flaring behaviour is considered as smaller than the typical flux uncertainties given in Table 4.14. The SED was then fitted by the Kurucz stellar model (ATLAS9 [202]). The result is shown in Figure 4.14. The best fit gives A_V=1.405±0.0376, T_{eff}=4750±125 K, log(g)=4.50±0.59, an age of 19Myrs, a mass of 1.5 Msun and a radius = 1.1 Rsun. Those parameters are consistent with both a G-K star and a RS CVn primary component. Others multi-wavelength observations by NOT (ATel #7994), by SAAO (ATel #7993), by

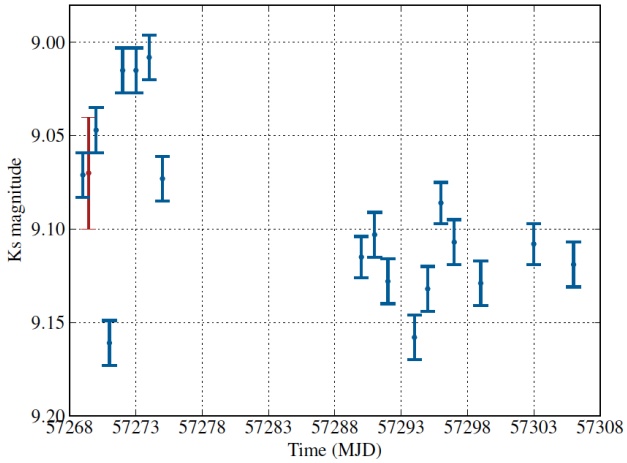

FIGURE 4.13 – Near infrared light curve of USNO-B1.0 0626-0501169 (Ks-band) starting ∼2 days after the ANTARES trigger (red point : ATel #8006.). The grey points correspond to a reference star.

CAHA (ATel #7998), by Wifes on the ANU telescope (ATel #7996) and in radio (VLA Jansky ATel #7999 and #8034) confirm this source origin.

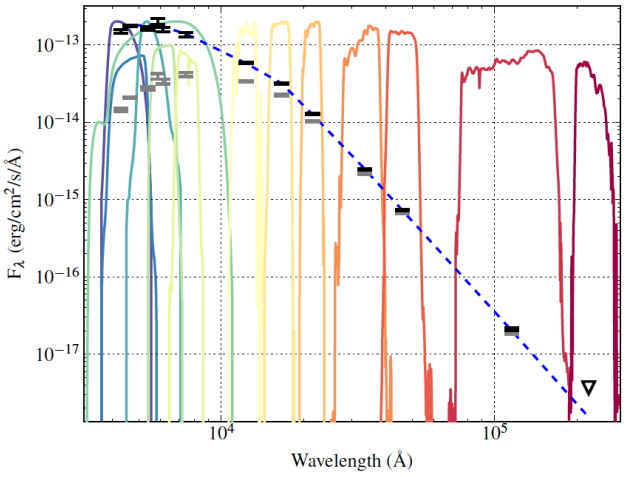

FIGURE 4.14 – Spectral energy distribution (black dots) and Kurucz stellar model fit (dash blue). The different bands are represented in color.

These observations point to USNO-B1.0 0626-0501169 being a young accreting G-K star or a binary system of chromospheric active stars (RS CVn), undergoing a flaring episode that produced the X-ray emission. Therefore, this source seems not to be the origin of the bright ANT150901A neutrino with a probability of 3 % of chance association. This probability has been computed taking into account the

large-scale spatial distribution of X-ray active stars to estimate the average number of active stars in a given direction using ROSAT and Swift catalogs, the flaring rate (proportion of time spent in an active state) and the position and the error region of the neutrino ANT150901.

4.3.3 Results of the long term follow-ups

The two main sources that we are looking in the long-term follow-up are the core-collapse supernova (rising light-curve in the following weeks) and the flares of AGNs. Among the 322 sent alerts, 224 have sufficiently good optical long-term follow-ups, i.e. at least 3 (2) nights of observation for TAROT (MASTER) network. Among these 224 alerts, 77 are triggered by the directional trigger and 153 by the single HE/VHE triggers. No significant slowly varying transient optical counterparts were found in association with a neutrino trigger. The expected number of accidental SN detections, i.e. a SN detection in coincidence with a background neutrino event, is estimated to be 0.4 in the 224 alerts assuming a rate of 1 SN per year within a sphere of 10 Mpc (i.e. 2.4×10^{-4} yr^{-1} Mpc^{-3}). This result is consistent with this small expectation SN number with a probability of $\sim$0.7. Note that there are some SN detected in the fields of view of the alerts but there are not compatible in time.

4.3.4 Test of the blazar origin with Fermi/LAT data

As described earlier, the TAToO neutrino sample represents a good sample to look for correlation with HE gamma-ray sources, in particular for the HE and VHE trigger samples. In regards to the recent IceCube and ANTARES possible association with blazars, it has also been tested with the TAToO sample. For each neutrino alert, we have looked at the Fermi catalogues (4FGL [203] and the previous versions) for the detected sources in a 2-degres cone around the direction of the alert (2° corresponds to 90 % of the ANTARES PSF). For the sources classified as blazar (FSRQ, BLL, BCU), we have used the FAVA tools to look for possible coincidence with gamma-ray flares at the time of the alert. FAVA (Fermi All-sky Variability Analysis) is a tool that blindly searches for transients over the entire sky observed by the Fermi/LAT [204]. No high-energy gamma-ray flaring blazars have been found associated to the neutrino alerts.

For all the alerts between 2012 and 2019, we have also looked for a statistical correlation between the TAToO neutrino sample (265 alerts) and the blazars sources of the 4FGL catalogue. The method looks if there is an excess of ANTARES events in the direction of the blazars [205]. In the 2-degres cone, there are 42 FSRQ, 45 BL Lacs and 31 blazars candidates of uncertain type. The statistical analysis consists in the comparison with the real event directions and the scrambled events (null hypothesis). This test is performed using the full blazar sample or only one of the FSRQ, BLL samples. No significant excess has been found. The maximum

correlation is $\sim 1\sigma$ for the FSRQ. Another test performed using the method proposed in [[100]] allows to compare the energetic of the blazars found int eh 2-degres cone with the overall blazar population. This seems to indicate that blazars found within the directions of the ANTARES events are average objects. There are several ways to improve this analysis, such as reducing the TAToO neutrino sample to only the VHE alerts to reduce the look-else-where effect, add the timing information (looking for flares) and look in blazar catalogues in other wavelengths (radio or X-ray).

4.3.5 Results of the radio follow-up

A search for radio counterparts to two candidate high-energy neutrino events detected in November 2013 (ANT131121A) and March 2014 (ANT140323A) was performed using the Murchison Widefield Array [206]. Such triggers have directions consistent ($< 0.4°$) with the positions of galaxies within 20 Mpc of Earth. Two galaxies match in each case : NGC1374 and ESO358-015 match ANT131121A, and ESO499-037 and PGC29194 match ANT140323A. PGC29194 (the Antlia Dwarf Galaxy), at a distance of 1.3 Mpc, is located just 6' from the neutrino position. Figure 4.15 shows radio images for both neutrino triggers about 20-days prior to, at the time of, and over 1 year after (deep image) the trigger. Both neutrino events also had an optical follow-up. For ANT131121A, 12 observations of 6 images were performed with the TAROT telescope in Chile from 2 - 61 days after the trigger. No optical transient was identified, to a limiting magnitude of 19. For ANT140323A, a total of 8 images was taken with ROTSE 3b in Texas (starting $\sim$15 hr after the trigger) and 10 images with TAROT Chile up to 45 days after the trigger according to the long-term strategy. No transient counterpart was found to limiting magnitudes of 16.4 (prompt) and 18.7 (long-term).

No strongly varying radio counterpart has been identified for the two triggers. Using 5σ upper limits of 90 - 340 mJy, the upper limit for low-frequency radio emission has been set to 10^{37} erg s^{-2} (at 150 MHz) for progenitors at 20 Mpc. These limits are not strongly constraining of late-time emission from even the most luminous radio supernovae or GRBs at these distances. Optical limits are more stringent for these distances. The use of archival data has limitations. Neither trigger was optimally placed within the MWA field of view : ANT131121A was $\sim 8°$ from the pointing center, and ANT140323A was $\sim 17°$ away. Particularly in the latter case, the fall-off in primary beam response means that noise in the region of the image near the trigger position is higher than is ideal. If the neutrino sources are instead not in nearby galaxies, but originate in binary neutron star mergers, the limits constrain the progenitors to be at $z \geq 0.2$ ($\sim$1 Gpc).

It is notable that Fornax A, one of the brightest radio sources in the sky (associated with NGC1316 at a distance of < 20 Mpc) is close ($\sim 3°$) to the position of ANT131121A, although it is strongly ruled out as the progenitor given the

positional uncertainties of the ANTARES trigger. However, this region of the sky is densely populated by galaxies (including about 10 bright members of the Fornax Cluster within the neutrino error circle), illustrating the importance of EM observations coincident in time with neutrino triggers to resolve ambiguity as to the progenitor. ANTARES is now sending a sub-sample of the neutrino alerts in real-time to MWA. Analysis of MWA data is still on-going.

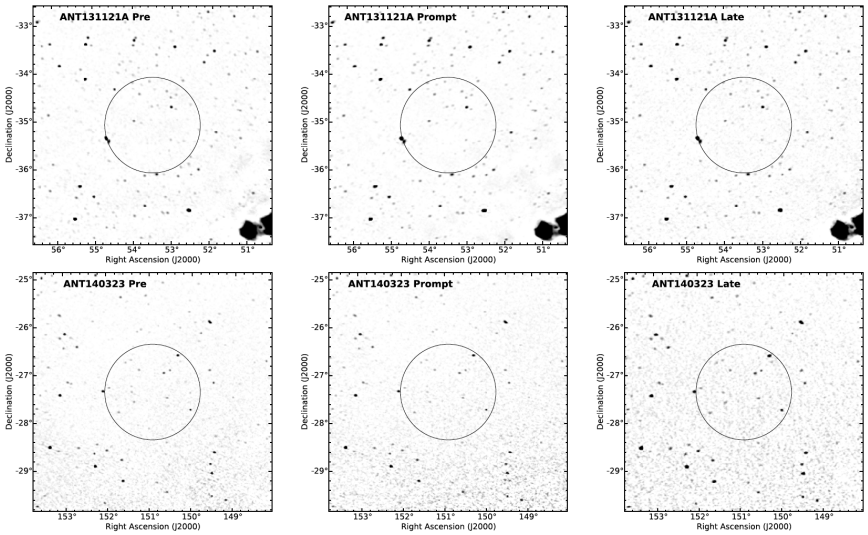

FIGURE 4.15 – 5×5° cutouts from median-combined deep images on each of the two triggers (top : ANT131121A ; bottom : ANT140323A). From left to right, images were taken ∼20 days prior to, at the time of, and over the course of ∼1 yr after the trigger time. Some faint image artifacts are visible, particularly in the top panels around the bright source Fornax A. In the bottom panels, enhanced noise is visible towards the bottom due to the effects of the fall-off in sensitivity towards the edge of the primary beam. The grey-scale runs from 0 to 1 Jy/beam. The black circles represent the 1σ ANTARES error.

4.3.6 Results of the H.E.S.S. follow-up

Since 2016, ANTARES and H.E.S.S. have signed an MoU to exchange information and alerts. Exploiting the intimate connection between high-energy neutrinos and very high-energy gamma rays, the very high gamma-ray H.E.S.S. telescopes have followed two ANTARES alerts shortly after the neutrino detection : ANT150901A and ANT170130A. For ANT150901, the observations started on September 3rd, 2015, at 18 :58 UT as soon as the necessary observation conditions were reached. No very-high energy gamma-ray source has been identified in the 1.5 h observations. An upper limit on the gamma-ray flux to F(E > 320 GeV ; 99% C.L.) < 2.7 × 10^{-8} $m^{-2}s^{-1}$‘[200]. The neutrino ANT170130A direction has also been followed

by H.E.S.S. with a very short delay, 32 s during 1 hour and again 45 min the night after (Figure 4.16 left). The analysis on site shows no source detection in the neutrino field of view. The significance map of the region around the reconstructed neutrino direction is shown on Figure 4.16 right [207].

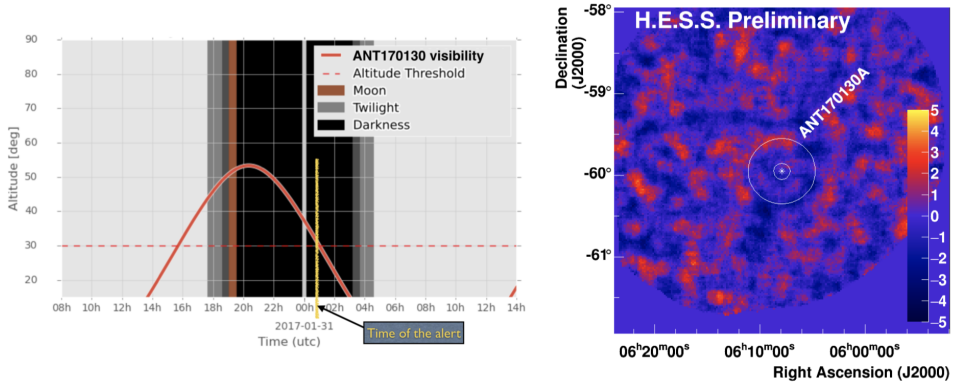

FIGURE 4.16 – Left : Visibility of the ANTARES alert received 2017-01-30 at the H.E.S.S. site. Right : H.E.S.S. significance map of the regions around the ANTARES alert ANT170130A. The inner circle illustrates the size of the H.E.S.S. PSF and the outer circle denotes the 50% containment angular uncertainty on the neutrino direction of 0.4 degrees [cite 1709.00466].

4.3.7 New ANTARES-FERMI/LAT coincidence trigger

Recently, within the AMON multi-messenger analysis framework [208], one new real-time alert stream has been set in the case of the coincidence between Fermi/LAT high-energy photons and ANTARES neutrinos [209]. One coincidence with a False Alarm Rate lower than 1 every 4 years is sent publicly via a GCN notice and a more detailed GCN circular. Two triggers of this type have already been sent publicly :

— ANTARES-200108A (GCN #26674) is a coincidence event between a single ANTARES neutrino (p-value = 0.027) and one Fermi/LAT photon (778.3 MeV). The false alarm rate for the coincidences of this quality or better is 1 per 0.419 years. This neutrino has also been selected as VHE alert and sent to our private partners on his own.

— ANTARES-200127A (GCN #26915) is a coincidence between one high-energy neutrino-induced muon event detected by ANTARES (p-value=0.433) and two Fermi LAT photons (2.18 GeV and 33.28 GeV). The false alarm rate is 1 per 4.036 years.

The results of the follow-up by IceCube (GCN #26699), Master (GCN #26684), INTEGRAL (GCN #26683) and Fermi-GBM (GCN #26676) have been reported

in the GCN. For the last trigger, only the results of IceCube (GCN #26922) and Master (GCN #26920) have been reported. No counterpart has been found for both alerts.

4.4 Conclusions and perspectives

We have started this alert program in September 2008, starting a stable alert sending mid 2009, and this system is operational without discontinuities since then. To achieve this, we have developed robust and simple tools (BBFit, run control). For the alert sending system, it has been a continuous integration and improvement during the whole project : adding the refined positioning, adding new telescopes and therefore new communication protocols with them (GCN socket, VO Event, mail). Adding these patches to the code has made it difficult to maintain the application. It is important for the development of the future alert sending tools for KM3NeT to start with a very versatile and modular architecture, and to fix one unique communication protocol.

All the ANTARES neutrino data are private. So, we had to sign plenty of MoUs with the different partners. It is sometimes difficult to manage these 12-13 MoUs. The example of IceCube sending their neutrino alerts is a really good example to follow. On average, they succeed to obtain a larger follow-up coverage than ANTARES with a limited network. Especially, if one observatory finds a counterpart candidate, the astronomy community is always reacting very fast for its characterisation. It is remarkable that the astronomy community is somehow capable of self-organized itself. The only ANTARES alert, ANT150901A, sent publicly has been followed by 19 observatories. Moreover, for the observatory, getting the visibility by publishing the results of the follow-up, positive or negative, is a key to get their effort recognised and therefore, to obtain their funding. In ANTARES, this question was raised many times and have created sometimes some little tension. Having MoUs is also a good thing since it provides a direct contact within the observatory, a common agreement on the observing strategies and some persons who are doing the data/image analysis. So, I think it is important to set both systems in parallel for the future alert sending of KM3NeT.

The last question which should ask our self is about the neutrino selection for the alert. We have sent a bit more than 300 alerts to the robotic telescopes without finding what were our primary targets. We have not found any GRB afterglow, neither core-collapse supernovae (CCSNe). Ten years ago, GRB was a very popular candidate for neutrino production (see Section 2). Nowadays, direct searches by IceCube and ANTARES have set stringent constraints on the association GRB/neutrino. Only few percents of the detected GRBs can contribute to the neutrino diffuse flux. Note that this does not rule out low-luminosity GRBs to have a larger contribution.

For the CCSNe, we were looking for hidden jets inside the supernovae [210, 211, 212]. This model is quite popular since it can make the link between the long GRB and the CCNSe populations. The neutrinos are emitted in the jets soon after the explosion and the optical emission is following the standard rising light curve of the CCSNe in the first weeks. The non-observations of the supernovae timely correlated with the neutrinos rule out most of the parameter spaces of this model. The main limitations of the ANTARES neutrino selection are that we select only medium energies (1-50 Tev) for the single events due to the limited instrumented volume and only muon neutrinos were selected in real-time. We have known since the beginning that with this selection, the event sample is largely dominated by atmospheric neutrinos. Either the hook was not adapted or there was no fish in the Universe Sea.

For KM3NeT, we should send the single neutrino alerts with even higher energies (>100 TeV), *a la IceCube*. We have seen that the precision is the key to obtain good follow-up, therefore, it is important to obtain the best angular resolution in real-time, using the most optimal reconstruction algorithms, the dynamical positioning and a good control of the absolute pointing accuracy. We should also be able to reconstruct all event topologies, especially the cascade one. If the angular resolution is good enough, this channel is particularly interesting since the atmospheric background contamination is very low. Even at low energies (<5 TeV), we can still use the alert sending to look for neutrino sources. With the improved statistic of KM3NeT, we can imagine smarter event selection based on all-flavor neutrino bursts.

4.5 TAToO group and publications

TAToO is a group effort from CPPM (M. Ageron, V. Bertin, J. Brunner, D. Dornic), APC (A. Coleiro), LAM (S. Basa), CEA-IRFU (F. Schüssler, B. Vallage) with the support of all the ANTARES Collaboration. There were also few students/postdocs working me with invaluable contributions : I. Al Samarai [2009-2011], M. Vecchi [2009-2010], A. Mathieu [2013-2015] and D. Turpin [2014-2016].

Up to now, there are 5 main publications with TAToO results (more will come) :
- The ANTARES telescope neutrino alert system (TATOO), ANTARES Collaboration, Astropart. Phys. 35 (2012) 530-536.
- Optical and X-ray early follow-up of ANTARES neutrino alerts, , ANTARES, ROTSE, TAROT, Zadko and Swift Collaborations, JCAP 1602 (2016) 062
- The Zadko Telescope : Exploring the transient Universe, D.-M. Coward et al., Publ. Astron. Soc. Aust 34 (2017) e005.
- Murchison Widefield Array Limits on Radio Emission from ANTARES Neutrino Events, MWA, ANTARES, TAROT, ROTSE Collaborations, Astrophys. J. Lett 820 (2016) L24.

— D. Dornic, S. Basa, P.A. Evans, J.A. Kennea, J.P. Osborne, and V. Lipunov, ANTARES Collaboration, the Swift-XRT team and MASTER team, ANTARES neutrino detection and possible Swift X-ray counterpart, GCN #18231 and ATeL #7987 (2015).

5 Online analyses of multi-messenger alerts and electromagnetic transient events

By constantly monitoring at least one complete hemisphere of the sky, neutrino telescopes are well designed to detect neutrinos emitted by transient astrophysical events. We have performed with the ANTARES telescope real-time searches for neutrino candidates coincident with Swift and Fermi gamma-ray bursts, IceCube high energy neutrino events and gravitational wave candidates observed by LIGO/Virgo. By requiring temporal coincidence, this approach increases the sensitivity and the significance of a potential discovery.

In the same online analysis framework, we have also developed a dedicated real-time analysis to look for neutrino events in both time and space coincidence with transient events announced by public alerts distributed through the Gamma-ray Coordinated Network (GCN) or by private alerts transmitted via special channels. The online selection is optimised to select a quite pure neutrino sample (similar cuts as in the standard point-like source search) : only upgoing track events with a reconstruction quality parameter, $\Lambda >$ -5.2 are used in the analysis (with an atmospheric muon contamination lower than 10 %). The typical rate of events in ANTARES is given in Figure 2.14. In 2012, there were about 4-5 events per day, but actually, this rate is only about 1-2 events per day.

If some associations are found interesting in online, more optimized offline analyses are then performed to improve the online search. Offline searches are also performed for neutrino counterparts to catalogued transients.

5.1 Follow-up of IceCube high-energy neutrinos

A coincident detection by both IceCube and ANTARES would be a significant proof of the astrophysical origin of these neutrino candidates and would point directly to the position of the source in the sky. By looking in real-time if ANTARES finds neutrino events in coincidence with the IceCube neutrino triggers will boost the significance of the neutrinos and therefore will provide additional lights to convince the astronomy community to perform the most optimal EM

follow-up. Since 2016, IceCube has been sending public triggers for high-energy starting events (HESE) and extremely high-energy track candidates (EHE). The events are received by the Astrophysical Multi-messenger Observatory Network (AMON [208]) and distributed to the community via an alert of the GCN. In June 2019, IceCube is provided in replacement two new very-high energy track event samples : gold (with a probability to be astrophysical p>50 %) and bronze (p>30 %) samples. In July 2020, IceCube has provided another alert stream based on very high-energy cascades with a typical resolution uncertainties of 15-20 degrees (50 % radius) and a typical rate of 8 / year. Except two test events in July , no automatic event has been sent yet. The list of triggers is available at this address : https://gcn.gsfc.nasa.gov/amon.html.

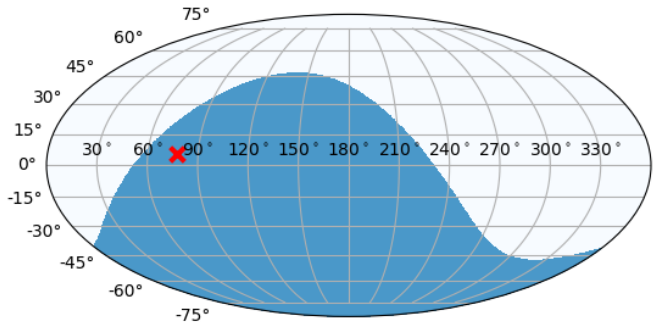

FIGURE 5.1 – Skymap in equatorial coordinates showing in blue the visible ANTARES field of view at the time of IC170922. The direction of the IC event is drawn as a red cross.

In this context, we are performing a follow-up analysis of each IceCube event whose position is below the horizon of ANTARES (which could consequently yield to an up-going event at the time of the alert). Up to now, ANTARES has received 58 neutrino triggers from IceCube and has followed 20 alerts (7 HESE, 3 EHE, 3 gold and 7 bronze). The rest of the triggers was either retracted by the IceCube Collaboration or in the wrong hemisphere. Figure 5.1 shows the direction of the IceCube event IC170922 and the ANTARES visibility at the time of the event. No neutrino candidates were found compatible with one of the alerts within a cone of 3 degrees centered on the IceCube event coordinates and a time window of ±1 hour and an extended one of ±1 day. These non-detections have been used to derive preliminary 90 % confidence level upper limits on the radiant neutrino fluence of

these events of the order of ∼15 GeV cm^{-2} and ∼30 GeV cm^{-2} for the E^{-2} and the E$^{-2.5}$ spectral models respectively (see Table 5.1). These results have been published as GCN circulars and Astronomer's Telegrams typically after one day after the alerts (Table 5.2).

IceCube event	Elevation (deg)	Fluence U.L. (GeV cm^{-2})	
		$dN/dE \propto E^{-2}$	$dN/dE \propto E^{-2.5}$
IC160731A (EHE/HESE)	-28°	14 (2.8 TeV - 3.1 PeV)	27 (0.4 - 280 TeV)
IC160814A (HESE)	-26°	16 (2.9 TeV - 3.3 PeV)	43 (0.5 - 250 TeV)
IC161103A (HESE)	-26°	13 (3.8 TeV - 3.8 PeV)	22 (0.7 - 370 TeV)
IC170321A (EHE)	-57°	16 (2.5 TeV - 2.5 PeV)	26 (0.5 - 220 TeV)
IC170922A (EHE)	-14°	15 (3.3 TeV - 3.4 PeV)	34 (0.5 - 280 TeV)
IC171015A (HESE)	-45°	14 (2.7 TeV - 2.9 PeV)	27 (0.4 - 240 TeV)
IC180908A (EHE)	-41°	18 (2.4 TeV - 2.6 PeV)	36 (0.4 - 250 TeV)
IC190104A (HESE)	-39°	16 (3.2 TeV - 3.5 PeV)	30 (0.6 - 315 TeV)
IC190124A (HESE)	-44°	15 (3.1 TeV - 3.6 PeV)	25 (0.6 - 316 TeV)
IC190504A (HESE)	-18°	16 (3.1 TeV - 3.5 PeV)	32 (0.6 - 316 TeV)
IC190619A (gold)	-19°	13 (3.9 TeV - 3.9 PeV)	33 (0.7 - 320 TeV)
IC190712A (bronze)	-13°	16 (4.6 TeV - 4.3 PeV)	40 (0.8 - 420 TeV)
IC191119A (gold)	-37°	16 (3.4 TeV - 3.6 PeV)	28 (0.7 - 340 TeV)
IC191231A (bronze)	-17°	15 (5.3 TeV - 5.0 PeV)	32 (1.0 - 470 TeV)
IC200127A (bronze)	-18°	15 (6.8 TeV - 6.3 PeV)	29 (1.0 - 610 TeV)
IC200421A (bronze)	-25°	15 (3.9 TeV - 4.9 PeV)	27 (0.7 - 380 TeV)
IC200530A (gold)	-0.04°	80 (6 TeV - 6 PeV)	110 (1 - 560 TeV)
IC200620A (bronze)	-32°	15 (5 TeV - 4 PeV)	30 (0.8 - 400 TeV)
IC200911A (bronze)	-7°	14 (10 TeV - 8 PeV)	34 (1.5 - 740 TeV)
IC200916A (bronze)	-29°	18 (4 TeV - 4.5 PeV)	33 (1 - 430 TeV)

TABLE 5.1 – Preliminary ANTARES fluence upper limits at 90% C.L. for each IceCube neutrino candidate. For each fluence, the 5-95 % energy range is given.

5.2 Follow-up of gravitational wave events

Current modeling of binary black-hole merger evolution does not imply EM or neutrino counterpart. However, in a sufficient circumbinary dense region, an accretion disk might form and/or a relativistic jet connected to the accretion could be released. Accreting black holes can drive relativistic outflows [213]. In this case, the process might lead to gamma-ray emission with a potential high-energy neutrino counterpart if a hadronic component is present [214, 215, 216, 217, 218, 219]. With more GW detections, we start to probe systems with asymmetric masses,

IceCube event	GCN	ATels
IC160731A (EHE/HESE)	/	9324
IC160814A (HESE)	19885	9440
IC161103A (HESE)	20134	9715
IC170321A (EHE)	20926	10189
IC170922A (EHE)	21923	10773
IC171015A (HESE)	22019	10854
IC180908A (EHE)	23218	12024
IC190104A (HESE)	23611	12359
IC190124A (HESE)	23793	12423
IC190504A (HESE)	24400	12731
IC190619A (gold)	24866	12878
IC190712A (bronze)	25064	12937
IC191119A (gold)	26266	13295
IC191231A (bronze)	26623	13380
IC200127A (bronze)	26811	13409
IC200421A (bronze)	27619	13654
IC200530A (gold)	27871	13770
IC200620A (bronze)	28002	13820
IC200911A (bronze)	28415	14008
IC200916A (bronze)	28446	14025

TABLE 5.2 – References of the publication in GCN and in Astronomer's Telegram of the ANTARES follow-up of IceCube public triggers.

or very large masses, which are less theoretically known, leaving room for possible discoveries. An EM counterpart, presumably associated with a hadronic emission is more expected from neutron star/black hole (NSBH) or neutron star/neutron star (BNS) mergers. Most of the models are based either on the formation of a gamma-ray burst [220, 221, 222] or a magnetar [223]. The other goal of the neutrino follow-up is that the angular resolution of ANTARES ($\sim$0.4° at $\sim$10 TeV) compared to the size of the gravitational wave error box (a few hundreds of square degrees on the sky) offers the possibility to drastically reduce the size of the region of interest in case of a coincident neutrino detection.

During the first observing run O1 in 2015, three GWs coming from binary black hole (BBH) mergers have been detected by LIGO for the first time [224]. As the online analysis was not ready for these events, only offline analyses have been performed by the ANTARES Collaboration [225, 226]. About one year later, during the second observing run O2 (November 30, 2016 to August 25, 2017), the upgraded LIGO and VIRGO detectors have detected GW from a total of seven binary black hole mergers (plus 3 additional sources found in the offline analyses) and a binary

neutron star (BNS) merger GW170817. Only for this last event, electromagnetic counterparts have been identified as a short gamma-ray burst followed by a kilonova [13, 227]. During the run O2, the LIGO/VIRGO Collaboration has triggered 15 alerts identified by online analysis using a loose false-alarm-rate threshold of one per month. These triggers were shared with partner collaborations who have signed MoU with LIGO/Virgo for electromagnetic and neutrino follow-up. Each of these alerts were followed by the ANTARES neutrino telescope by searching for a potential neutrino counterpart. The online analysis consists in looking for *(i)* temporal coincidences within a ± 500 s and a ± 1 hour time windows around the GW alert [228] and *(ii)* spatial overlap between the 90% probability contour and the ANTARES visibility region at the time of the GW event. Figure 5.2 illustrates the principle of the real-time GW analysis. LIGO and VIRGO are sending few notices for each GW candidate with updated information (Preliminary, Initial, Update, Retraction). Each new type is processed as it is a new GW trigger. At the end, we provide the results of the last stable revision. This analysis schema has been applied to all the GW candidate triggers we have received and the results are that no up-going neutrino candidates temporally coincident with all the GW candidates was found with ANTARES. The results of the nearly real-time analyses have been transmitted to LIGO/Virgo follow-up community via the GCN. Table 5.3 lists the different GCN circulars sent by ANTARES. In general, the online analyses performed on each GW candidates are followed by a more optimised all-sky analyses [227, 229].

GW name	Type	GCN Id
G268556	BBH	20517
G270580	BBH	20621
G274296	BBH	20704
G275404	BBH	20751
G275697	BBH	20765
G277583	BBH	20866
G284239	BBH	21066
G288732	BBH	21223
G296853	BBH	21433
G297595	BBH	21479
G298048	BNS	21522 / 21601 / 21631
G298936	BBH	21659
G299232	BBH	21696 / 21769

TABLE 5.3 – Characteristics of the GW candidates distributed by LIGO/VIRGO during run O2.

The third observing run O3 has started April 1st, 2019, with even more upgraded

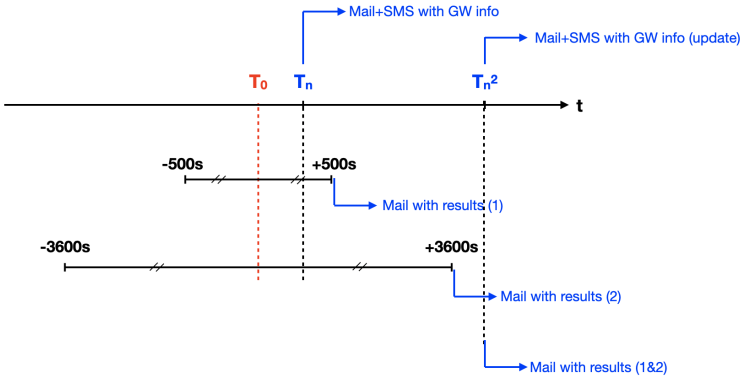

FIGURE 5.2 – Principle of the online GW analysis. T_0, T_n and T_{n2} correspond to the time of the detection, the time of the reception of the first notice and the time of the successive notices for one GW trigger. At the time T_n and when the results of the two searches are available, one mail is sent to the ANTARES GW subgroup. A SMS is also sent to faster the communication within the group.

interferometers. Up to the end of March 2020, 78 alerts have been distributed publicly, 22 retracted by LIGO/VIRGO after further investigations. Among the 56 events, 37 are BBH, 5 Mass Gap, 4 NSBH, 6 BNS, 1 unmodeled and 3 probably coming from terrestrial noise (5.4 left). We have performed real-time analysis for 51 GW triggers (5.4 right). Two triggers have not been analysed since the GW were classified quickly as terrestrial noise, 2 with the error region not in the ANTARES hemisphere while for the other event, ANTARES was in maintenance during the event. Figure 5.3 illustrates the errors contours of of GW event S190602aq together with the ANTARES visibility at the time of the event. The main characteristics of the 51 GW candidates and the results of the neutrino search are summarised in Table 5.4.

Figure 5.5 and Figure 5.6 show the distribution of the reconstructed GW parameters (distance and 90 % C.L. error region) and the fraction of the 90 % C.L. error region visible by ANTARES at T_0 as upgoing directions. Unfortunately, during this run, most of the GW candidates were reconstructed with a large error region, typically above 1000 deg^2. Only few events were reconstructed within less than 100 sq. deg. This makes the EM follow-up even more difficult and the detection of a neutrino at the end all the more important.

For those events, we have performed similar analyses as done for the run O2 events, but in a completely automatised way. Up to now, no up-going muon track neutrino has been found in time and space coincidence with each alert of run O3 (Table 5.4). All the results have been reported via the publication of a circular to the GCN. The results contain a sky map of the visible region of ANTARES (as

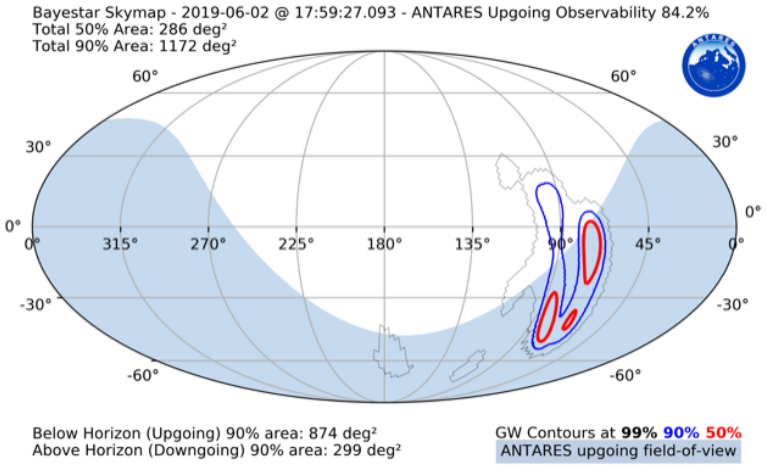

FIGURE 5.3 – Skymap in equatorial coordinates showing the 99 % (black), 90 % (blue) and 50 % (red) probability contours of S190602aq together with the ANTARES field-of-view at the event time (blue part of the map).

upgoing) at the time of the GW candidate together with the GW error regions, the fraction of the GW 90 % error region covered by the ANTARES field of view, the number of events in time/space coincidence and the expected number of atmospheric background events in the region visible by ANTARES. This false alarm rate is computed directly in the data using an off-region before the GW trigger. The results are reported for two search time windows : ±500 s and ±1 hour centered on the time of the GW. The typical delay between the detection time of the GW candidates and the time of the ANTARES results circular is around 4.5 hours. Note that one necessary condition to submit our results was to receive a confirmation circular by LIGO/VIRGO. If we use this time as a reference, the results have been published on average in less than 2h (Figure 5.7). The offline analysis has started for a few events that has been already published by LIGO/VIRGO [230, 231, 232].

TABLE 5.4 – Characteristics of the GW candidates distributed by LIGO/VIRGO during run O3. The coverage indicates the fraction of the 90 % GW error box falling in the visibility of the ANTARES neutrino telescope at the time of the event. The error box is the one given at the time of the analysis, some more refined GW parameters may have arrived later.

GW name	Type	Error box (deg^2)	Distance (Mpc)	Coverage (%)	GCN Id
S190408an	BBH	387	1473		

Continued on next page

Table 5.4 – continued from previous page

GW name	Type	Error box	Distance	Coverage	GCN
S190412m	BBH	156	812	9.3	24105
S190421ar	BBH	1917	1628	52	24156
S190425z	BNS	10183	156		
S190426c	BNS	1932	377	45	24271
S190503bf	BBH	448	421	98	24387
S190510g	Terrestrial	3462	237		
S190512at	BBH	399	1388	83	24516
S190513bm	BBH	691	1987	55	24539
S190517h	BBH	939	2950	83.3	24581
S190518bb	retracted				
S190519bj	BBH	967	3154	34	24602
S190521g	BBH	1163	3931	56	24628
S190521r	BBH	388	1136	30	24634
S190524q	retracted				
S190602aq	BBH	1172	797	84	24719
S190630ag	BBH	8493	926	68.6	24924
S190701ah	BBH	67	1849	99.9	24952
S190706ai	BBH	1100	5263	48.7	25009
S190707q	BBH	1375	874	58.3	25013
S190718y	Terrestrial	7246	227	77.5	25091
S190720a	BBH	1599	869	41.6	25120
S190727h	BBH	1357	2839	55.1	25168
S190728q	BBH	977	874	38.1	25194
S190808ae	retracted				
S190814bv	NSBH	772	267	99.9	25330
S190816i	retracted				
S190822c	retracted				
S190828j	BBH	603	1946	53.1	25508
S190828l	BBH	948	1528	56.8	25507
S190829u	retracted				
S190901ap	BNS	13613	241	54.1	25611
S190910d	NSBH	3829	632	50.9	25700
S190910h	BNS	24226	230	50	25711
S190915ak	BBH	528	1584	45.6	25758
S190923y	MassGap	2107	438	41.7	25816
S190928c	retracted				
S190930s	MassGap	1998	709	25.9	25881
S190930t	NSBH	24220	108	50	25882
S191105e	BBH	1253	1183	66.4	26189
S191109d	BBH	1487	1810	79.1	26210

Continued on next page

Table 5.4 – continued from previous page

GW name	Type	Error box	Distance	Coverage	GCN
S191110x	retracted				
S191110af	unmodeled	1261		56	26230
S191117j	retracted				
S191120aj	retracted				
S191120at	retracted				
S191124be	retracted				
S191129u	BBH	1011	742	51.6	26307
S191204r	BBH	433	678	92.9	26336
S191205ah	NSBH	6378	385	28	26352
S191212q	retracted				
S191213g	BNS	1393	201	75.1	26404
S191213ai	retracted				
S191215w	BBH	923	1770	42.3	26443
S191216ap	BBH	300	376	15.9	26458
S191220af	retracted				
S191222n	BBH	2324	2518	53.1	26550
S191225aq	retracted				
S200105ae	Terrestrial	7719	283	35.6	26643
S200106au	retracted				
S200106av	retracted				
S200108v	retracted				
S200112r	BBH	6199	1125	38.4	26718
S200114f	Unmodeled	403		6	26742
S200115j	MassGap	920	340	76	26762
S200116ah	retracted				
S200128d	BBH	2521	3702	50.1	26912
S200129m	BBH	53	755		
S200208q	BBH	1120	2142	68.5	27016
S200213t	BNS	2587	201	31.9	27049
S200219ac	BBH	1251	3533	55.5	27135
S200224ca	BBH	69	1575		
S200225q	BBH	403	995	42.4	27201
S200302c	BBH	6704	1820	49.5	27284
S200303ba	retracted				
S200308e	retracted				
S200311bg	BBH	52	1115		
S200316bj	MassGap	1117	1178	26.6	27390

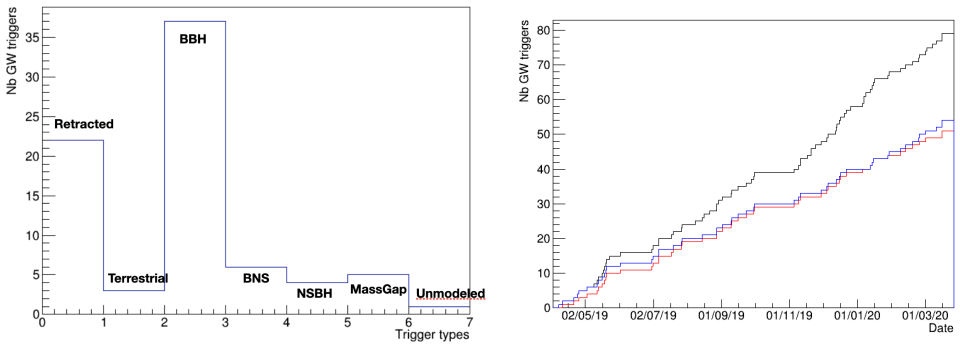

FIGURE 5.4 – (Left) Online classification of the GW candidates detected during run o3. (Right) Cumulative number of the GW candidates detected during run o3 as a function of the date. In black : all GW triggers, in blue, the one analysable (not terrestrial and not retracted at the time of the analysis) and in red, the analysed GW candidates by ANTARES.

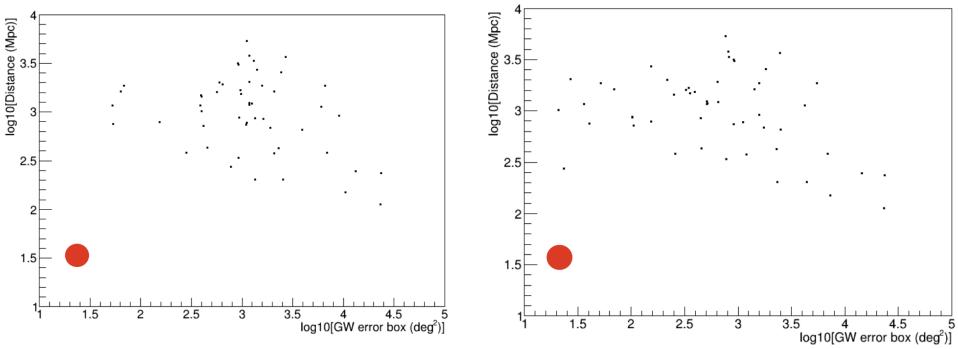

FIGURE 5.5 – Size of the 90 % C.L. error region of the GW candidates calculated with the textitBayestar (left) and the *LALinference* (right) GW analysis pipeline as a function of the inferred GW distance. The red dots correspond to the BNS GW170817.

5.3 Follow-up of gamma-ray bursts

Transient astrophysical events are observed all over the electromagnetic spectrum. Gamma-ray bursts (GRB) are mainly detected by X-ray and gamma-ray satellites such as Swift, Fermi-GBM. Once a GRB is detected, an alert message is sent publicly via the GCN within a few tens of seconds. ANTARES is able to react in real-time to this type of alerts. Only the bursts with their direction visible on the ANTARES hemisphere are analysed. A dedicated search for muon-track neutrino counterparts in the optimized online data set is performed in real-time within [-250 s ; +750 s] time window around the detection time and in a cone of max [2°,error box Fermi] radius centered on the GRB position (Figure 5.8). The

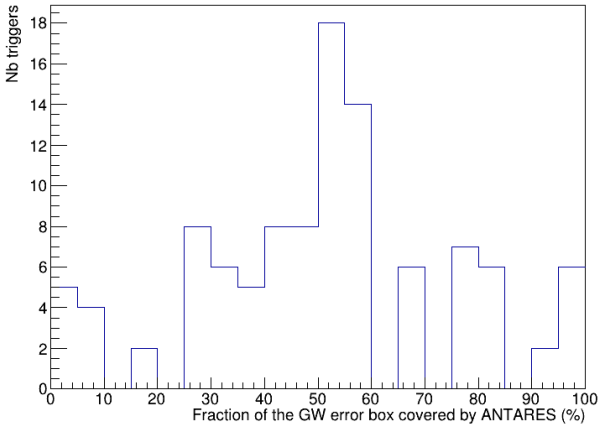

FIGURE 5.6 – Fraction of the 90 % C.L. error region of the GW candidates visible by ANTARES at T_0 as upgoing directions.

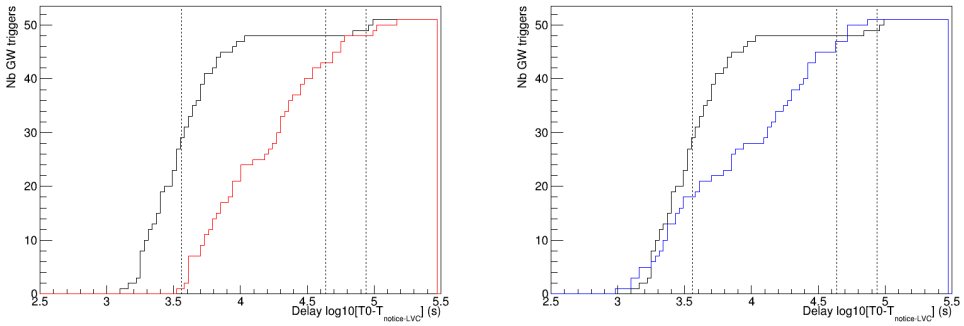

FIGURE 5.7 – Delay between the time of the GW candidates and the reception time of the first notice (black) and the submission times of the circular with the ANTARES results (red). The blue curve corresponds to the time difference between the reception of the GW confirmation circular and the ANTARES circulars.

event selection is relaxed compared to the typical point-like source search and is more optimized for a transient analysis ($\Lambda >$ -5.4). The analysis is performed automatically and a mail is sent to a subgroup with the results of the search. To ensure the quality of the data at the alert time, the detector stability is checked over several hours before the alert. This analysis has been operational since the beginning of 2014 and up to now ≈98 % of the alerts have been processed. During this about 7 years of operation (01/2014-05/2020), there were 265 Swift and 637 Fermi-GBM bursts. The bursts detected at the same time by both satellites are tagged as Swift. Figure 5.9 shows the directions of these two GRB samples. No online neutrino signal has been detected in this search.

In case of a coincident neutrino detection, a dedicated offline analysis is run to

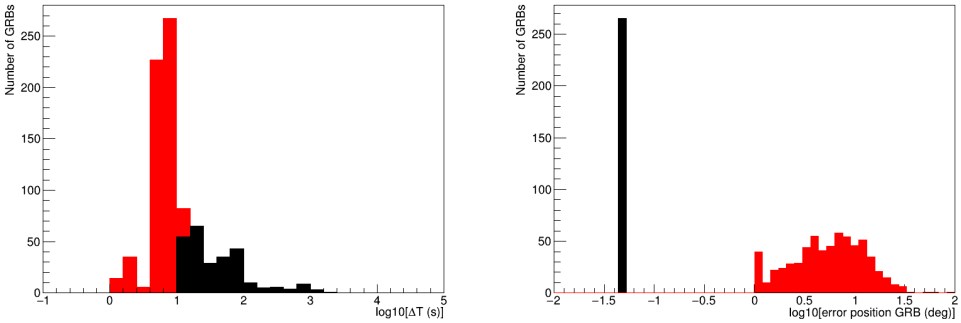

FIGURE 5.8 – (Left) Time delays between the burst detection and the received notice. (Right) Error in the position of the GRBs detected. Swift and Fermi-GBM GRBs are shown in blue and red.

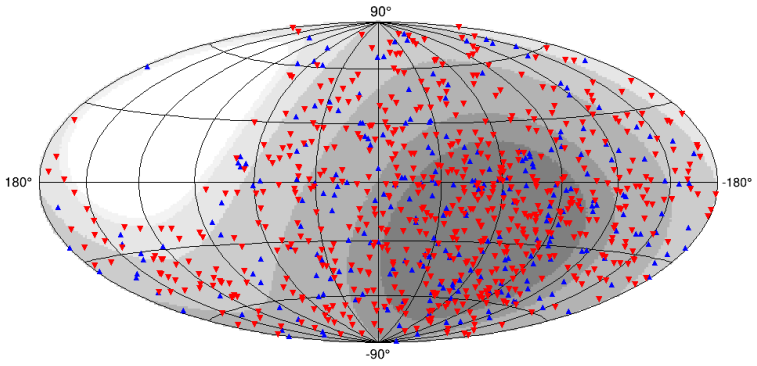

FIGURE 5.9 – Skymap on galactic coordinates with the positions of the Fermi (red triangles) and Swift (black triangles) GRBs followed by ANTARES up to May 2020. The shade of grey indicates the ANTARES visibility.

confirm the result and compute its significance (expected to be higher than 3σ in most of the cases). For example, dedicated offline analyses have been performed by the ANTARES Collaboration with improved event selections [233, 234].

5.4 Follow-up of other transient triggers

Since mid 2019, HAWC has started to issue short TeV transient alerts from 0.2 to 100 s, targeting in particular GRBs. HAWC has the same advantage of ANTARES such as monitor half of the sky in permanence with a high-duty cycle. Detecting TeV sources is particularly interesting for the high-energy neutrino searches since it first proves that the sources are powerful cosmic accelerator and in hadronic scenarios, those gamma-rays have more or less the same energy as the detected neutrino by ANTARES. The alerts are channeled via the AMON framework and then distributed by the GCN. HAWC has sent 14 triggers, 4 of them have been

followed by ANTARES (only the alerts with a direction in the ANTARES visibility at the time of the alert). The alert parameters are available at this address : https://gcn.gsfc.nasa.gov/amon_hawc_events.html. Figure 5.10 shows the direction of the HAWC alerts together with the integrated ANTARES visibility. The same analysis strategy as for the IceCube neutrino alerts is applied and the results are then published as a circular to the GCN. Table 5.5 summarizes the main alert parameters and lists the GCN published for this analysis.

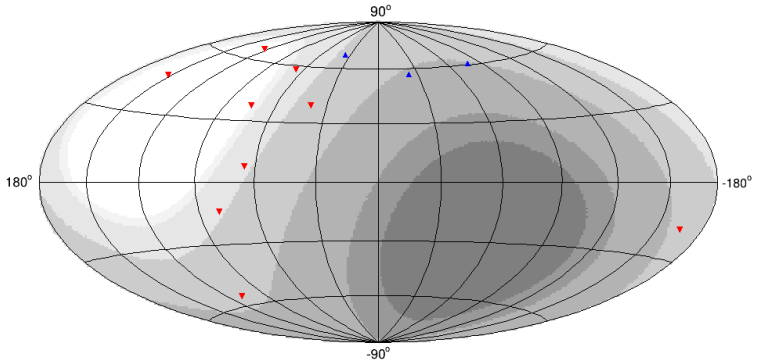

FIGURE 5.10 – Skymap on galactic coordinates with the positions of the HAWC alerts (red triangles) up to May 2020. The blue triangles indicate the analysed alerts.The shade of grey indicates the ANTARES visibility.

5.5 Perspectives

Public alerts are common for the EM transients, especially gamma-ray burst, soft-gamma-ray repeaters, supernovae, etc. It is clear that to measure the parameters and thus study these astrophysical sources in detail, it is necessary to obtain simultaneous multi-wavelength data. This can only happen with a synergy between different instruments based on efficient, fast and reliable communication between them. The GCN is in the center of this strategy as a fast dispatcher of triggers and results. Recently, multi-messenger actors have also adopted a similar strategy of the public alert distribution, IceCube in 2016, LIGO/VIRGO in 2019, HAWC in 2020. With the run O3 of LIGO/VIRGO and the new alert selection of IceCube, it has reached some maturity with about 110 triggers in one year. We have developed an online analysis framework, fully automatised, that looks for time/space coincidence with the time/direction of the MM and EM transient external triggers. We have followed all these public alerts at the condition that at the time of the trigger, its direction is visible as the up-going in ANTARES. Despite the fact that we have not found any coincidence with the online, this program has highlighted the multi-messenger program of ANTARES to a broad community. Most of the work

Event Id	Direction RA, Dec (deg)	Error (arcmin)	δT (s)	Vis (%)	GCN
HAWC-200815A (9579_392)	11.231,+11.497	48	0.2	44	/
HAWC-200814A (9575_1797)	177.794, +19.945	48	0.2	39	/
HAWC-200709A (1009500_793)	252.377, +15.204	24	100.00	42	28074
HAWC-200329A (109213_248)	192.271,+51.610	36	10.00	0	/
HAWC-200314A (1009197_466)	255.693,+48.088	24	100.00	0	/
HAWC-200227A (1009170_1051)	151.036,+60.598	24	100.00	0	/
HAWC-200226A (19170_50)	182.802,-0.608	48	1.00	50	27242
HAWC-200221A (19164_862)	291.308,+32.239	35	1.00	0	/
HAWC-191210A (9066_1171)	210.803,-1.515	48	0.20	35	26391
HAWC-191208A (1009064_586)	228.875,+40.243	24	100.00	0	/
HAWC-191019A (8991_1097)	217.499,+25.807	48	0.20	50	26049
HAWC-190927A (108961_355)	248.727,+21.210	24	10.00	0	/
HAWC-190917A (18941_372)	321.848,+30.973	48	1.00	0	/
HAWC-190806A (1008846_957)	78.390,+6.610	24	100.00	0	/

TABLE 5.5 – Summary of HAWC transient triggers and ANTARES publication in GCN. Error is the location uncertainty (radius, 50 % containment). δT is the trigger duration interval. Vis is the visibility of the alert direction during one day.

remains on the writing and validation of the GCN circular. This step can also be automatised in the future.

Other alert distribution systems are used by VHE, radio or optical communities, such as the Transient Server for the optical transients such as supernovae, the Fermi's advocate for the Fermi flaring sources, Astronomer's Telegram for the VHE transients... As most of them are written by human with sometimes large delays (weeks), it is more difficult to automatised this type of analyses. For the most interesting transients, we are also doing the follow-up in offline still using the online data. For example, the neutrino analysis results on the FRB associated with the magnetar SGR 1935+2154 were reported in the ATel # 13721.

As a coincident observation by two experiments significantly decreases the probability of false alerts, fast confirmation is essential to allow observatories with limited follow-up capabilities, e.g. due to limited sky coverage or observation time, to efficiently prioritise and schedule their resources. This search has the additional capability of "amplifying" incoming alerts if a coincident neutrino signal is found. In such a case, the priority of following up the alert will be high for all partner instruments on the network. A further advantage is that a subsequent offline analysis of data collected by different instruments upon an alert may yield a significant

result from a combination of signals that by themselves would not be considered significant enough for reporting.

We plan to adapt a similar plan in the KM3NeT Collaboration. So, we are actually building the real-time analysis framework based on (see Section 6 for details) :

— All-sky/all flavor neutrino reconstruction : adding real-time capabilities to select efficiently cascade events and being able to look for neutrino signal in the down-going region are the principal upgrades we are working on.
— Implementation of a more sensitive cross-match method based on either a binned or likelihood-based analysis to calculate the corresponding sensitivities of KM3NeT according to the most up-to-date neutrino models.
— Possibility to follow variable sources such as flares of AGNs, in an automatic way over a longer time scale of several days to one year.

5.6 Online group and publications

The real-time follow-up is a group effort from CPPM (M. Ageron, D. Dornic) and APC (A. Coleiro, A. Kouchner). For the GW alerts, this group includes also T. Pradier (IPHC) and M. Colomer-Molla (APC). At the end, it represents the processing of more than one hundred of alerts, with a fast reaction ; most of the alerts were followed and results published in typically few hours.

There is no publication in a journal dedicated to the follow-up results, but there are 107 GCNs and 28 ATels up to September 2020.

6 Neutrino astronomy with the KM3NeT neutrino telescope

6.1 The KM3NeT neutrino detector

A second neutrino telescope is in construction in the Mediterranean Sea : KM3NeT [67], one very large detector for the highest energies (ARCA, Astroparticle Research with Cosmics in the Abyss) and one densely instrumented detector for lower neutrino energies (ORCA, Oscillation Research with Cosmics in the Abyss). ARCA will be located about 100 km offshore from Porto Palo di Capo Passero in the South of Italy at a depth of 3500 m (36° 16' N 16° 06' E) and ORCA 40 km offshore Toulon in the South of France at a depth of 2450 m (42° 48' N 06° 02' E). The main goals of KM3NeT are to study of neutrino oscillations, with as flagship measurement the determination of the neutrino mass ordering and to perform neutrino astronomy with improved angular resolution over a very large energy range. Both detectors are based on the same detection principle, i.e. the Cherenkov light induced by charged secondary particles emerging from neutrino interactions is detected using a three-dimensional deep-sea grid of photo-sensors with single-photon sensitivity and nanosecond time resolution. Thanks to the versatile design concept of KM3NeT detector elements, the same technology can be used at both sites. One building block of KM3NeT will host 115 vertical detection lines (DUs) with 18 digital optical modules (DOM) each, where each module is equipped with 31 3-inch photomultiplier tubes installed in a 17-inch glass sphere (Figure 6.1). Each ARCA DUs are 700 m in height, with DOMs spaced 36 m apart in the vertical direction, with an average inter-DU distance of about 90 m. For KM3NeT/ORCA, each string is 200 m in height with DOMs spaced 9 m apart in the vertical direction and a mean inter-DU distance of about 20 m. ORCA will comprise one building block with an instrumented volume of 8 mega tons of water. ARCA will consist of two building blocks covering 1.1 cubic kilometres. The construction is in progress on both sites, and by mid 2021, a larger sensitivity is already expected in the whole energy range compared to the ANTARES detector.

As in ANTARES, the readout of the KM3NeT detector is based on the "all-data-to-shore" concept in which all analogue signals from the PMTs that pass a preset threshold (typically 0.3photo-electrons) are digitised and sent to shore to be processed in real time. The physics events are filtered from the background using a designated software in a computer cluster located at each shore station. To

maintain all available information for the offline analyses, each event will contain a snapshot of all the data in the detector during the event. The events are then stored in ROOT files and transmitted to two computing centers in France (CC-IN2P3) and in Italy (CNAF-Bologna) for the offline reconstruction and further data analysis. In parallel to the data writing, the events are also processed by an online analysis framework where the event's direction and energy are reconstructed using dedicated algorithms as track and shower topologies, then, they are classified as track, cascade neutrinos and atmospheric muons. The neutrino sample is finally analysed to look for time/space coincidences with external EM/multi-messenger events and to select very "interesting" neutrinos for the alert sending program. A low-level data stream is also processed in real-time for the CCSN analysis.

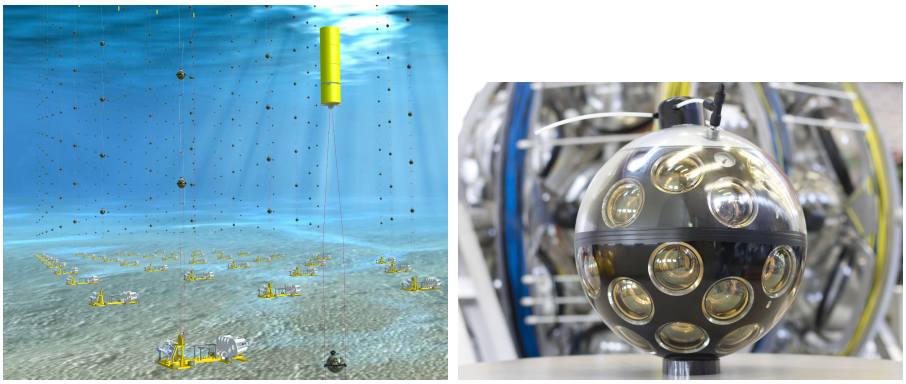

FIGURE 6.1 – (left) Artistic view of the KM3NeT detector. (Right) Picture of a DOM (17 inc diamater).

Thanks to the unprecedented angular resolution, the extended energy range (1 GeV ; >10 PeV) and the full sky coverage, KM3NeT will play an important role in the rapidly evolving multi-messenger field. This even implies a significant discovery potential already during the construction phase. A good sensitivity over such a large energy coverage can only be obtained by combining the data of the two detectors. This combination has already been applied to search for the next galactic CCSN (See Section 6.3).

One of the main goals of KM3NeT is to look for the astrophysical neutrino sources and to characterize them thanks to its good angular resolution. ARCA is dedicated for the neutrino astronomy looking for all-flavor astrophysics neutrino signal above about 50 TeV. With the very large volume of ARCA, the sea medium and the performances of the optical modules, a good angular resolution better than 0.2° (Figure 6.2 left) is achieved for very high energy muon neutrino tracks (>10 TeV). For galactic sources, the angular resolution is around 0.2° for o(10 TeV) neutrinos while for extra-galactic sources, the resolution is around 0.1° for o(100 TeV) neutrinos. For the highest energies, this angular resolution can reach 0.05° (>10 Pev). However, the estimation of the energy is quite poor due to the

limited size of the detector compared to the track length with a resolution of 0.2 in log10(E). The angular resolution of cascade events is worse, 1.5° above 50 TeV (Figure 6.2 right). For contained events, the energy can be reconstructed with about 5 % resolution. Cascade events can be used in astronomy thanks to the smaller atmospheric background contamination. It is one of the most promising windows to detect astrophysical sources.

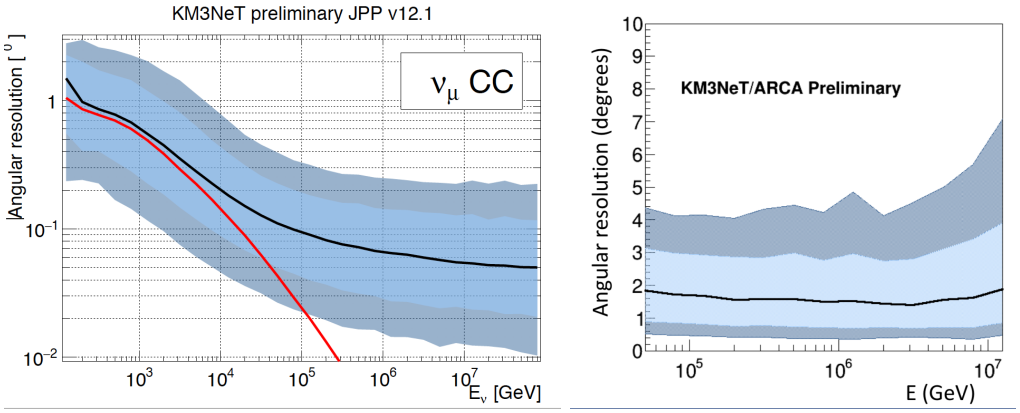

FIGURE 6.2 – Median angular resolution as a function of the energy for tracks (left) and cascades (right) detected in ARCA.

We can also do neutrino astronomy at low energies with ORCA. For example, cosmic ray acceleration in winds of X-ray/γ-ray binaries, in chocked GRBs or in hidden jets in core-collapse SN may provide low-energy neutrinos <1 TeV. Even at lower energies (< 10 GeV), we may expect neutrinos from solar flares. At 100 (10) GeV, the angular resolutions for tracks are around 2 (7)° (Figure 6.3). Above 1 TeV, this resolution is < 1°. For cascade events, the angular resolution is very similar (Figure 6.3). Even if it is worse, it can still be used to look for cosmic neutrinos as we will mainly use multiple events, e.g. 2-3 neutrinos in the same time/angular windows (the angular resolution is improved by $1/\sqrt{N}$, N is the number of neutrinos).

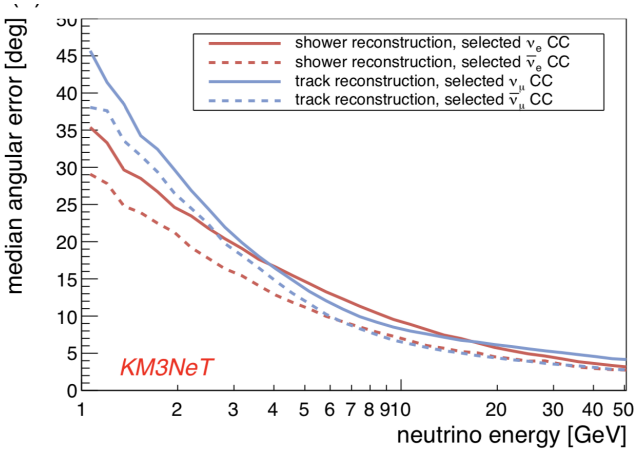

FIGURE 6.3 – Median angular resolution as a function of the energy for tracks and cascades detected in ORCA at energies below 50 GeV.

6.2 Online analysis with KM3NeT neutrino

With the scientific return from ANTARES, we are designing the KM3NeT real-time analysis platform. It must be able to process all events with the track and cascade reconstruction algorithms from ORCA and ARCA, select in real time a neutrino sample of all flavours, receive and filter triggers from the external community, quickly search for coincidences in time/space around these alerts, provide the results, select a sample of interesting events to send alerts, manage the connections to our partner's servers, perform the CCSN analysis. Figure 6.4 shows the functional scheme of the real-time physics analysis framework. In this figure, for each process, we have also indicated the time of each step. In about 10 s, the results of both track and shower reconstructions are available. After being reconstructed, each event enters in different classifiers to select first up-going events and then neutrino tracks from the atmospheric muon background. The classifier is based on a Boost Decision Tree (LightGBM) using the parameters of the reconstruction (direction, quality, charge and number of triggered hits, etc.). The BDT is trained and tested using full Monte-Carlo simulations of ORCA 7 lines. In this simulation, two energy samples are used : one low energy, 1-100 GeV, used for the neutrino oscillation studies and one intermediate energy, 50 GeV - 5 TeV, create specifically for the astronomy. The two classifiers for neutrino tracks take in average < 1 s per event. With 6 DUs on ORCA, we are able to identify about 150 (120) neutrino candidates per day with 10 (5) % muon contamination. These events are very low energy o(10 GeV). Above 50 GeV, the numbers are $\sim$5 with 10 % contamination. With this selection, the atmospheric background contribution is reduced by a factor 2 10^5 while keeping around half of the signal. There is still room for improvements that will be done in the coming months. Figure 6.5 shows an event display for an atmospheric muon and an up-going neutrino candidate reconstructed

with ORCA. At this time, the cascade neutrino classifier has not yet been developed.

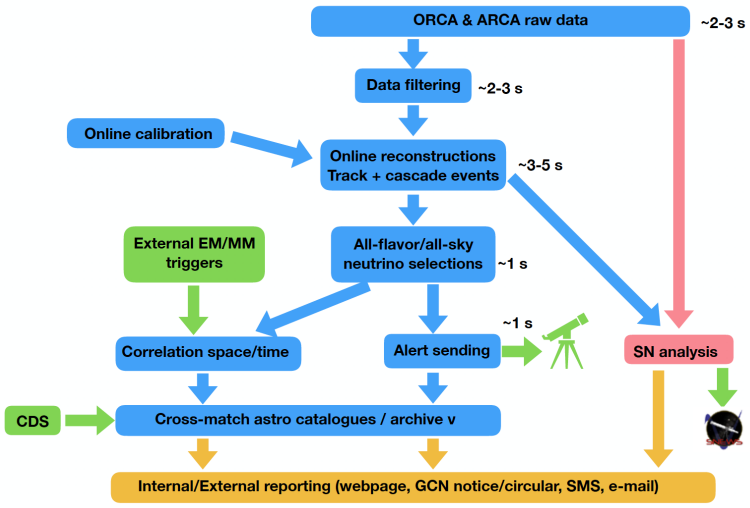

FIGURE 6.4 – Data flow diagram in the online analysis framework.

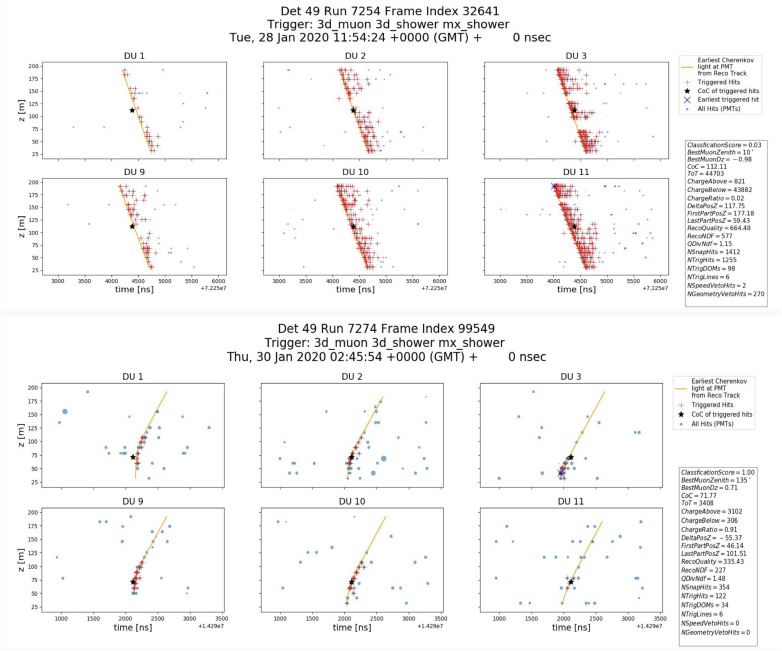

FIGURE 6.5 – Example of a muon (top) and a neutrino (bottom) event display (ORCA6). For each figure, the hits of the events (dots) are display in the altitude-time space. The line shows the reconstructed track.

The filtering and the reconstruction are using an ideal detector. In the current version, the dynamical positioning is in development in the Collaboration and

therefore cannot be used in the processing. It is a long term plan to implement a similar calibration set as in offline to reduce the differences between both samples. To facilitate the maintenance, we are using the offline reconstruction functions both to track and cascade events in the real-time framework. The code design of these algorithms have been slightly modified in order to be compliant with the event by event analyses needed for an online system. The algorithms are implemented directly in the DAQ system with separated computers to not perturb the standard acquisition system. At trigger level, the event rate of each of the two KM3NeT detectors is about 100 Hz, completely dominated by atmospheric muons (the rate of neutrinos is ∼1 mHz). To account for this large rate of events, the event reconstruction processes are distributed in a farm of several CPUs. Based on MC simulations, the number of CPUs to process online events is estimated to 400 cores per building block. A first distribution has been developed in the ORCA shore station on a single 24-core computer and is already in operation with the current ORCA 6-string detector. Figure 6.6 displays the main preliminary performances of the actual online analysis in term of processing time and of angular resolution.

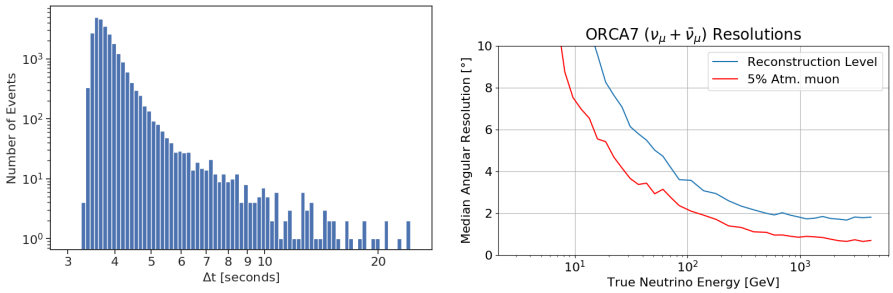

FIGURE 6.6 – Performances of the online analysis for the ORCA6 detector. Right : Median angular resolution for neutrinos vs. true neutrino energy for ORCA7 neutrino track events. Left : Processing time from the raw PMT data recorded in 6-line ORCA to the end of processing, including data filtering, track reconstruction and the event classification.

Figure 6.7 shows a detailed scheme of the architecture and the data flow of the online analysis framework. This architecture is composed of three main parts : one specific to ORCA (blue rectangle), one to ARCA (green rectangle) and one common to both detectors (red rectangle). In order to limit the huge data flow of each detector, the heavy processing is performed directly on the shore station, and it contains the event reconstructions, the classifiers and the supernova monitor (Figure 6.8). The common part contains some services (tools to make event display, event storage, monitoring and the internal/external reporting), the SN final processing processes (SN trigger, SN alert and SNEWS sender), the neutrino alert sending module and the online analysis module.

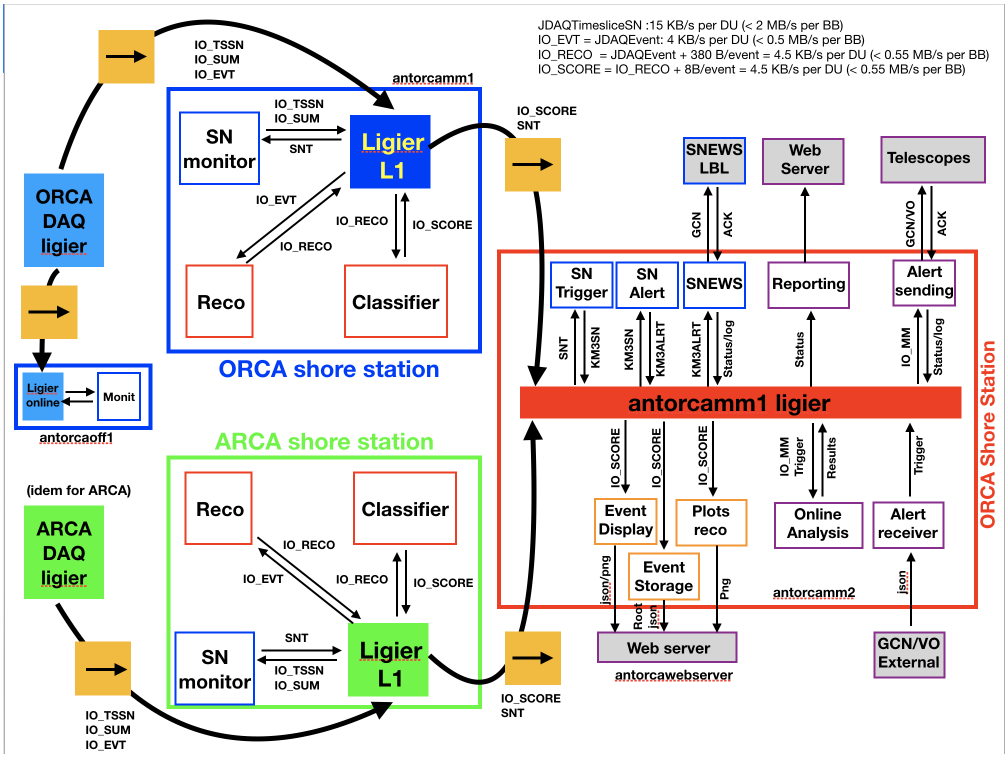

FIGURE 6.7 – Architecture scheme of the KM3NeT real-time analysis framework.

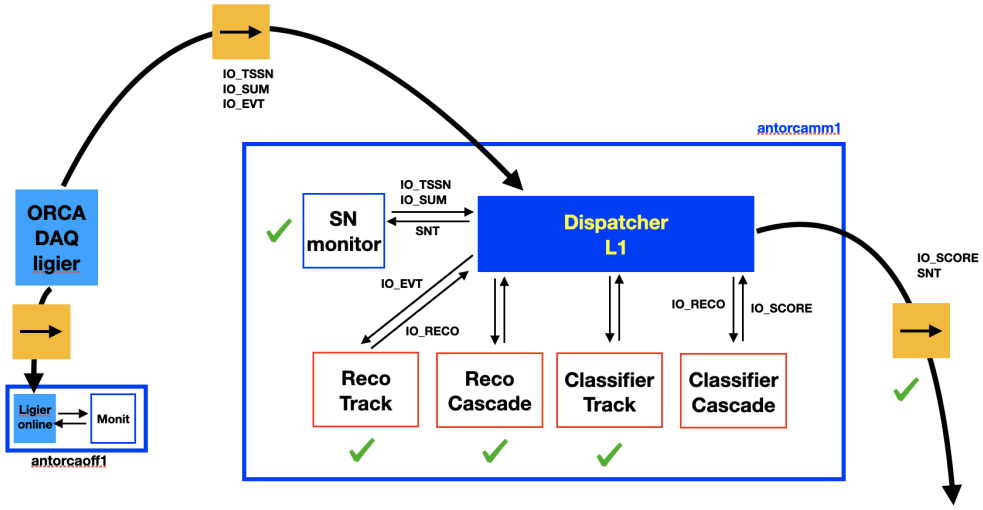

FIGURE 6.8 – Architecture scheme of the ORCA online data processing. The yellow boxes with an arrow correspond to data copy for selected data tags.

In the neutrino alert selection module is running an analysis that will select "interesting neutrino signals based on the event classification and the event parameters (energy, quality, direction, time profile, etc.) In this context, "interesting" neutrino

means a potential cosmic candidate : either a very high-energy neutrino events or a burst of multiple low-energy neutrinos. Figure 6.9 illustrates the functional scheme of the KM3NeT alert loop processing. Once selected, the alert information is gathered in a VO Event in the alert management module and the alert is sent via the COMET broker to the external facilities. The VO event and the additional event information are stored in the multi-messenger data base (MM DB) and the alert details are then available on a dedicated website for the online shifters.

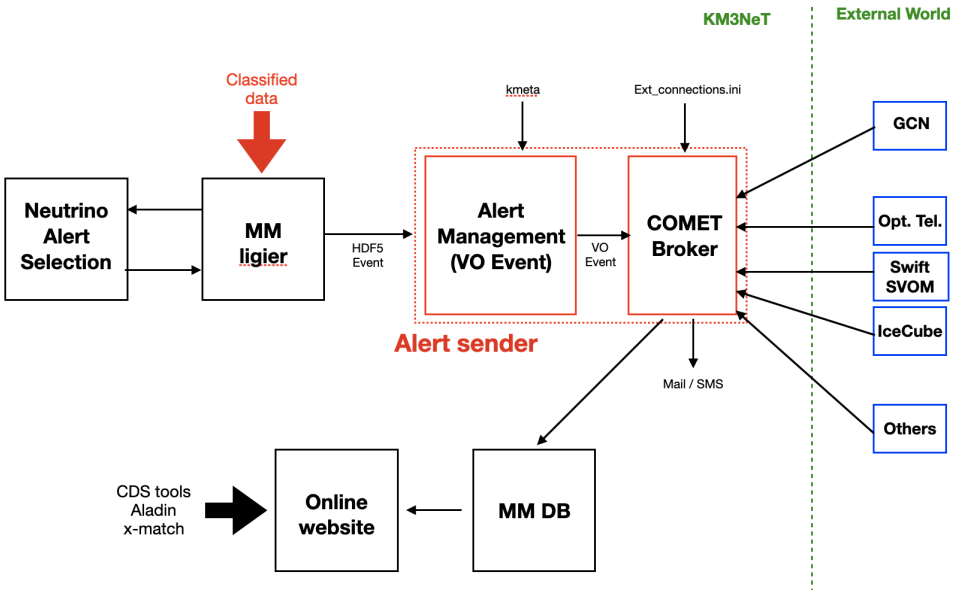

FIGURE 6.9 – Functional scheme of the KM3NeT alert loop processing.

Most of the high-energy electromagnetic alerts are transmitted via the GCN network. This network was first developed to distribute gamma-ray burst triggers from various satellites. It has been then extended to others types of sources such as LIGO/VIRGO gravitational alerts, ANTARES and IceCube neutrino triggers, others X-ray/gamma-ray transients (soft gamma-ray repeaters, tidal disruption events, etc.). The trigger distribution is performed completely automatically without humans-in-the-loop to allow the fastest dissemination. The trigger notices are transmitted either by sockets or by VO Events. A notice contains a unique ID, the alert and the notice UTC times, the astronomical coordinates and the associated error boxes and some key parameters about the events (fluence, duration, type, etc.). The typical alert rate is about few per day. Figure 6.10 illustrates the functional scheme of the external alert reception and processing in the KM3NeT online framework. The alert receiver module assures the connection to the GCN server, the reception and the parsing of the notices and a log of the notice information. An alert filter selecting only interesting triggers for KM3NeT has been implemented. This filter is using the type of sources that are promising neutrino emitters, the

visibility of the sources, the size of the error boxes, the delay between the times of the trigger and the notice reception and the false alarm rate. In the current version, we are only selecting gamma-ray burst and LIGO/VIRGO, SNEWS, HAWC and IceCube neutrino triggers for which the direction is below the KM3NeT horizon (mainly the Southern Sky). At the end of the filter module, the selected triggers are distributed to the multi-messenger message dispatcher, an application running on the computer that allows transmitting information (event file, JSON) between different applications.

A very simple analysis is currently implemented to test the analysis chain and to get quick results. It is based on a counting analysis : looking for a signal excess in predefined search angular and time windows. The background is directly extracted from the data using an off-time window prior to the signal time window. The length of the search time window is adapted to each type of external alerts. It is a compromise between the amount of background and the duration of the astrophysical phenomena. For example, for a gamma-ray burst, we are using [T0 - 250s, T0 + 750s] as time window (T0 is the time of the GRB) largely dominated by the GRB duration. The size of the search window and the final event selection are optimized together based on Monte-Carlo simulations. To not bias the analysis, this event selection criteria and the radius of the search cone are fixed in advance (like in a "prescription"). The main advantage of this type of analysis does not rely on the Monte-Carlo simulations to obtain the results. More sophisticated analysis methods based on a maximum likelihood ratio will be implemented in the future when the knowledge of the online data will improve. The trigger information and the results of the online analysis are stored in the MM DB and are available on a dedicated website for the online shifters.

Some Collaborations are not using the GCN to transmit their transient triggers. For example, the flare's activities of active galactic nuclei are distributed by others ways (Astronomer's Telegram, Fermi AGN advocates, private communication). The Transient Name Server (TNS) is also heavily used by the optical community.

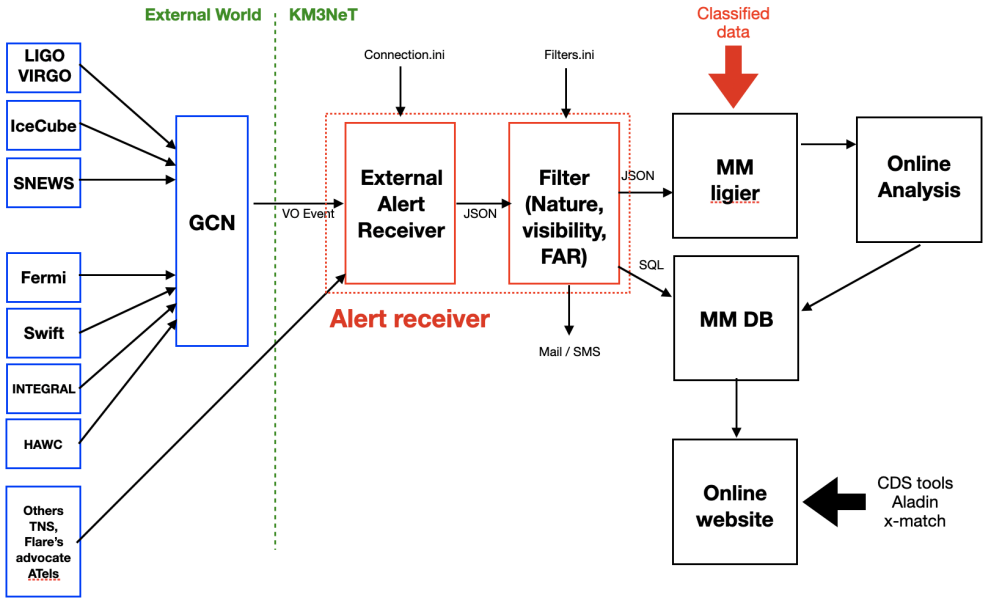

FIGURE 6.10 – Functional scheme of the external trigger online processing.

To advertise the KM3NeT online group, we have implemented an automatic mail and SMS reporting. Two mails are sent for each selected trigger : one at the reception of the notice with the main characteristics of the trigger and one after the end of the search time window with the results of the analysis. When the trigger is particularly interesting or when we have a positive correlation, SMS is sent the online group to accelerate the verification of the analysis. For the reporting task, we plan to publish some circulars to the GCN to advertise the astronomy community.

6.3 Core-collapse supernova analysis

Supernova is an explosive phenomena that may occur at the end of the life of massive stars. The explosion mechanism is not fully understood, but neutrinos play a fundamental role in it, 99 % of gravitational energy is released through neutrinos. In 1987, the first astrophysical neutrino signal was identified in coincidence with a core-collapse supernova (CCSN) located in the Large Magellanic Cloud ($\sim$50 kpc). The detection of only a few tens of neutrinos was a major discovery. More than 4000 papers have been published related to this event. With the upgraded instruments actually running or in construction, $\sim$o(10^3-10^5) neutrinos are expected for the next galactic CCSN, so the future observation of CCSN neutrinos will clearly be a major breakthrough in particle physics, astrophysics and nuclear physics.

The most recent estimate of the CCSN rate in the Milky Way is about 1-3 per century. The computation of this rate is on a particular importance for the

neutrino telescope. In the last 2000 years, less than ten galactic SNe have been detected. No detection has been reported since about 3 centuries. There are several methods used in the past to try to infer this rate based on the count of massive stars in the galaxies [235], on the count of extra-galactic SNe on similar galaxies than the Milky Way as Andromeda [236], on the ^{26}Al abundance [237], on the neutron star birth rate [238], on the historical supernova remnants [239]. A recent paper [240] has performed a combination of the rates infers by all these methods to 1.63±0.46 per century, corresponding to a time between consecutive core-collapse events, 61^{+24}_{-14} years. As this rate is so low, we must be very well prepared for the next one since the probability to get two in a human life is very very poor.

The KM3NeT ORCA and ARCA neutrino telescopes in the Mediterranean Sea are expected to observe a significant number of neutrino interactions through the detection of Cherenkov light, mostly induced by inverse beta decay (IBD) processes on free protons in the sea water ($\bar{\nu_e} + p \rightarrow e^+ + n$). This main channel accounts for $\sim$ 97 % of the detected rate in KM3NeT. IBD interactions provide sensitivity only to the $\bar{\nu_e}$ flux. Elastic Scattering ($\nu + e \rightarrow \nu + e$) and interactions of neutrinos with oxygen atoms ($\nu_e + {}^{16}\mathrm{O} \rightarrow e^- + {}^{16}\mathrm{F}$, $\bar{\nu_e} + {}^{16}\mathrm{O} \rightarrow e^+ + {}^{16}\mathrm{N}$) also provide a small contribution. The outgoing electron or positron induces the production of Cherenkov light that can be detected by the PMTs. The unique characteristics of the KM3NeT DOMs (segmented photocathode, photon counting...) facilitate the detection of the MeV neutrinos emitted by nearby supernova explosions. The classical event-by-event reconstruction methods are only working for sufficiently extended event topologies, typically with a low energy threshold of about 1 GeV. The interaction of o(10-20 MeV) neutrinos produces a charged lepton (e^+/e^-) with a track length of the order of a few centimetres (energy deposit of $\sim$0.5 cm per MeV). The detection principle relies on a coherent increase of the PMT counting rates on a large number of the DOMs in a short time window. The detection of photons in coincidence between the different PMTs of KM3NeT DOMs allows to discriminate the CCSN signal against the optical background light. Radioactive decays are responsible for a constant background hit rate of $\sim$7 kHz per PMT. Bioluminescence can cause localised and diffused increases of the hit rates, up to the MHz range. A *high-rate-veto* mechanism is adopted in the front-end electronics to discard the data of PMTs when rates are detected above 20 kHz on a 100 ms basis. The last major background contamination comes from the signal of the atmospheric muons. The long track's signature of the atmospheric muons produces multiple coincidences on different DOMs. The main criterion to reject the muons is to veto the detection of multiple causally-connected hits over different DOMs.

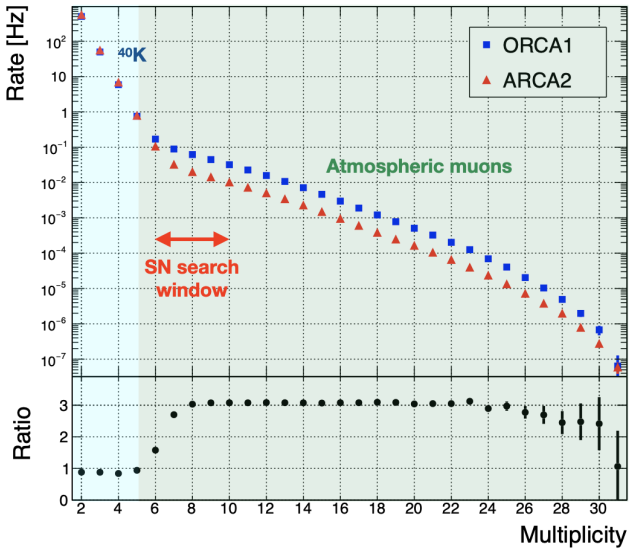

FIGURE 6.11 – Coincidence rates as a function of the multiplicity for ORCA and ARCA.

Coincidences at the few nanosecond-scales between the different PMTs of a DOM are a signature of a multi-photon emission typical of Cherenkov radiation. The number of PMTs in a DOM detecting a photon within a time window of 10 ns is later on referred to as multiplicity (M). CCSN neutrino interactions in the instrumented volume result in an increase of the counting rates of individual PMTs as well as at the various multiplicity levels. Radioactive decays in sea water and atmospheric muons are the dominant contributions to the multiplicity spectrum in the ranges $M \leq 5$ and $M \geq 7$, respectively. The contribution of coincidences from uncorrelated photons produced by bioluminescence or radioactive decays becomes negligible above $M = 3$. Atmospheric muons are mainly rejected by vetoing simultaneous detection of $M \geq 4$ events by several DOMs within one microsecond scale window. Figure 6.11 shows the coincidence rates as a function of the multiplicity for ORCA and ARCA. Note that the muon rate of ORCA is three times larger than the one on ARCA because of the different detector depths (2500 vs 3500 m). The water at both sites has the same salinity properties (i.e. similar ^{40}K contribution). Figure 6.12 shows the rejection efficiency of the atmospheric muon background computed from one building block of ORCA and ARCA.

The sensitivity of the CCSN search has been determined using state-of-the art 3D simulations from the MPA Garching group [241, 242, 243] that provides the time dependent CCSN neutrino spectrum for the accretion phase for a CCSN stellar progenitor of 11, 27 and 40 solar masses. Neutrino events are generated using custom softwares accounting for the cross-sections and the full event kinematics. The out-going leptons are then propagated in sea water with KM3Sim that takes

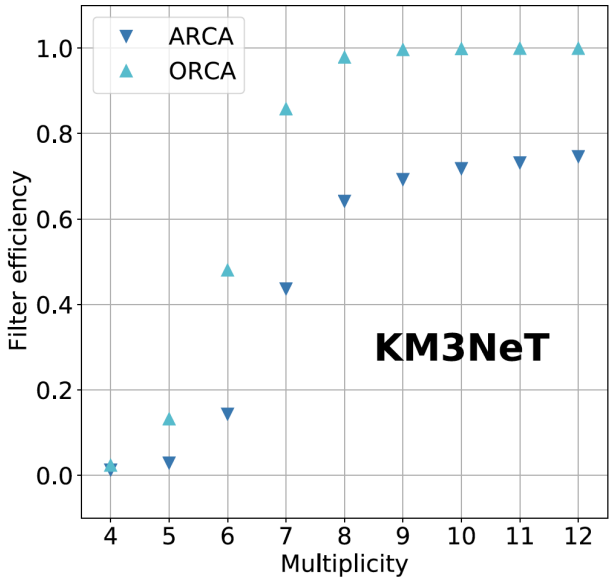

FIGURE 6.12 – Efficiency of the filter to reject atmospheric muon background, estimated with a simulation of KM3NeT ARCA and ORCA building blocks.

into account the lepton energy losses, the production of the Cerenkov light, the photon propagation in the water (absorption + scattering) and the PMT responses (angular acceptance and detection efficiency of the DOMs). Finally, the simulated photons are processed by JPP tools to reproduce the detector electronics, to filter the hits and to trigger the events. The expected number of signal events as a function of the multiplicity is shown in Table 6.1 for the 3 CCSN progenitors.

Background rates have been estimated from the data of the first ORCA and ARCA detection lines deployed in the sea. Simulations are used to optimise the multiplicity selection in order to discriminate the CCSN neutrino signal from background resulting in the criterion $7 \leq M \leq 11$. Figure 6.13 illustrates the SN

TABLE 6.1 – Expected number of signal events as a function of the multiplicity for one KM3NeT building block. Statistical uncertainties from the Monte Carlo simulation are reported.

Model	Multiplicity									
	2	3	4	5	6	7	8	9	10	11
11 $M_\odot$ (340 ms)	1119 ± 3	258 ± 1	100,4 ± 0,8	48,9 ± 0,5	25,8 ± 0,4	13,3 ± 0,3	7,2 ± 0,2	3,4 ± 0,1	1,29 ± 0,08	0,50 ± 0,05
27 $M_\odot$ (543 ms)	4806 ± 9	1120 ± 5	442 ± 3	218 ± 2	116,0 ± 1,5	64 ± 1	35,2 ± 0,8	19,4 ± 0,6	8,0 ± 0,4	1,9 ± 0,2
40 $M_\odot$ (572 ms)	15 240 ± 30	3650 ± 10	1449 ± 8	723 ± 6	399 ± 4	226 ± 3	127 ± 2	69,5 ± 1,8	36,6 ± 1,3	15,0 ± 0,8

expectation for the simulated signal for the 11 $M_\odot$, 27 $M_\odot$ and 40 $M_\odot$ models.

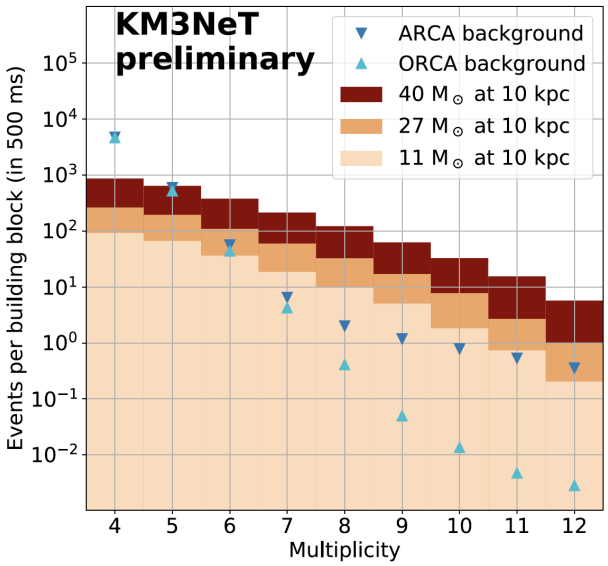

FIGURE 6.13 – Detected coincidence rate as a function of the multiplicity. Background rates are shown with points in light blue (ORCA) and dark blue (ARCA). Signal rates averaged over the duration of the simulation are shown as bars colored in shades of orange for the different models : light for 11 $M_\odot$, intermediate for 27 $M_\odot$, dark for 40 $M_\odot$.

.

The number of signal and background events at 10 kpc after the background filter and the multiplicity selection, together with the detection sensitivities, are given in Table 6.2 for each progenitor and for the two KM3NeT detectors. In Figure 6.14, the sensitivity of the combination of the KM3NeT ORCA and ARCA detectors is reported as a function of the distance to the source for the three considered progenitor models. The error bars include the systematic uncertainties on the PMT efficiency (±10 %), the active PMT fraction (±3 %), the filter efficiency (±15 %), the absorption length (±1 %), the IBD/ES cross sections (<1 %). The results of the more pessimistic scenario (11 $M_\odot$ progenitor), show that about 95 % of the Galactic CCSN Supernova progenitors can be observed by the KM3NeT detectors, taking into account the CCSN probability as a function of the distance in [244]. For the failed CCSN (ending in a black hole for the most massive supernovae), the detection reaches the Large Magellanic Cloud galaxy at about 50 kpc. Even with a reduced configuration, the ORCA 6-DUs has a 5σ discovery potential at 9 and 4 kpc for the heaviest and lightest progenitors, respectively.

TABLE 6.2 – Expectation values for the number of background and signal events after the background rejection in the 7-11 multiplicity selection, for ARCA and ORCA. The signal is given for a CCSN at 10 kpc. The corresponding sensitivity for each detector and progenitor is provided.

Progenitor mass	ARCA			ORCA		
	N_b	N_s	$\sigma_{10\ kpc}$	N_b	N_s	$\sigma_{10\ kpc}$
11 $M_\odot$	22.1	72.2	11	4.9	36.1	10
27 $M_\odot$	22.1	240	29	4.9	120	24
40 $M_\odot$	22.1	895	71	4.9	447	57

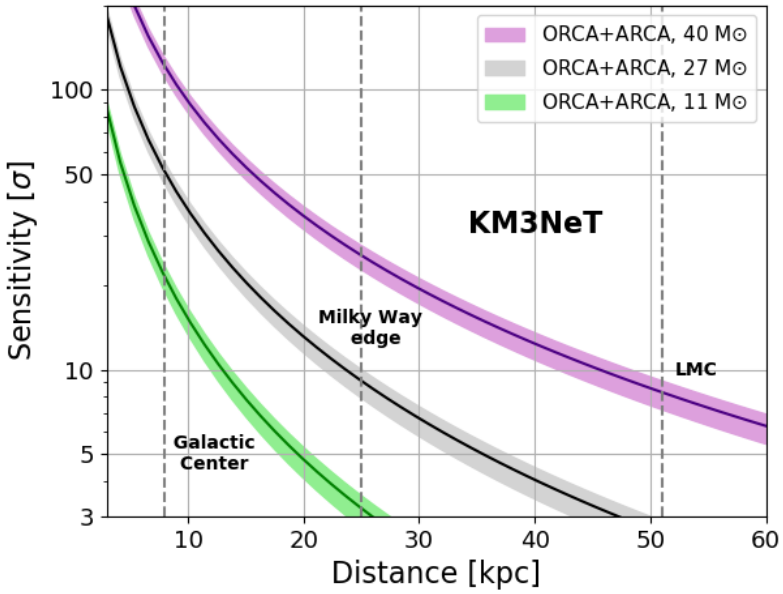

FIGURE 6.14 – KM3NeT detection sensitivity as a function of the distance to the CCSN for the three progenitors considered : 11 $M_\odot$ (green), 27 $M_\odot$ (black) and 40 $M_\odot$ (purple). The error bars include the systematic uncertainties.

In the online analysis framework, we have also developed a real-time CCSN analysis to handle the triggering of real-time alerts and the participation in the SNEWS (Supernova Early Warning System) network [245]. A dedicated data stream containing all coincidences above multiplicity M $\geq$ 4 is continuously acquired for online monitoring and permanent storage. The same data stream is simultaneously analysed in real time for the purpose of alert generation. Figure 6.16 illustrates the functional scheme of the CCSN analysis. The CCSN analysis will analyse in

real-time the SN streams of both ORCA and ARCA to look for a combined excess on the 7-11 multiplicity rate. If this rate surpassed the pre-defined threshold, a SN alert is emitted. It contains the time of the first time-slice (with a 100 ms uncertainty) and the combined significance. The threshold is fixed to obtain a corresponding false alarm rate (FAR) to 1 event every 8 days required by SNEWS. This first alert message is automatically transmitted in less than 20 s to the SNEWS server in Brookhaven to look for a coincidence with others neutrino detectors. In parallel, this alert triggers the DAQ to buffer all L1 data during a given period (for example, $\pm$10 minutes). The design concept is based on a common dispatcher used by multiple clients to receive and send data, making the outputs of all the processing stages simultaneously available to any client (Figure 6.16). This structure allows for the building of flexible and extensible data processing pipelines. These low-level data are then analysed by the quasi offline analysis to build the detected neutrino light-curve with 1 ms precision. Further applications will analyse this neutrino light curve to estimate the time of arrival (T_0). The time T_0 and the light-curve will then be transmitted to SNEWS in a second alert message in typically less than 10 minutes. This is of interest because the information, when combined with other detectors, can be used to determine the source localisation by triangulation [246, 247]. In addition, the relative start time of the electron anti-neutrino signal is tied to the flavour conversion processes in the star, in turn dependent on the neutrino mass ordering. Figure 6.15 gives an example of the fit of the rising-edge of the neutrino light-curve. The T_0 is then inferred from the fit results. At 8 kpc and for a 20 $M_\odot$, the time uncertainty is around 10 ms, reaching $\sim$5 ms for an equivalent source at 5 kpc. For a lighter progenitor, this uncertainty becomes larger, $\sim$9 ms at 5 kpc.

The CCSN analysis can also be triggered by an external trigger provided by SNEWS. This alert will be processed similarly as a self-generated alert. The analysis is supervised by the SN group of KM3NeT that will validate the analysis and then alert the SN decision group (which includes the KM3NeT management, the Multi-Messenger Coordinator and the head of the Publication Committee) that will decide if the results are worth to report to the Collaboration and to the public via a GCN circular. This decision should be made within 12 hours since the trigger. At the end, the self-generated or received alert and the results of the analysis will be stored in the MM database (MM DB).

This CCSN analysis is currently in operation with the ORCA 6-DUs detector. The current configuration allows for an alert to be produced within 20 seconds from the generation of the corresponding data offshore, a fast response compared to the current SNEWS latency.

With the maximum event statistic using all the coincidences ($M \geq 2$), it is possible to compute the detected neutrino light-curve with 1 ms time resolution.

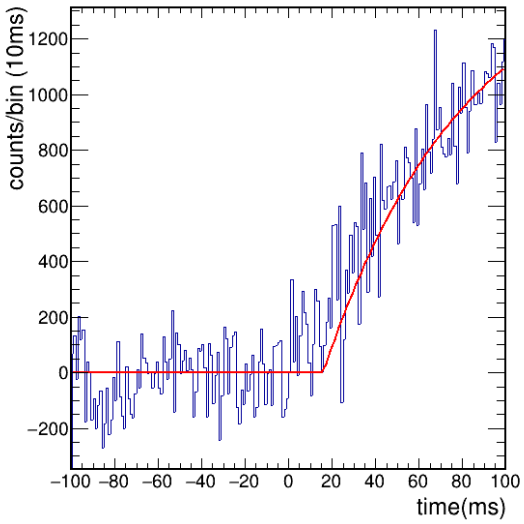

FIGURE 6.15 – Expected time distribution of the events (neutrino light-curve) for ARCA using all coincidences, assuming a 20 $M_\odot$ CCSN progenitor at 5 kpc.

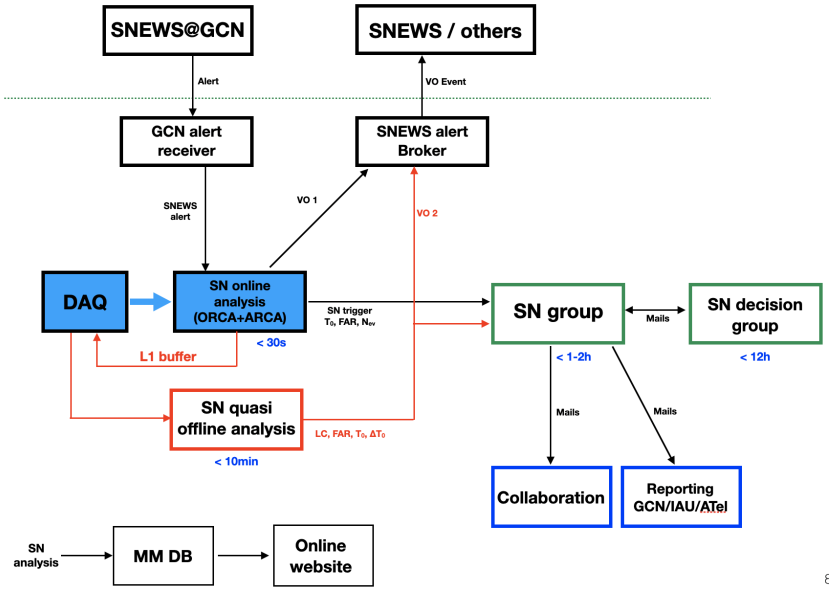

FIGURE 6.16 – Functional scheme of the CCSN analysis.

As reported before, it is used to estimate the time of the explosion and for the triangulation [247]. The SASI (Standing Accretion Shock Instability) oscillations are predicted to be developed fast and asymmetric hydrodynamic motions in the core during the accretion phase [241] in the state-of-the-art three-dimensional simulations of CCSNe. This phenomena produce oscillations of the core that can be

seen in the time profile of the neutrino emission. Figure 6.17 displays the simulated neutrino light-curves expected for a 20, 27 and 40 $M_\odot$ CCSN progenitors. The predicted SASI frequency is ∼80 Hz for the $20M_\odot$ and $27M_\odot$ progenitors, and of 140 Hz while for the 40 $M_\odot$ failed CCSN. A dedicated analysis has been developed in the KM3NeT SN group based on the Fourier transform of the neutrino light-curve. Depending if we applied a blind search or a search assuming a prior on the SASI frequency, the typical 3σ sensitivity is reached at distances between 3 and 5 kpc, depending on the progenitor models.

One other interesting characteristic of the CCSN physics is the neutrino energy spectrum. Following [242], the CCSN neutrino energy spectrum can be described with three parameters : the normalisation of the flux, Λ, the mean energy and the pinching parameter, α. Using the fact that the multiplicity distribution of coincidences dependents on the flux spectral features (Figure 6.18). In particular, higher energy events tend to produce more photons and be detected at higher multiplicity. The capability to estimate the mean energy of the neutrino has been evaluated using a chi-square method in an offline analysis. The results are the following : the precision on the mean energy is about 0.25 MeV (corresponding to ∼2% energy resolution) when α and Λ are fixed, and stays below 0.5 MeV if these two parameters are known with a 10% uncertainty. In the latter case, the determination of the pinching parameter is not reliable anymore, as the fit reaches the edges of the allowed range. If Λ and α are left free in the fit, the results indicate that the sensitivity is completely lost.

As said before, the CCSN events are very rare, there is probably only once-in-a-generation opportunity. So, it requires a coincidence between few neutrino detectors to be sure that there is a detection. This search of coincidence is performed by the SNEWS network. This observation by multiple neutrino detector worldwide can provide a clear supernova signal, providing an early warning for the subsequent electromagnetic follow-ups as well as informing others neutrino detectors with significant backgrounds to store their recent data. SNEWS requires that at least two neutrino detectors identify a signal within 10 s. If the alert has a false alarm rate larger than one per century, an alert message is sent publicly to the worldwide community within minutes. This alert is distributed through the GCN or via dedicated private channels with specific experiments. SNEWS is operational since 2005 and Super-Kamiokande, LVD, IceCube, Borexino, KamLAND, HALO and Daya Bay are involved (NOvA, KM3NeT and Baksan are in a test mode and will join soon).

Since SNEWS was established, the particle astrophysics and the multi-messenger landscape has evolved considerably. In this new area, false alarms are acceptable, reporting low-probability events will increase the detection potential. Moreover, neutrino detector technologies and data analysis techniques have progressed. It is now common to analyse the data in real-time and be able to not only trigger for a Galactic supernova, but also to provide details on the signal (light-curve, position...). This new paradigm has triggered the recent upgrade of the SNEWS

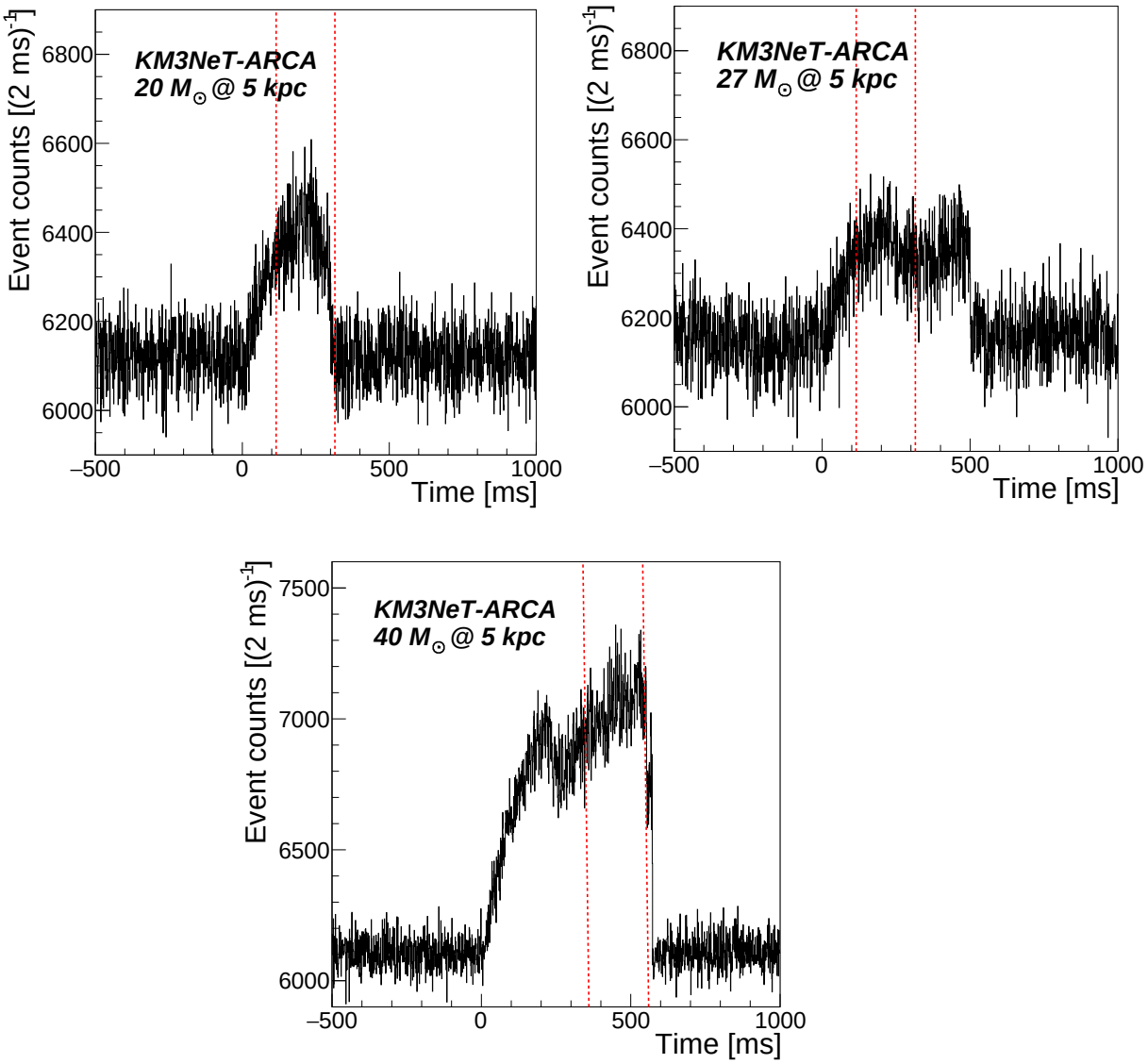

FIGURE 6.17 – Detected neutrino light-curves in the full ARCA detector. On the top for a source at 5 kpc, for the 20 $M_\odot$ (right) and the 27 $M_\odot$ CCSN progenitors (left). On the bottom, for a failed CCSN of 40 $M_\odot$ at 5 kpc. The dashed red lines indicate the domain of the applied Fourier transform.

system to SNEWS2.0. This new system is in development and will probably become operational in 2021. The main goals of SNEWS 2.0 are :

— Lowering the threshold for generating alerts and thus increasing the reach in distance and flux sensitivity ;

— Reducing the alert latency ;

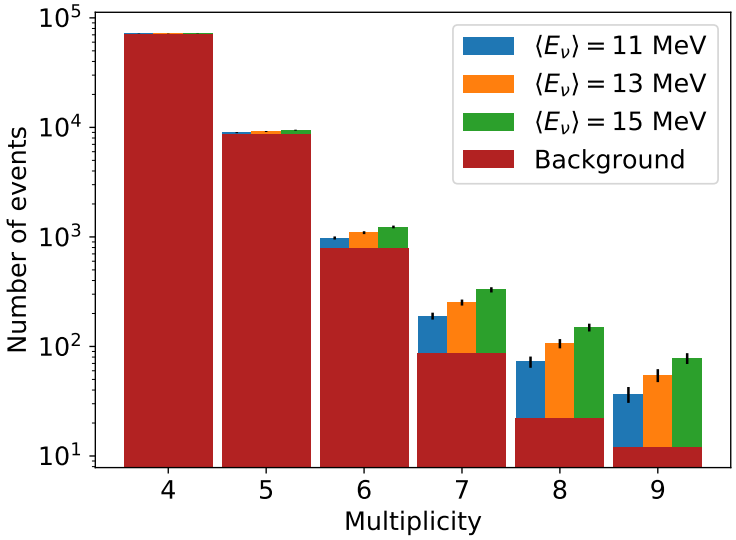

FIGURE 6.18 – Expected multiplicity distribution of detected events in ARCA and ORCA detectors for CCSN $\bar{\nu}_e$ spectra having mean energies of 11, 13 and 15 MeV, $\alpha = 3$ and $\Lambda = 1$. The number of events due to the background of the detector is drawn in red.

— Enhancing the pointing ability by combining information from individual experiments with triangulation via timing differences between detectors ;
— Implementation of a pre-supernova alert (lower neutrino energy, $\sim$ a few MeV) based on the rising neutrino flux which precedes core-collapse. Its detection is limited to nearby stars, at distances up to $\sim$1 kpc ;
— Development of a follow-up observing strategy to prepare the astronomical community ; and engage amateur astronomer through alert dissemination.

To achieve these goals, it requires the sharing of the trigger but also detailed information on the neutrino signals such as a very precise estimation of the time of the explosion and event the neutrino light-curve with at least 1 ms time resolution. In the KM3NeT SN group, we have developed a new method to combine the experimental neutrino light-curves coming from different neutrino detectors to infer the location of the next Galactic supernova [247]. This approach is based on the determination of the arrival time delay of the neutrino signal at different experiments using a direct neutrino light-curve matching. The arrival time delay and its uncertainty between two neutrino detectors are estimated with chi-square and cross-correlation methods. A direct comparison of the detected light-curves offers the advantage to be model-independent. Millisecond time resolution on the arrival time delay at two different detectors is needed. Using the computed time delay between different combinations of currently operational and future detectors, a triangulation method is used to infer the supernova localisation in the sky. The combination of IceCube, Hyper-Kamiokande, JUNO and KM3NeT/ARCA provides

a 90 % confidence area of 140±20 deg^2 (∼70 deg^2 at 1σ level). Figure 6.19 shows the inferred location of a CCSN at the Galactic Center using the 4 neutrino detectors. This location uncertainty can be reduced further by intersecting this area with the CCSN progenitors distribution in the Milky Way and combining with the confidence areas from the Super-Kamiokande and JUNO detectors performing stand-alone source localisation. These low-latency analysis methods will be implemented in the SNEWS2.0 alert system.

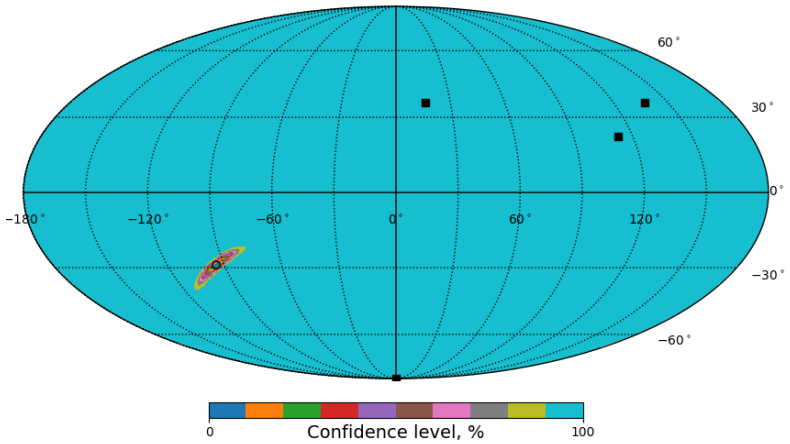

FIGURE 6.19 – Confidence area in equatorial coordinates for a CCSN at the Galactic Centre (black dot) computed using triangulation between four detectors : IceCube, KM3NeT/ARCA, Hyper-Kamiokande and JUNO. Their positions are indicated by the black squares.

6.4 Perspectives

The construction of the KM3NeT detection lines has just started at both sites. ORCA has started to take multi-line data on Feb 19 2018 with 2 lines. On Feb 17 2019, 2 more new lines have been added to the network and finally 2 additional lines have been deployed end of January 2020 completing the phase 1 of the ORCA project. 4 new strings are expected to be deployed beginning of 2021. In the coming years, new DUs will be connected to reach 115 lines to complete the building block in 2025. ARCA has already taken some data with 1 and 2 lines in 2018. An upgraded of the seafloor network has prevented to add more strings. It is planned to resume the ARCA data taking beginning of 2021 and start to add additional DUs mid 2021 to reach the completion in 2027. With the early data, we have performed a lot of studies to understand the behaviour of the detectors by setting the calibration procedures and by implementing very detailed Monte Carlo simulations that reproduce quite well the data taking. With the ORCA4 and ORCA6 detectors,

we have started to develop the online analysis framework. Most of the elements are in operation (online reconstruction, neutrino classifier, reception of external transient triggers, alert sending). We are in a phase of deep test using the muon neutrino track channel. The implementation of the cascade reconstruction and selection have just started and probably more DUs are needed to better tune the parameters (due to the event containment in the instrumented volume). Once the analysis performed will be completed and we will have a sufficient number of string sin operation, we plan to start to follow the main transient and multi-messenger triggers in an automatic way and to send first neutrino alerts to our main partners based on the neutrino track selections both with ORCA and ARCA. We will not only send single high energy events, but also double/triple coincidences of neutrino candidates coming from the same direction and in a given time window. As these criteria require a large event statistic, it is more adapted to low energy neutrinos. When we will have more working lines in both sites, we will start to define more advanced neutrino selection to be all-flavor and all-sky.

6.5 KM3NeT online and SN groups

Most of the work on the implementation of the KM3NeT online analysis platform has been performed with two postdocs, G. Maggi [2017-2019] and F. Huang [2018-2020] and two engineers at CPPM, M. Ageron and W. Assal. This work is done also with the support of the DAQ and software working group of KM3NeT.

For the supernova analysis, we have built a KM3NeT SN group composed of V. Kulikovskiy, A. Coleiro and myself with two PhD students : M. Colomer-Molla (APC) and M. Lincetto (CPPM). Within this group, we have studied the CCSN science cases for KM3NeT and implemented a real-time analysis to look for low energy neutrino. There are 2 publications :

— A. Coleiro, M. Colomer-Molla*, D. Dornic, V. Kulikovskiy*, M. Lincetto, *Combining neutrino experimental light-curves for pointing to the next Galactic Core-Collapse Supernova*, Eur.Phys.J.C 80 (2020) 9, 856, arxiv :2003.04864.

— The KM3NeT Collaboration, *Core-Collapse Supernova neutrinos with KM3NeT*, to be submitted.

— SNEWS 2.0 : A Next-Generation SuperNova EarlyWarning System for Multi-messenger Astronomy, to be submitted

7 SVOM : a transient catcher and a multi-wavelength observatory

7.1 SVOM

The aim of SVOM (Space-based multi-band astronomical Variable Objects Monitor) is to continue the exploration of the transient universe with a set of space-based multi-wavelength instruments, following the way opened by Swift. SVOM [183] is a space mission developed in cooperation between the Chinese Space Agency (CNSA), the Chinese Academy of Science (CAS) and the French Space Agency (CNES), which is dedicated to the detection, localization and study of GRBs and other high-energy transient phenomena (X-ray bursts, soft gamma repeaters, AGN, novae, etc.). The launch date is expected mid 2022 with a nominal mission lifetime of 3 years plus 2 years of extended mission.

The system is based on an instrumental setup comprising 4 instruments on-board the satellite and 3 instruments on the ground (Figure 7.1). Fast communications from the satellite to the ground are ensured with a VHF emitter on-board and a dedicated network of ground receivers. The instrumentation in space includes ECLAIRs, a coded-mask γ-ray imager and spectrometer (4 - 150 keV, FOV = 89×89°), GRM, a γ-ray spectrometer (15 keV - 5 MeV), MXT, a low-energy X-ray telescope (0.2 - 10 keV, FOV = 1×1°), and VT, a 40-cm optical telescope (FOV = 26×26 arcmin). The ground instruments are based on two 1-m Ground Follow-up Telescopes (GFTs) and GWAC (Ground Wide Angle Camera). Figure 7.2 shows the spectral and time coverage of each SVOM instrument as a function of the time for a GRB trigger.

SVOM satellite will be put in an orbit at ∼600 km altitude with a slight inclination to avoid the disturbances existing in the polar areas. The duration of one orbit is 90 min. In order to facilitate measuring the redshifts of GRBs detected by ECLAIRs, the instruments of SVOM will be pointed close to the anti-solar direction. Most of the year, the optical axis of the SVOM instruments will be pointed at about 45° from the anti-solar direction. This pointing is interleaved with avoidance periods during which the satellite passes away from the Sco-X1 source and the Galactic Plane (B1 attitude law). This strategy ensures that SVOM GRBs will be in the night hemisphere and quickly observable from the ground by large telescopes.

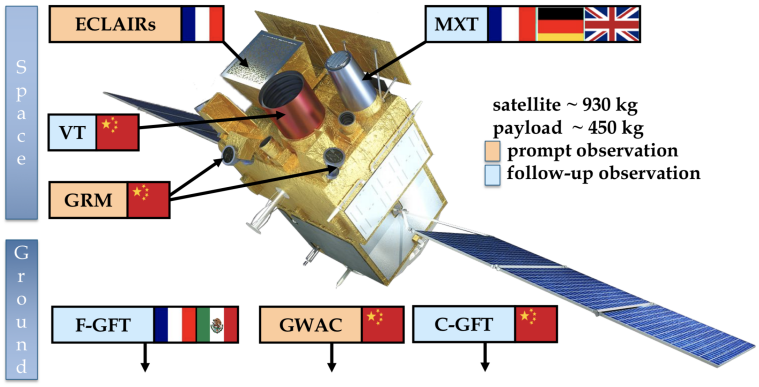

FIGURE 7.1 – Schematic view of the SVOM spacecraft with its multi-wavelength instruments.

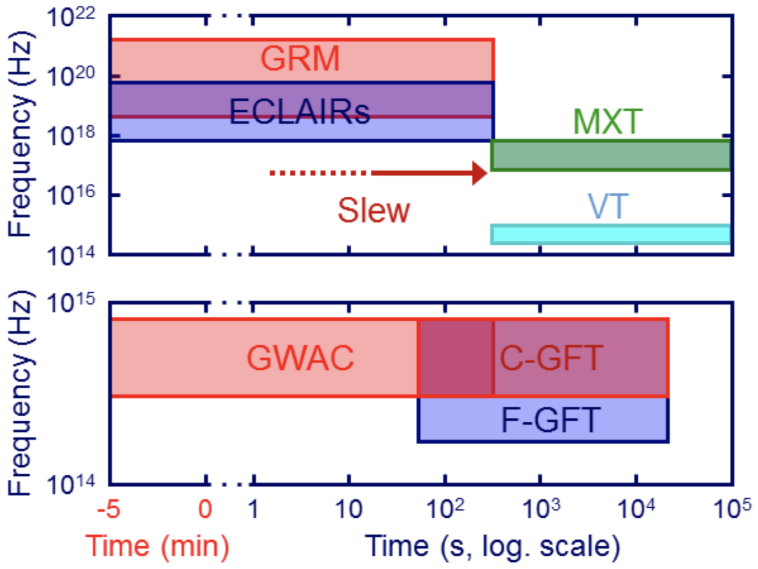

FIGURE 7.2 – Spectral coverage of the GRB prompt emission and its afterglow with SVOM instruments, as a function of time.

As GRBs are transient phenomena with the flux varying rapidly, the time is a key issue in the SVOM observing strategy. The burst is first detected by the wide-field instrument ECLAIRs (with an error box of 13 arcmin radius) then an alert is transmitted to the ground in less than one minute via the VHF network (45 ground stations distributed around the Earth below the orbit) for the observation by the dedicated robotic telescopes as well as the large ground telescopes. In the mean time, for very bright bursts, the satellite is able to reposition itself very quickly to complete the observations in the soft X-ray domain with the MXT and in the visible domain with the VT. This slew lasts around 5 minutes. The MXT

and VT instruments continue to follow the burst during 14 orbits. On the ground, the telescopes are directly receiving the alert message and can start the observation less than one minute after the trigger if the direction is directly observable. The information provided by the ground instrument is crucial to confirm the transient nature, reduce the error box of the burst localisation and identify quickly if the burst is at large distance. If the burst is interesting, the follow-up group may decide to trigger large telescopes such as VLT, GTC, Keck in order to measure the redshift and characterise the environment of the burst.

The success of the Swift mission for catching GRBs and others transients relies on the unique combination of space agility, fast communication with ground, multi-wavelength observing capability, and long lifetime. These capabilities have permitted the detection of nearly 1000 GRBs and the measure of 300 redshifts. The SVOM mission intends to follow the path of Swift being the satellite, which detects the GRBs. The main improvement of SVOM compared to Swift is mainly a better synergy between the instruments on-board the satellite and the ground observatories with the development of three facilities (GWAC, C-GFT, F-GFT) performed by the Collaboration. Moreover, the anti-solar altitude law of the satellite maximises the follow-up probability by the robotic telescopes. Within a mass and volume significantly lower than Swift (500 kg vs 1500 kg), SVOM will locate 70-80 GRBs/yr, allowing to measure >40 redshifts/yr (vs 30/yr for Swift) thanks to a pointing strategy optimized for GRB follow-up with large telescopes on Earth. The low-energy threshold of ECLAIRs has been adjusted at 4 keV (15 keV for Swift/BAT) increasing the detection of soft GRBs like X-ray rich GRBs or X-ray flashes and highly redshifted GRBs. This low energy threshold and the improve sensitivity below 20 keV (×3 at 10 keV) will particularly improve the access to the soft population for which Swift is not well suited. This is especially interesting in connection with the identification of associated supernovae with some of these bursts. As said before, the low-energy threshold is of prime importance for the detection of very high redshift GRBs. Simulations indicate that ∼15 GRBs at z>5 can be detected during the nominal duration of the mission (3 years) compared to only 8 for Swift in nearly 10 years of mission. Moreover, SVOM combines a very good spectral coverage of the prompt gamma-ray emission (4 keV – 5 MeV), which allows with a single mission to characterize the energy spectrum, in particular the parameter E_{peak}. Following the burst on many consecutive orbits will allow detecting ultra-long GRBs like the 15000 s for GRB111209A at z=0.677. The VT will have also a higher sensitivity compared to the UVOT instrument on-board of Swift (x10 in the visible) providing accurate positions for more than 70% of the GRB.

The SVOM observing program will consist on the Core program (GRB detection and follow-up), the Target of Opportunity (ToO, alerts from outside world) and the General program (others sources follow-up such as AGN, X-ray binaries, etc.). While GRBs will occupy a small fraction of the SVOM observing time, the broad

wavelength coverage and good sensitivity of the on-board instrumentation allows performing non-GRB sciences on selected topics during the remaining time such as Earth environment studies, supernovae and galaxy observation, X-ray survey, etc. Nominal ToO can be proposed to the SVOM PIs and, if accepted, it should be performed within 48h. ToO are used generally for unplanned observations. The goal is to devote at least 15% (1 ToO/day) of the useful lifetime of the nominal mission to the ToO observations and at least 40% (5 ToO/day) in case of the extended mission. For very fast "interesting" alerts, a subclass, ToO-EX (exceptional) can be processed as soon as possible (average delay of 12h). Finally, a third class of ToO, ToO-MM has been introduced for the follow-up of non-well localized alerts, such as the one of the gravitational wave and the neutrino ones. It relies on tiling to cover large error boxes. Figure 7.3 illustrates the time sharing of the 3 main observing programs for the nominal and the extended scenarios. The extended mission (3 years after the launch) involves a higher ToO fraction and more GP time outside the B1 law (from 10% to 50%).

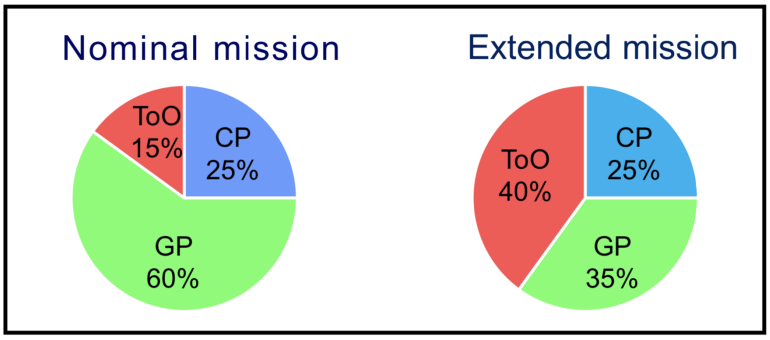

FIGURE 7.3 – Allocated observation-time fraction of the three SVOM scientific programs : Core Program (CP), Target of Opportunity Program (ToO), General Program (GP).

7.2 The COLIBRI telescope

One of the key instruments of the ground follow-up involves a robotic 1-m class ground telescope equipped with a panchromatic camera, allowing simultaneous observations in the visible and near infrared domains. This Ground Follow-up Telescope (GFT), named COLIBRI (Figure 7.4), will have several unique features : very high availability for alert observations, very good sensitivity (1.3 m mirror diameter), fast pointing speed (on target in less than 30 sec), multi-band photometric capability (from 400 to 1700 nm), and a field of view covering the SVOM trigger error box (26 arcminutes). It will be installed in 2021 in the OAN (Observatorio Astronòmico Nacional) site located in North of Mexico, at an altitude

of 2800 m. The COLIBRI project is joint between French and Mexico. It involves several partners in France (CEA, CPPM, IRAP, LAM, OHP) and Mexico (UNAM).

FIGURE 7.4 – Picture of the COLIBRI mount.

COLIBRI will be unique in the world level as no other telescope with such capabilities exists or is in construction and will play an important role in the SVOM strategy :

— Its global response time allows it to start very quickly the observations (< 30 s). It will become possible to study the mechanisms associated with the prompt emission and also the transition between the prompt and the afterglow emissions.
— Its sensitivity in the infrared domain is also unique. It will become possible to search for the so-called dark GRBs, which are events detected in the X-ray domain but not in the optical domain.
— It also plays an important role in the SVOM overall system by providing photometric redshifts and then by identifying the highest ones. It will in particular be possible to activate very large telescopes (NTT, VLT...) immediately from the GFT, which is critical for the cosmological bursts.
— This facility will provide a service to astroparticle, as it could be used to search for the EM counterparts of high-energy neutrinos detected by KM3NeT, or of gravitational wave candidates detected by advanced LIGO and Virgo.

7.3 Optical follow-up of SVOM and MM triggers

COLIBRI will have a follow-up efficiency of about 18 % in prompt raising to 66 % integrated over 24 hours for the SVOM detected GRBs. Figure 7.5 shows these efficiencies as a function of the delay between the GRB and the observation. These efficiencies have been computed on the simulated GRB detection between 2020 and 2050 provided by the CNES consisting of about 55 GRBs per year. This calculation takes also into account the observing conditions of the telescope : elevation of the GRB direction larger than 15°, the Sun elevation lower than -15°, the moon elevation lower than 0 or the distance between the moon and the GRB directions larger than 30°. Two scenarios have been studied : 100% and 76% availability. This latter case simulated the dead-time of the telescope, which includes 10% maintenance, 15% bad weather (10% in Spring and Autumn and 20% in Winter and Summer). As it is very difficult to look for optical sources in the Galactic plane due to the dust absorption, the case with a Galactic cut |b|>10° is also studied. Figure 7.6 summarizes the results of this efficiency study. Once it has started to observe, the typical duration of the observations is around 8 hours (Figure 7.7). These probabilities will be increased adding the Chinese telescopes of SVOM (C-GFT and the GWAC), by typically a factor ∼2.

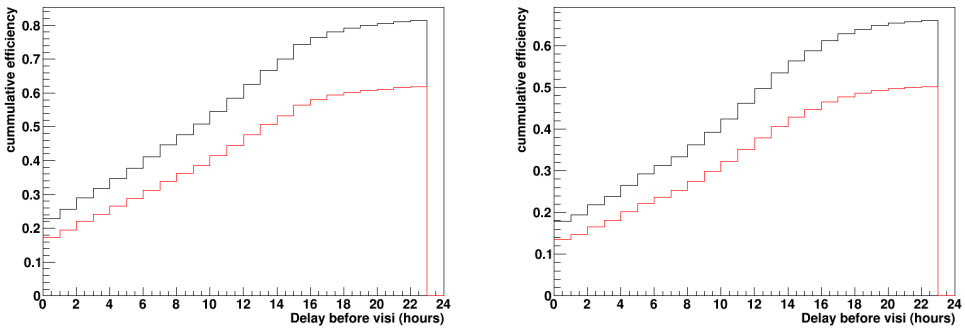

FIGURE 7.5 – Follow-up efficiencies as a function of the delay between the GRB and the optical observation for both the nominal (left) and extended (right) mission scenarios. The black and red curves correspond to the 100% and 76% availability, respectively.

Figure 7.8 shows the limiting magnitudes reached by the telescope [248]. COLIBRI will detect the vast majority of GRB afterglows, including those of short GRBs and those of dark GRBs (with CAGIRE). Due to the fast decay of GRB afterglows, their quick localization is essential for their spectroscopic follow-up with the largest facilities. Arriving in the first minute after the trigger, it will permit to study the transition between the prompt emission and the afterglow and to assess the role of the reverse shock, with a temporal resolution of few to several seconds. The afterglows of GRBs that are not immediately visible can still be detected with

	Nominal Mission Phase					
	F-GFT Availability 81% (Sp+A) +72%(W+S)		F-GFT Availability 76%		F-GFT Availability 100%	
F-GFT %GRB Access	With galactic equator	Without galactic equator	With galactic equator	Without galactic equator	With galactic equator	Without galactic equator
Immediate only	17.8	18.8	17.3	18.4	23.6	24.1
Immediate and	62.3	66.6	61.8	66.1	81.3	87.0

	Extended Mission Phase					
	F-GFT Availability 81% (Sp+A) +72% (W+S)		F-GFT Availability 76%		F-GFT Availability 100%	
F-GFT %GRB Access	With galactic equator	Without galactic equator	With galactic equator	Without galactic equator	With galactic equator	Without galactic equator
Immediate only	13.8	17.8	13.6	17.5	17.8	23.1
Immediate and	50.4	62.3	50.3	62.0	66.1	81.5

FIGURE 7.6 – Results of this efficiency studies.

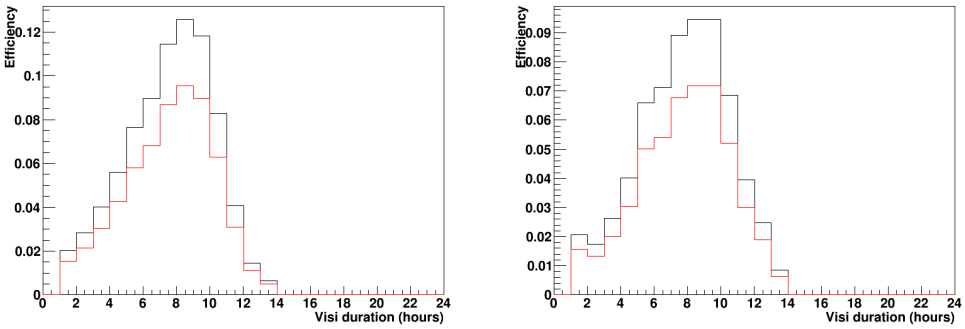

FIGURE 7.7 – Distributions of the duration of the observations for the SVOM GRB triggers for both the nominal (left) and extended (right) mission scenarios. The black and red curves correspond to the 100% and 76% availability, respectively.

observations starting a few hours after the burst.

7.4 COLIBRI softwares

In this section, the software tools of COLIBRI are described. The main component is named Telescope Control System (TCS) under the responsibility of UNAM. TCS is the heart of COLIBRI, it will control the telescope, the instruments and the dome ; monitor conditions and determine when to open and close ; select and execute observing blocks ; manage alerts ; archive the data in the local data storage. The observing blocks are provided by a dedicated scheduler (LAM task).

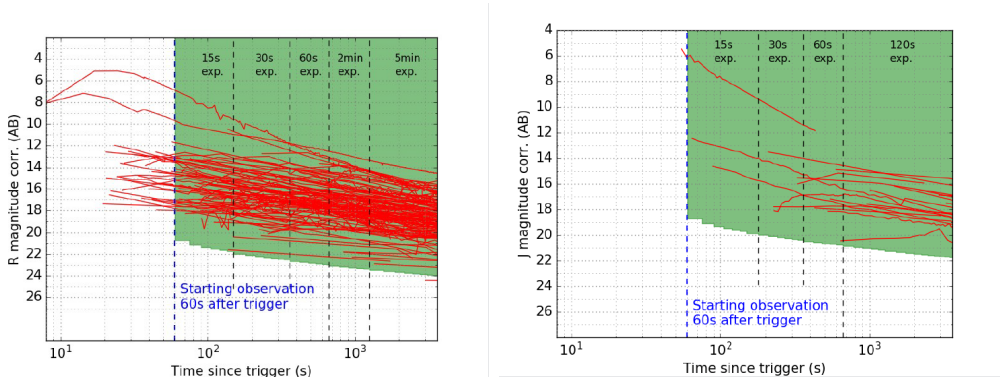

FIGURE 7.8 – Sensitivity of the GFT (5 sigma limit, green area) in the infrared (left) and visible (right) arm [248]. The light curves of ancient bursts are also given for reference (red lines). The observations begin within 60 seconds after the detection on-board the satellite (delay to transmit the alert to the GFT : 30 sec, delay for the telescope to start an observation : 30 sec).

It will take the observing requests of the astronomers, verify its feasibility and if there are validated by the Time Allocation Committee (TAC), translate them in observing blocks. The list of observing blocks are then scheduled according to their priorities and visibilities. The schedule is performed again after each observation to take into account the fast varying conditions due to the weather changes or alert interruptions. The PLC (Program Logic Controller), provided by OHP, is an automaton that that will control the safety of the observatory : safety of persons (anti-intrusion in robotic observation, emergency buttons) and of material in case of environmental events (weather, power failure...). For this, the PLC will monitor the different sensors in the infrastructure and in the environment.

The reduction and analysis pipelines (GP1) will be used to correct the raw images from the instrumental biases and to calibrate the astrometry and photometry. The pipeline will perform sky subtraction, co-add, and produce source catalogs. For GRB and multi-messenger alerts, it will also perform the analysis of the images to identify the optical counterpart and to characterize it (refined coordinates, multi-band light-curve, photo redshift estimation, etc.). It is under the responsibility of N. Butler (ASU) for the pipeline development and maintenance and on the CPPM for the interfaces with the other entities.

Finally, the instrument center of COLIBRI (GIC) is in charge of the long-term monitoring of the observatory, the validation of the calibration files, the visualization of the scientific products for the SVOM alerts, the creation of dedicated observing strategies, the organisation of the instrument expert shifts. It is provided by CPPM. The SVOM interfaces are essentially managed by the GIC for the data

exchanges between COLIBRI and the French Science Center (FSC) and by TCS for the SVOM trigger reception. It includes two components : the local GIC close to the telescope and the GIC located in the CC-IN2P3 cloud.

For the last few years, I am coordinating the software group of COLIBRI ($\sim$ 10 persons). I am the scientific responsible of the instrument center and I am also in charge of testing and integrating the GP1 pipeline in the control center of the telescope.

7.5 Perspectives and synergies between KM3NeT and SVOM

As explained in the Introduction, I have joined the SVOM project for two main scientific reasons : gamma-ray bursts are particularly interesting astrophysical sources by itself and to assure a good follow-up of the KM3NeT neutrino alerts/sources by the SVOM instruments. Since then, I have assured the link between the two experiments.

GRB by itself are very important sources for the high-energy astroparticle community. We have seen in the Section 2, that GRBs are particularly attractive cosmic accelerators. The recent detections of VHE emission from 3 GRBs up to a few hundreds of GeV by MAGIC and H.E.S.S. have also proven the acceleration of particles up to these very high energies. These detections are clearly very encouraging for CTA [249] which should detect multiple GRBs with a relatively high statistic. One of the next challenges will be to push the limit on the maximum photon energy with CTA, HAWC [250] and LHAASO [251] in the Northern hemisphere and the project SWGO [252] in the Southern hemisphere. So far, no high-energy neutrino signal has been correlated with the prompt GRB emission, leading to a very stringent limit (<10%) on the fraction of standard GRBs that contribute to the high-energy neutrino diffuse flux (using standard hadronic modelisation). The contribution of a dominant population of low-luminosity and/or choked GRBs, largely missed by current gamma-ray satellites, may still be an important source of high-energy neutrino. Thanks to the ECLAIRs low-energy threshold of 4 keV, SVOM will be more efficient in the detection of such GRB populations therefore providing a new sample to search for correlated neutrino emission. Thanks to the performance of its instruments, to their large multi-wavelength coverage, and to the excellent space-ground synergy, SVOM will provide a sample of well characterized GRBs, which is primordial for the detailed search of point-like neutrino sources.

SVOM with its ground- and space-based instruments will offer large and complementary follow-up capability through ToOs. The performances of SVOM (fields

of view and instrument sensitivities) are perfectly tailored to follow all neutrino alerts with the MXT and VT instruments on-board and ground-based telescopes (GFTs and GWAC). Figure 7.9 illustrates the follow-up strategies with SVOM instruments for future multi-messenger alerts. Even if the sensitivity of the MXT is lower than the one of the XRT telescope of Swift, thanks to its large field of view (1 degree), it is well adapted to the follow-up of not-well localized alerts. Following the example of the TAToO-Swift ToO program, we want to secure the link between KM3NeT and SVOM as we strongly believe that this alert program will be one of the prime source finding programs.

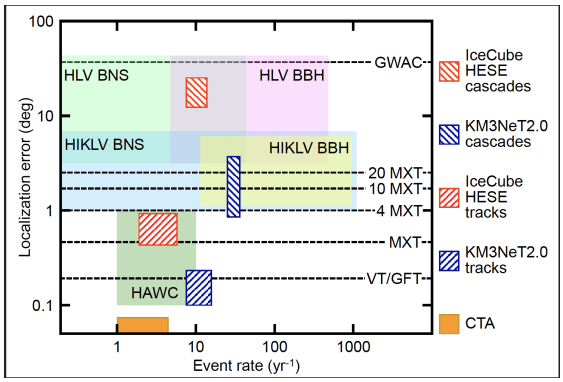

FIGURE 7.9 – Anticipated event rate and localization error for some forthcoming detectors operating in the field of multi-messenger astronomy [183]. Predictions are shown for two configurations of gravitational-wave detectors : Hanford- Livingston-Virgo (HLV) and Hanford-India-Kagra-Livingston-Virgo (HIKLV) and two sources : binary neutron stars (BNS) and binary black-holes (BBH). Predictions are also shown for two phase 2 high-energy neutrino detectors : IceCube for high-energy starting events (HESE) detected as cascades or tracks and KM3NeT, again for events detected as cascades or tracks. Predictions are finally shown for two high-energy gamma-ray detectors, HAWC and CTA. Horizontal dotted lines indicate the SVOM follow-up instrument capabilities with 4 MXT, 10 MXT and 20 MXT corresponding to different MXT tilings with 4, 10 and 20 tiles.

One of the key ingredients of the models of high-energy transient sources such as blazar or micro-quasar to account for the multi-messenger observations is the X-ray/gamma-ray observations simultaneously with the high-energy messengers (see Section 2). In a pure hadronic model or in a lepto-hadronic model, the X-ray/gamma-ray observations fix the leptonic or the proton cascade contributions (i.e. synchrotron processes). It is a key element to quantify the expected flux of neutrinos at high energies. SVOM will be a major partner for this with the ToO program to obtain simultaneous multi-wavelength observations and by providing

an X-ray catalogue for transient sources with the light curves and spectra (General Program) that can serve as a basis for the offline search of neutrino coincidences.

8 Conclusion and perspectives

Doing neutrino astronomy is a long dream for neutrino telescopes. The story starts about 50 years ago with the deployment of the prototype DUMAND offshore the coast of Hawaii. Nowadays, there are two key players, IceCube at the South Pole and ANTARES in France. The last decade is marked by the IceCube results, with the discovery of an astrophysical neutrino flux in the 10 TeV – 10 PeV energy range. Up to now, the arrival directions of the most energetic neutrinos seem to be consistent with a uniform distribution across the sky. Neutrino emission at the observed flux level has been predicted from a variety of source classes, including γ-ray bursts, blazars, starburst galaxies, galaxy clusters, and others. No firm detection of point like neutrino sources have been identified. The best candidate, so far, is the association between one very high-energy neutrino, IC170922, and a flare of the blazar TXS 0506+056, with a $\sim 3\sigma$ probability. However, this cannot be the entire story : multiple independent analyses indicate that only a fraction of the diffuse neutrino flux can come from γ-ray blazars. The current lack of established neutrino point sources — despite a firm detection of a diffuse neutrino flux — indicates a dominant population of low-luminosity extragalactic sources. For example, with the current knowledge of the hadronic interaction models, we can exclude a dominant contribution of highly energetic blazars and gamma-ray bursts. Source populations either with sufficiently large local densities — like starburst galaxies, galaxy clusters, low-luminosity AGN, radio-quiet AGN or star-forming galaxies with AGN outflows — or with high local rate densities — like (extragalactic) jet-powered SNe including hypernovae and interaction-powered SNe — are presently consistent with the observations.

Two additional players are entering in the game in the Northern hemisphere : GVD in Lake Baikal and KM3NeT in the Mediterranean Sea. Both detectors are already collecting data with first detection units and will reach significantly better sensitivities for the detection of cosmic neutrinos surpassing by far the ANTARES one. The main advantages of KM3NeT are the good angular precision, thanks to the clear water being the best medium with very low scattering. KM3NeT will achieve a precision of <0.1 degrees for the muon neutrino tracks at very high energies, and $<1.5^\circ$ for the cascade events (ν_e, ν_τ + all flavor neutrino neutral current interactions). This is a factor 5 - 10 improvements compared to IceCube. With KM3NeT, we will be able to perform a very efficient all-flavour neutrino astronomy. In the 2030s, IceCube is also planning a major upgrade, IceCube Gen-2, with an instrumented volume greater than 10 km^3, enlarging the cosmic neutrino

statistics by a factor 10. Having multiple neutrino observatories with different detection techniques and environments will help in the detection of the neutrino source population and in reducing the systematic errors of the measurements.

The detection of 50-60 gravitational waves clearly marks a major step in the multi-messenger astronomy. Unfortunately, only for one source, there is a detected EM counterpart (GW170817) identified in a real-time multi-wavelength observing campaign. With improved detectors in the future, the detection of these GWs will become routinely, with one detection every day. It will be then possible to study the GW population and detect peculiar candidates (large masses or large mass gap BBH, NS-BH and BNS with different observing angles, etc.). It will be possible to detect few events where a significant high-energy neutrino signal is expected. Moreover, in most of the hadronic models, we can expect a simultaneous production of neutral and charged pions in cosmic-ray interactions that suggests that the sources of high-energy neutrinos may also be strong 10 TeV –10 PeV γ-ray emitters. Only a few hints of PeVatron candidates have been detected by the current air shower Cherenkov telescopes, all of them being galactic sources. For extragalactic sources, the γ-ray emission is not directly observable because of the strong absorption of photons by e^+-e^- pair production in extragalactic background photons. There is a natural link between the sciences of CTA and high-energy neutrino telescopes. Real-time multi-messenger campaigns are crucial in unveiling the sources of the most energetic particles and the acceleration mechanisms at work. Neutrinos would provide insights into the physics of stellar explosions, compact object mergers, and relativistic jets, as well as particle acceleration processes. It relies on the quasi-online communication of potentially interesting observations to partner instruments ("alerts"), with latencies of a few minutes, at most. Such alerts are the only way to achieve simultaneous observations of transient phenomena by pointing instruments. With the arrival of the next generation multi-wavelength observatories (LSST, SKA, etc.), we expect an explosion of the number of EM triggers, it is very important to develop a real-time analysis infrastructure completely autonomous. This analysis framework will be a key element of the multi-messenger program of KM3NeT being a showcase of the experiment.

We have seen that the X-ray/γ-ray sky is very rich and simultaneous observation together with neutrino, GW or other EM wavelengths are crucial to understand the micro-physics of these cataclysmic events. SVOM, being launched in 2021-22, will be at the heart of this time-domain astronomy. This multi-wavelength facility is perfectly tailored for such multi-messenger and transient analyses. In particular, COLIBRI will participate to the optical and NIR follow-up of the KM3NeT alerts. The fast follow-up with the NIR camera is important to characterize the counterpart candidates. In case of galactic CCSN, infrared observations may be the only solution to find the optical counterpart in the galactic plane (due to the dust absorption).

To conclude, multi-messenger astronomy is in its infancy and it has already provided few impressive results. It should not be forgotten that about 5 years ago, no gravitational waves or high-energy neutrino sources were identified. The future looks bright with the arrival of several new generation observatories such as SKA, CTA, LSST, SVOM, ATHENA, KM3NeT, upgraded LIGO/VIRGO/KAGRA, etc.

Bibliographie

[1] Pawan Kumar et Bing Zhang. « The physics of gamma-ray bursts & relativistic jets ». In : *Phys. Rept.* 561 (2014), p. 1-109. doi : 10.1016/j.physrep.2014.09.008. arXiv : 1410.0679 [astro-ph.HE] (cf. p. 8).

[2] C.Megan Urry et Paolo Padovani. « Unified schemes for radio-loud active galactic nuclei ». In : *Publ. Astron. Soc. Pac.* 107 (1995), p. 803. doi : 10.1086/133630. arXiv : astro-ph/9506063 (cf. p. 8).

[3] K. Hirata et al. « Observation of a Neutrino Burst from the Supernova SN 1987a ». In : *Phys. Rev. Lett.* 58 (1987). Sous la dir. de K.C. Wali, p. 1490-1493. doi : 10.1103/PhysRevLett.58.1490 (cf. p. 9).

[4] R.M. Bionta et al. « Observation of a Neutrino Burst in Coincidence with Supernova SN 1987a in the Large Magellanic Cloud ». In : *Phys. Rev. Lett.* 58 (1987), p. 1494. doi : 10.1103/PhysRevLett.58.1494 (cf. p. 9).

[5] E.N. Alekseev, L.N. Alekseeva, I.V. Krivosheina et al. « Detection of the Neutrino Signal From SN1987A in the LMC Using the Inr Baksan Underground Scintillation Telescope ». In : *Phys. Lett. B* 205 (1988), p. 209-214. doi : 10.1016/0370-2693(88)91651-6 (cf. p. 9).

[6] Kei Kotake, Katsuhiko Sato et Keitaro Takahashi. « Explosion mechanism, neutrino burst, and gravitational wave in core-collapse supernovae ». In : *Rept. Prog. Phys.* 69 (2006), p. 971-1144. doi : 10.1088/0034-4885/69/4/R03. arXiv : astro-ph/0509456 (cf. p. 9).

[7] B.P. Abbott et al. « GW170817 : Observation of Gravitational Waves from a Binary Neutron Star Inspiral ». In : *Phys. Rev. Lett.* 119.16 (2017), p. 161101. doi : 10.1103/PhysRevLett.119.161101. arXiv : 1710.05832 [gr-qc] (cf. p. 9, 45).

[8] B.P. Abbott et al. « Gravitational Waves and Gamma-rays from a Binary Neutron Star Merger : GW170817 and GRB 170817A ». In : *Astrophys. J. Lett.* 848.2 (2017), p. L13. doi : 10.3847/2041-8213/aa920c. arXiv : 1710.05834 [astro-ph.HE] (cf. p. 9, 45).

[9] M.G. Aartsen et al. « Neutrino emission from the direction of the blazar TXS 0506+056 prior to the IceCube-170922A alert ». In : *Science* 361.6398 (2018), p. 147-151. doi : 10.1126/science.aat2890. arXiv : 1807.08794 [astro-ph.HE] (cf. p. 9, 15, 16).

[10] M.G. Aartsen et al. « Multimessenger observations of a flaring blazar coincident with high-energy neutrino IceCube-170922A ». In : *Science* 361.6398 (2018), eaat1378. DOI : 10.1126/science.aat1378. arXiv : 1807.08816 [astro-ph.HE] (cf. p. 9, 15).

[11] A. Abramowski et al. « Acceleration of petaelectronvolt protons in the Galactic Centre ». In : *Nature* 531 (2016), p. 476. DOI : 10.1038/nature17147. arXiv : 1603.07730 [astro-ph.HE] (cf. p. 9).

[12] S.J. Smartt et al. « A kilonova as the electromagnetic counterpart to a gravitational-wave source ». In : *Nature* 551.7678 (2017), p. 75-79. DOI : 10.1038/nature24303. arXiv : 1710.05841 [astro-ph.HE] (cf. p. 9).

[13] B.P. Abbott et al. « Multi-messenger Observations of a Binary Neutron Star Merger ». In : *Astrophys. J. Lett.* 848.2 (2017), p. L12. DOI : 10.3847/2041-8213/aa91c9. arXiv : 1710.05833 [astro-ph.HE] (cf. p. 9, 79).

[14] V. Acciari, S. Ansoldi, Lucio Angelo Antonelli et al. « Teraelectronvolt emission from the γ-ray burst GRB 190114C ». In : *Nature* 575 (nov. 2019), p. 455-458. DOI : 10.1038/s41586-019-1750-x (cf. p. 9).

[15] H. Abdalla et al. « A very-high-energy component deep in the γ-ray burst afterglow ». In : *Nature* 575.7783 (2019), p. 464-467. DOI : 10.1038/s41586-019-1743-9. arXiv : 1911.08961 [astro-ph.HE] (cf. p. 9).

[16] M.G. Aartsen et al. « The IceCube Neutrino Observatory : Instrumentation and Online Systems ». In : *JINST* 12.03 (2017), P03012. DOI : 10.1088/1748-0221/12/03/P03012. arXiv : 1612.05093 [astro-ph.IM] (cf. p. 11).

[17] M. Ageron et al. « ANTARES : the first undersea neutrino telescope ». In : *Nucl. Instrum. Meth. A* 656 (2011), p. 11-38. DOI : 10.1016/j.nima.2011.06.103. arXiv : 1104.1607 [astro-ph.IM] (cf. p. 11, 18).

[18] M.G. Aartsen et al. « Observation of High-Energy Astrophysical Neutrinos in Three Years of IceCube Data ». In : *Phys. Rev. Lett.* 113 (2014), p. 101101. DOI : 10.1103/PhysRevLett.113.101101. arXiv : 1405.5303 [astro-ph.HE] (cf. p. 11, 48).

[19] Austin Schneider. « Characterization of the Astrophysical Diffuse Neutrino Flux with IceCube High-Energy Starting Events ». In : *PoS* ICRC2019 (2020), p. 1004. DOI : 10.22323/1.358.1004. arXiv : 1907.11266 [astro-ph.HE] (cf. p. 11).

[20] Hans Martin Niederhausen et Yiqian Xu. « High Energy Astrophysical Neutrino Flux Measurement Using Neutrino-induced Cascades Observed in 4 Years of IceCube Data ». In : *PoS* ICRC2017 (2018), p. 968. DOI : 10.22323/1.301.0968 (cf. p. 11).

[21] M.G. Aartsen et al. « Observation and Characterization of a Cosmic Muon Neutrino Flux from the Northern Hemisphere using six years of IceCube data ». In : *Astrophys. J.* 833.1 (2016), p. 3. doi : 10.3847/0004-637X/833/1/3. arXiv : 1607.08006 [astro-ph.HE] (cf. p. 11).

[22] J. Stettner. « Measurement of the Diffuse Astrophysical Muon-Neutrino Spectrum with Ten Years of IceCube Data ». In : *PoS* ICRC2019 (2020), p. 1017. doi : 10.22323/1.358.1017. arXiv : 1908.09551 [astro-ph.HE] (cf. p. 11).

[23] M.G. Aartsen et al. « The IceCube Neutrino Observatory – Contributions to the 36th International Cosmic Ray Conference (ICRC2019) ». In : *36th International Cosmic Ray Conference*. Juil. 2019. arXiv : 1907.11699 [astro-ph.HE] (cf. p. 11, 12, 48).

[24] Andrea Palladino et Walter Winter. « A multi-component model for observed astrophysical neutrinos ». In : *Astron. Astrophys.* 615 (2018), A168. doi : 10.3204/PUBDB-2018-01376. arXiv : 1801.07277 [astro-ph.HE] (cf. p. 11).

[25] A. Albert et al. « All-flavor Search for a Diffuse Flux of Cosmic Neutrinos with Nine Years of ANTARES Data ». In : *Astrophys. J. Lett.* 853.1 (2018), p. L7. doi : 10.3847/2041-8213/aaa4f6. arXiv : 1711.07212 [astro-ph.HE] (cf. p. 11).

[26] J. Stettner. « Study of the high-energy diffuse neutrino flux with the ANTARES telescope ». In : *PoS* ICRC2019 (2020), p. 0891 (cf. p. 11, 13).

[27] Thomas K. Gaisser. « Neutrino Astronomy 2017 ». In : *13th Rencontres du Vietnam : Neutrinos 2017*. Jan. 2018. arXiv : 1801.01551 [astro-ph.HE] (cf. p. 12, 13).

[28] D. Gaggero, D. Grasso, A. Marinelli et al. « Diffuse cosmic rays shining in the Galactic center : A novel interpretation of H.E.S.S. and Fermi-LAT γ-ray data ». In : *Phys. Rev. Lett.* 119.3 (2017), p. 031101. doi : 10.1103/PhysRevLett.119.031101. arXiv : 1702.01124 [astro-ph.HE] (cf. p. 14).

[29] S. Adrian-Martinez et al. « A Search for Neutrino Emission from the Fermi Bubbles with the ANTARES Telescope ». In : *Eur. Phys. J. C* 74.2 (2014), p. 2701. doi : 10.1140/epjc/s10052-013-2701-6. arXiv : 1308.5260 [astro-ph.HE] (cf. p. 14).

[30] Hallmann S. « Search for Neutrino Emission from the Fermi Bubbles at Low Galactic Latitudes with the ANTARES Telescope ». In : *PoS* ICRC2019 (2020), p. 0905 (cf. p. 14).

[31] Fusco L. « Search for high-energy neutrinos from local superbubbles with the ANTARES telescope ». In : *PoS* ICRC2019 (2020), p. 0892 (cf. p. 14).

[32] A. Albert et al. « First all-flavor neutrino pointlike source search with the ANTARES neutrino telescope ». In : *Phys. Rev. D* 96.8 (2017), p. 082001. doi : 10.1103/PhysRevD.96.082001. arXiv : 1706.01857 [astro-ph.HE] (cf. p. 14).

[33] Tessa Carver. « Ten years of All-sky Neutrino Point-Source Searches ». In : *36th International Cosmic Ray Conference*. Août 2019. arXiv : 1908.05993 [astro-ph.HE] (cf. p. 15).

[34] Illuminati G. « Searches for point-like sources of cosmic neutrinos with 11 years of ANTARES data ». In : *36th International Cosmic Ray Conference*. Août 2019, p. 920 (cf. p. 15, 33).

[35] Julien Aublin, Giulia Illuminati et Sergio Navas. « Searches for point-like sources of cosmic neutrinos with 11 years of ANTARES data ». In : *PoS* ICRC2019 (2020), p. 920. doi : 10.22323/1.358.0920. arXiv : 1908.08248 [astro-ph.HE] (cf. p. 15).

[36] Simona Paiano, Renato Falomo, Aldo Treves et al. « The redshift of the BL Lac object TXS 0506+056 ». In : *Astrophys. J. Lett.* 854.2 (2018), p. L32. doi : 10.3847/2041-8213/aaad5e. arXiv : 1802.01939 [astro-ph.GA] (cf. p. 15).

[37] A. Albert et al. « The Search for Neutrinos from TXS 0506+056 with the ANTARES Telescope ». In : *Astrophys. J. Lett.* 863.2 (2018), p. L30. doi : 10.3847/2041-8213/aad8c0. arXiv : 1807.04309 [astro-ph.HE] (cf. p. 15).

[38] M. Ackermann et al. « The spectrum of isotropic diffuse gamma-ray emission between 100 MeV and 820 GeV ». In : *Astrophys. J.* 799 (2015), p. 86. doi : 10.1088/0004-637X/799/1/86. arXiv : 1410.3696 [astro-ph.HE] (cf. p. 15).

[39] M. Ackermann et al. « 2FHL : The Second Catalog of Hard Fermi-LAT Sources ». In : *Astrophys. J. Suppl.* 222.1 (2016), p. 5. doi : 10.3847/0067-0049/222/1/5. arXiv : 1508.04449 [astro-ph.HE] (cf. p. 15).

[40] Steven D. Bloom et Alan P. Marscher. « An Analysis of the Synchrotron Self-Compton Model for the Multi–Wave Band Spectra of Blazars ». In : *Astrophys. J.* 461 (1996), p. 657. doi : 10.1086/177092 (cf. p. 16).

[41] L. Maraschi, G. Ghisellini et A. Celotti. « A jet model for the gamma-ray emitting blazar 3C 279 ». In : *Astrophys. J.* 397 (1992), p. L5-L9. doi : 10.1086/186531 (cf. p. 16).

[42] Charles D. Dermer et Reinhard Schlickeiser. « Model for the high-energy emission from blazars ». In : *Astrophys. J.* 416 (1993), p. 458. doi : 10.1086/173251 (cf. p. 16).

[43] K. Mannheim. « The Proton blazar ». In : *Astron. Astrophys.* 269 (1993), p. 67. arXiv : astro-ph/9302006 (cf. p. 16).

[44] Thomas K. Gaisser, Francis Halzen et Todor Stanev. « Particle astrophysics with high-energy neutrinos ». In : *Phys. Rept.* 258 (1995). [Erratum : Phys.Rept. 271, 355–356 (1996)], p. 173-236. doi : 10.1016/0370-1573(95)00003-Y. arXiv : hep-ph/9410384 (cf. p. 16).

[45] Shan Gao, Anatoli Fedynitch, Walter Winter et al. « Modelling the coincident observation of a high-energy neutrino and a bright blazar flare ». In : *Nat. Astron.* 3.1 (2019), p. 88-92. doi : 10.1038/s41550-018-0610-1. arXiv : 1807.04275 [astro-ph.HE] (cf. p. 16, 17).

[46] Shan Gao, Martin Pohl et Walter Winter. « On the direct correlation between gamma-rays and PeV neutrinos from blazars ». In : *Astrophys. J.* 843.2 (2017), p. 109. doi : 10.3847/1538-4357/aa7754. arXiv : 1610.05306 [astro-ph.HE] (cf. p. 16).

[47] C. Righi, F. Tavecchio et S. Inoue. « Neutrino emission from BL Lac objects : the role of radiatively inefficient accretion flows ». In : *Mon. Not. Roy. Astron. Soc.* 483.1 (2019), p. L127-L131. doi : 10.1093/mnrasl/sly231. arXiv : 1807.10506 [astro-ph.HE] (cf. p. 16).

[48] M. Cerruti, A. Zech, C. Boisson et al. « Leptohadronic single-zone models for the electromagnetic and neutrino emission of TXS 0506+056 ». In : *Mon. Not. Roy. Astron. Soc.* 483.1 (2019), p. L12-L16. doi : 10.1093/mnrasl/sly210. arXiv : 1807.04335 [astro-ph.HE] (cf. p. 16).

[49] N. Sahakyan. « Lepto-hadronic γ-ray and neutrino emission from the jet of TXS 0506+056 ». In : *Astrophys. J.* 866.2 (2018), p. 109. doi : 10.3847/1538-4357/aadade. arXiv : 1808.05651 [astro-ph.HE] (cf. p. 16).

[50] A. Keivani et al. « A Multimessenger Picture of the Flaring Blazar TXS 0506+056 : implications for High-Energy Neutrino Emission and Cosmic Ray Acceleration ». In : *Astrophys. J.* 864.1 (2018), p. 84. doi : 10.3847/1538-4357/aad59a. arXiv : 1807.04537 [astro-ph.HE] (cf. p. 16).

[51] Anita Reimer, Markus Boettcher et Sara Buson. « Cascading Constraints from Neutrino Emitting Blazars : The case of TXS 0506+056 ». In : (déc. 2018). doi : 10.3847/1538-4357/ab2bff. arXiv : 1812.05654 [astro-ph.HE] (cf. p. 16).

[52] S. Hummer, M. Ruger, F. Spanier et al. « Simplified models for photohadronic interactions in cosmic accelerators ». In : *Astrophys. J.* 721 (2010), p. 630-652. doi : 10.1088/0004-637X/721/1/630. arXiv : 1002.1310 [astro-ph.HE] (cf. p. 16, 45).

[53] Haocheng Zhang, Ke Fang et Hui Li. « Variability and Optical Polarization Can Probe the Neutrino and Electromagnetic Emission Mechanisms of TXS~0506+056 ». In : (juil. 2018). arXiv : 1807.11069 [astro-ph.HE] (cf. p. 17).

[54] Ruo-Yu Liu, Kai Wang, Rui Xue et al. « Hadronuclear interpretation of a high-energy neutrino event coincident with a blazar flare ». In : *Phys. Rev. D* 99.6 (2019), p. 063008. DOI : 10.1103/PhysRevD.99.063008. arXiv : 1807.05113 [astro-ph.HE] (cf. p. 17).

[55] S. Garrappa et al. « Investigation of two Fermi-LAT gamma-ray blazars coincident with high-energy neutrinos detected by IceCube ». In : *Astrophys. J.* 880.2 (2019), 880 :103. DOI : 10.3847/1538-4357/ab2ada. arXiv : 1901.10806 [astro-ph.HE] (cf. p. 17).

[56] Francis Halzen, Ali Kheirandish, Thomas Weisgarber et al. « On the Neutrino Flares from the Direction of TXS 0506+056 ». In : *Astrophys. J. Lett.* 874.1 (2019), p. L9. DOI : 10.3847/2041-8213/ab0d27. arXiv : 1811.07439 [astro-ph.HE] (cf. p. 17).

[57] Kai Wang, Ruo-Yu Liu, Zhuo Li et al. « Jet-cloud/star interaction as an interpretation of neutrino outburst from the blazar TXS 0506+056 ». In : (sept. 2018). arXiv : 1809.00601 [astro-ph.HE] (cf. p. 17).

[58] Xavier Rodrigues, Shan Gao, Anatoli Fedynitch et al. « Leptohadronic Blazar Models Applied to the 2014–2015 Flare of TXS 0506+056 ». In : *Astrophys. J. Lett.* 874.2 (2019), p. L29. DOI : 10.3847/2041-8213/ab1267. arXiv : 1812.05939 [astro-ph.HE] (cf. p. 17).

[59] M.G. Aartsen et al. « The contribution of Fermi-2LAC blazars to the diffuse TeV-PeV neutrino flux ». In : *Astrophys. J.* 835.1 (2017), p. 45. DOI : 10.3847/1538-4357/835/1/45. arXiv : 1611.03874 [astro-ph.HE] (cf. p. 17).

[60] Robert Stein et al. « A high-energy neutrino coincident with a tidal disruption event ». In : (mai 2020). arXiv : 2005.05340 [astro-ph.HE] (cf. p. 17).

[61] J.A. Aguilar et al. « The data acquisition system for the ANTARES Neutrino Telescope ». In : *Nucl. Instrum. Meth. A* 570 (2007), p. 107-116. DOI : 10.1016/j.nima.2006.09.098. arXiv : astro-ph/0610029 (cf. p. 18).

[62] S. Adrián-Martínez et al. « Time calibration with atmospheric muon tracks in the ANTARES neutrino telescope ». In : *Astropart. Phys.* 78 (2016), p. 43-51. DOI : 10.1016/j.astropartphys.2016.02.001. arXiv : 1507.04182 [physics.ins-det] (cf. p. 19).

[63] S. Adrian-Martinez et al. « The Positioning System of the ANTARES Neutrino Telescope ». In : *JINST* 7 (2012), T08002. DOI : 10.1088/1748-0221/7/08/T08002. arXiv : 1202.3894 [astro-ph.IM] (cf. p. 19).

[64] S. Adrian-Martinez et al. « Search for Cosmic Neutrino Point Sources with Four Year Data of the ANTARES Telescope ». In : *Astrophys. J.* 760 (2012), p. 53. doi : 10.1088/0004-637X/760/1/53. arXiv : 1207.3105 [hep-ex] (cf. p. 20, 41, 53).

[65] A. Albert et al. « An algorithm for the reconstruction of neutrino-induced showers in the ANTARES neutrino telescope ». In : *Astron. J.* 154.6 (2017), p. 275. doi : 10.3847/1538-3881/aa9709. arXiv : 1708.03649 [astro-ph.IM] (cf. p. 20).

[66] A. Albert et al. « An algorithm for the reconstruction of high-energy neutrino-induced particle showers and its application to the ANTARES neutrino telescope ». In : *Eur. Phys. J. C* 77.6 (2017), p. 419. doi : 10.1140/epjc/s10052-017-4979-2. arXiv : 1703.02432 [astro-ph.HE] (cf. p. 20).

[67] S. Adrian-Martinez et al. « Letter of intent for KM3NeT 2.0 ». In : *J. Phys. G* 43.8 (2016), p. 084001. doi : 10.1088/0954-3899/43/8/084001. arXiv : 1601.07459 [astro-ph.IM] (cf. p. 21, 90).

[68] ANTARES collaboration, A. Albert, M. André et al. « Long-term monitoring of the ANTARES optical module efficiencies using ^{40}K decays in sea water ». In : *arXiv e-prints*, arXiv :1805.08675 (mai 2018), arXiv :1805.08675. arXiv : 1805.08675 [astro-ph.IM] (cf. p. 22, 24).

[69] M. Tavani, A. Bulgarelli, G. Piano et al. « Extreme particle acceleration in the microquasar CygnusX-3 ». In : *Nature* 462.7273 (déc. 2009), p. 620-623. doi : 10.1038/nature08578. arXiv : 0910.5344 [astro-ph.HE] (cf. p. 27).

[70] I. F. Mirabel et L. F. Rodríguez. « A superluminal source in the Galaxy ». In : *Nature* 371.6492 (sept. 1994), p. 46-48. doi : 10.1038/371046a0 (cf. p. 28).

[71] Guillaume Dubus. « Gamma-ray binaries and related systems ». In : *Astronomy and Astrophysics Review* 21, 64 (août 2013), p. 64. doi : 10.1007/s00159-013-0064-5. arXiv : 1307.7083 [astro-ph.HE] (cf. p. 28).

[72] G. S. Vila et G. E. Romero. « Leptonic/hadronic models for electromagnetic emission in microquasars : the case of GX 339-4 ». In : *Mon. Not. Roy. Astron. Soc.* 403.3 (avr. 2010), p. 1457-1468. doi : 10.1111/j.1365-2966.2010.16208.x. arXiv : 1001.0959 [astro-ph.HE] (cf. p. 28).

[73] G. S. Vila, G. E. Romero et N. A. Casco. « An inhomogeneous lepto-hadronic model for the radiation of relativistic jets. Application to XTE J1118+480 ». In : *A & A* 538, A97 (fév. 2012), A97. doi : 10.1051/0004-6361/201118106. arXiv : 1112.2560 [astro-ph.HE] (cf. p. 28).

[74] Carolina Pepe, Gabriela S. Vila et Gustavo E. Romero. « Lepto-hadronic model for the broadband emission of Cygnus X-1 ». In : *A & A* 584, A95 (déc. 2015), A95. doi : 10.1051/0004-6361/201527156. arXiv : 1509.08514 [astro-ph.HE] (cf. p. 28).

[75] R. D. Blandford et D. G. Payne. « Hydromagnetic flows from accretion disks and the production of radio jets. » In : *Mon. Not. Roy. Astron. Soc.* 199 (juin 1982), p. 883-903. doi : 10.1093/mnras/199.4.883 (cf. p. 28).

[76] María Díaz Trigo, James C. A. Miller-Jones, Simone Migliari et al. « Baryons in the relativistic jets of the stellar-mass black hole candidate 4U 1630-47 ». In : *Nature* 504 (2013), p. 260. doi : 10.1038/nature12672. arXiv : 1311.5080 [astro-ph.HE] (cf. p. 28).

[77] Simone Migliari, Robert P. Fender et Mariano Mendez. « Iron emission lines from extended x-ray jets in SS 433 : Reheating of atomic nuclei ». In : *Science* 297 (2002), p. 1673. doi : 10.1126/science.1073660. arXiv : astro-ph/0209131 (cf. p. 28).

[78] Sebastian Heinz, Michael G. Burton, Catherine Braiding et al. « Lord of the Rings : A Kinematic Distance to Circinus X-1 from a Giant X-Ray Light Echo ». In : *Astrophys. J.* 806.2 (2015), p. 265. doi : 10.1088/0004-637X/806/2/265. arXiv : 1506.06142 [astro-ph.HE] (cf. p. 28, 35).

[79] Amir Levinson et Eli Waxman. « Probing Microquasars with TeV Neutrinos ». In : *Phys. Rev. Lett.* 87 (17 oct. 2001), p. 171101. url : https://link.aps.org/doi/10.1103/PhysRevLett.87.171101 (cf. p. 28, 33).

[80] C. Distefano, D. Guetta, E. Waxman et al. « Neutrino flux predictions for known galactic microquasars ». In : *Astrophys. J.* 575 (2002), p. 378-383. doi : 10.1086/341144. arXiv : astro-ph/0202200 (cf. p. 28, 33-36).

[81] Romero, G. E., Torres, D. F., Kaufman Bernadó, M. M. et al. « Hadronic gamma-ray emission from windy microquasars ». In : *A&A* 410.2 (2003), p. L1-L4. doi : 10.1051/0004-6361:20031314-1. url : https://doi.org/10.1051/0004-6361:20031314-1 (cf. p. 28).

[82] Hugo R. Christiansen, Mariana Orellana et Gustavo E. Romero. « High-energy neutrino emission from x-ray binaries ». In : *Phys. Rev. D* 73 (2006), p. 063012. doi : 10.1103/PhysRevD.73.063012. arXiv : astro-ph/0509214 (cf. p. 28).

[83] Diego F. Torres et Francis Halzen. « LS I +61 303 as a potential neutrino source on the light of MAGIC results ». In : *Astropart. Phys.* 27 (2007), p. 500-508. doi : 10.1016/j.astropartphys.2007.02.004. arXiv : astro-ph/0607368 (cf. p. 28).

[84] F. L. Vieyro et G. E. Romero. « Particle transport in magnetized media around black holes and associated radiation ». In : *A & A* 542, A7 (juin 2012), A7. doi : 10.1051/0004-6361/201218886. arXiv : 1204.4469 [astro-ph.HE] (cf. p. 28, 29).

[85] A. Neronov et M. Ribordy. « Neutrino signal from gamma-ray loud binaries powered by high energy protons ». In : *Phys. Rev. D* 79 (2009), p. 043013. doi : 10.1103/PhysRevD.79.043013. arXiv : 0812.0306 [astro-ph] (cf. p. 28).

[86] N. Sahakyan, G. Piano et M. Tavani. « Hadronic Gamma-Ray and Neutrino Emission from Cygnus X-3 ». In : *Astrophys. J.* 780.1, 29 (jan. 2014), p. 29. doi : 10.1088/0004-637X/780/1/29. arXiv : 1310.7805 [astro-ph.HE] (cf. p. 28).

[87] Stephane Corbel, P. Kaaret, R.P. Fender et al. « Discovery of x-ray jets in the microquasar H 1743-322 ». In : *Astrophys. J.* 632 (2005), p. 504-513. doi : 10.1086/432499. arXiv : astro-ph/0505526 (cf. p. 29).

[88] J. C. A. Miller-Jones, P. G. Jonker, T. J. Maccarone et al. « A Deep Radio Survey of Hard State and Quiescent Black Hole X-Ray Binaries ». In : *Astrophys. J.l* 739.1, L18 (sept. 2011), p. L18. doi : 10.1088/2041-8205/739/1/L18. arXiv : 1106.0097 [astro-ph.HE] (cf. p. 29).

[89] J.C.A. Miller-Jones, A. Moin, S.J. Tingay et al. « The first resolved imaging of milliarcsecond-scale jets in Circinus X-1 ». In : *Mon. Not. Roy. Astron. Soc.* 419 (2012), p. 49. doi : 10.1111/j.1745-3933.2011.01176.x. arXiv : 1110.3996 [astro-ph.HE] (cf. p. 29, 35).

[90] V. Sguera, G. E. Romero, A. Bazzano et al. « Dissecting the Region of 3EG J1837-0423 and HESS J1841-055 with INTEGRAL ». In : *Astrophys. J.* 697.2 (juin 2009), p. 1194-1205. doi : 10.1088/0004-637X/697/2/1194. arXiv : 0903.1763 [astro-ph.HE] (cf. p. 29).

[91] Federico García, Deborah N. Aguilera et Gustavo E. Romero. « Exploring jet-launching conditions for supergiant fast X-ray transients ». In : *A & A* 565, A122 (mai 2014), A122. doi : 10.1051/0004-6361/201323157. arXiv : 1404.7243 [astro-ph.HE] (cf. p. 29).

[92] Franco Giovannelli et Lola S. Graziati. « A :0535+26 / HDE :245770 - a Typical X-Ray / Be-System ». In : *Space Science Reviews* 59.1-2 (jan. 1992), p. 1-81. doi : 10.1007/BF01262537 (cf. p. 29).

[93] Luis A. Anchordoqui, Diego F. Torres, Thomas P. McCauley et al. « Neutrinos from Accreting Neutron Stars ». In : *Astrophys. J.* 589.1 (mai 2003), p. 481-486. doi : 10.1086/374551. arXiv : hep-ph/0211231 [hep-ph] (cf. p. 29).

[94] Jeffrey D. Scargle. « Studies in astronomical time series analysis : 5. Bayesian blocks, a new method to analyze structure in photon counting data ». In : *Astrophys. J.* 504 (1998), p. 405. doi : 10.1086/306064. arXiv : astro-ph/9711233 (cf. p. 29).

[95] Jeffrey D. Scargle, Jay P. Norris, Brad Jackson et al. « Studies in Astronomical Time Series Analysis. VI. Bayesian Block Representations ». In : *Astrophys. J.* 764 (2013), p. 167. doi : 10.1088/0004-637X/764/2/167. arXiv : 1207.5578 [astro-ph.IM] (cf. p. 29).

[96] J. Neyman. « Outline of a Theory of Statistical Estimation Based on the Classical Theory of Probability ». In : *Phil. Trans. Roy. Soc. Lond. A* 236.767 (1937), p. 333-380. doi : 10.1098/rsta.1937.0005 (cf. p. 33).

[97] James C.A. Miller-Jones, R.P. Fender et E. Nakar. « Opening angles, Lorentz factors and confinement of x-ray binary jets ». In : *Mon. Not. Roy. Astron. Soc.* 367 (2006), p. 1432-1440. doi : 10.1111/j.1365-2966.2006.10092.x. arXiv : astro-ph/0601482 (cf. p. 34).

[98] R. D. Blandford et A. Konigl. « Relativistic jets as compact radio sources ». In : *Astrophys. J.* 232 (1979), p. 34. doi : 10.1086/157262 (cf. p. 35).

[99] S. Adrian-Martinez et al. « Search for muon-neutrino emission from GeV and TeV gamma-ray flaring blazars using five years of data of the ANTARES telescope ». In : *JCAP* 12 (2015), p. 014. doi : 10.1088/1475-7516/2015/12/014. arXiv : 1506.07354 [astro-ph.HE] (cf. p. 37).

[100] A.V.cow Plavin, Y.Y. Kovalev, Y.A. Kovalev et al. « Observational evidence for the origin of high-energy neutrinos in parsec-scale nuclei of radio-bright active galaxies ». In : *Astrophys. J.* 894 (2020), p. 101. doi : 10.3847/1538-4357/ab86bd. arXiv : 2001.00930 [astro-ph.HE] (cf. p. 37, 69).

[101] D.R. Lorimer, M. Bailes, M.A. McLaughlin et al. « A bright millisecond radio burst of extragalactic origin ». In : *Science* 318 (2007), p. 777. doi : 10.1126/science.1147532. arXiv : 0709.4301 [astro-ph] (cf. p. 37).

[102] D. Thornton et al. « A Population of Fast Radio Bursts at Cosmological Distances ». In : *Science* 341.6141 (2013), p. 53-56. doi : 10.1126/science.1236789. arXiv : 1307.1628 [astro-ph.HE] (cf. p. 37, 38).

[103] E. Petroff, E.D. Barr, A. Jameson et al. « FRBCAT : The Fast Radio Burst Catalogue ». In : *Publ. Astron. Soc. Austral.* 33 (2016), e045. doi : 10.1017/pasa.2016.35. arXiv : 1601.03547 [astro-ph.HE] (cf. p. 38, 40, 49).

[104] E.F. Keane et al. « A Fast Radio Burst Host Galaxy ». In : *Nature* 530 (2016), p. 453-456. doi : 10.1038/nature17140. arXiv : 1602.07477 [astro-ph.HE] (cf. p. 38).

[105] Tomonori Totani. « Cosmological Fast Radio Bursts from Binary Neutron Star Mergers ». In : *Pub. Astron. Soc. Jpn.* 65 (2013), p. L12. doi : 10.1093/pasj/65.5.L12. arXiv : 1307.4985 [astro-ph.HE] (cf. p. 38).

[106] Jie-Shuang Wang, Yuan-Pei Yang, Xue-Feng Wu et al. « Fast Radio Bursts from the Inspiral of Double Neutron Stars ». In : *Astrophys. J. Lett.* 822.1 (2016), p. L7. doi : 10.3847/2041-8205/822/1/L7. arXiv : 1603.02014 [astro-ph.HE] (cf. p. 38).

[107] Bing Zhang. « Fast Radio Bursts from Interacting Binary Neutron Star Systems ». In : *Astrophys. J. Lett.* 890 (2020), p. L24. doi : 10.3847/2041-8213/ab7244. arXiv : 2002.00335 [astro-ph.HE] (cf. p. 38, 45).

[108] Kelly Gourdji, Antonia Rowlinson, Ralph A.M.J. Wijers et al. « Constraining a neutron star merger origin for localized fast radio bursts ». In : (mar. 2020). arXiv : 2003.02706 [astro-ph.HE] (cf. p. 38).

[109] Haoxiang Lin et Tomonori Totani. « Detectability of radio afterglows from Fast Radio Bursts produced by Binary Neutron Star Mergers ». In : (mai 2020). arXiv : 2005.08112 [astro-ph.HE] (cf. p. 38).

[110] Bing Zhang. « A possible connection between Fast Radio Bursts and Gamma-Ray Bursts ». In : *Astrophys. J. Lett.* 780 (2014), p. L21. doi : 10.1088/2041-8205/780/2/L21. arXiv : 1310.4893 [astro-ph.HE] (cf. p. 38, 45).

[111] Divya Palaniswamy, Randall B. Wayth, Cathryn M. Trott et al. « A Search for Fast Radio Bursts Associated with Gamma-Ray Bursts ». In : *Astrophys. J.* 790.1 (2014), p. 63. doi : 10.1088/0004-637X/790/1/63. arXiv : 1406.1850 [astro-ph.HE] (cf. p. 38).

[112] Kohta Murase, Peter Meszaros et Derek B. Fox. « Fast Radio Bursts with Extended Gamma-Ray Emission ? » In : *Astrophys. J. Lett.* 836.1 (2017), p. L6. doi : 10.3847/2041-8213/836/1/L6. arXiv : 1611.03848 [astro-ph.HE] (cf. p. 38).

[113] Heino Falcke et Luciano Rezzolla. « Fast radio bursts : the last sign of supramassive neutron stars ». In : *Astron. Astrophys.* 562 (2014), A137. doi : 10.1051/0004-6361/201321996. arXiv : 1307.1409 [astro-ph.HE] (cf. p. 38, 39, 47).

[114] Vikram Ravi et Paul D. Lasky. « The birth of black holes : neutron star collapse times, gamma-ray bursts and fast radio bursts ». In : *Mon. Not. Roy. Astron. Soc.* 441.3 (2014), p. 2433-2439. doi : 10.1093/mnras/stu720. arXiv : 1403.6327 [astro-ph.HE] (cf. p. 38, 47).

[115] Xiang Li, Bei Zhou, Hao-Ning He et al. « Model-dependent estimate on the connection between fast radio bursts and ultra-high energy cosmic rays ». In : *Astrophys. J.* 797.1 (2014), p. 33. doi : 10.1088/0004-637X/797/1/33. arXiv : 1312.5637 [astro-ph.HE] (cf. p. 38, 39, 47).

[116] Ue-Li Pen et Liam Connor. « Local Circumnuclear Magnetar Solution to Extragalactic Fast Radio Bursts ». In : *Astrophys. J.* 807.2 (2015), p. 179. doi : 10.1088/0004-637X/807/2/179. arXiv : 1501.01341 [astro-ph.HE] (cf. p. 38).

[117] J.M. Cordes et Ira Wasserman. « Supergiant Pulses from Extragalactic Neutron Stars ». In : *Mon. Not. Roy. Astron. Soc.* 457.1 (2016), p. 232-257. doi : 10.1093/mnras/stv2948. arXiv : 1501.00753 [astro-ph.HE] (cf. p. 38).

[118] S.B. Popov et K.A. Postnov. « Millisecond extragalactic radio bursts as magnetar flares ». In : (juil. 2013). arXiv : 1307.4924 [astro-ph.HE] (cf. p. 38).

[119] Yuri Lyubarsky. « A model for fast extragalactic radio bursts ». In : *Mon. Not. Roy. Astron. Soc.* 442 (2014), p. 9. doi : 10.1093/mnrasl/slu046. arXiv : 1401.6674 [astro-ph.HE] (cf. p. 38).

[120] Wenbin Lu, Pawan Kumar et Bing Zhang. « A unified picture of Galactic and cosmological fast radio bursts ». In : (mai 2020). arXiv : 2005.06736 [astro-ph.HE] (cf. p. 38, 49).

[121] Kohta Murase, Kazumi Kashiyama et Peter Mészáros. « A Burst in a Wind Bubble and the Impact on Baryonic Ejecta : High-Energy Gamma-Ray Flashes and Afterglows from Fast Radio Bursts and Pulsar-Driven Supernova Remnants ». In : *Mon. Not. Roy. Astron. Soc.* 461.2 (2016). [Erratum : Mon.Not.Roy.Astron.Soc. 467, 3542–3543 (2017)], p. 1498-1511. doi : 10.1093/mnras/stw1328. arXiv : 1603.08875 [astro-ph.HE] (cf. p. 38, 39).

[122] Michael F. Bietenholz et Norbert Bartel. « On the Possibility of Fast Radio Bursts from Inside Supernovae : The Case of SN 1986J ». In : *Astrophys. J.* 851.2 (2017), p. 124. doi : 10.3847/1538-4357/aa98d9. arXiv : 1707.07746 [astro-ph.HE] (cf. p. 38).

[123] Xiao-Feng Cao et Yun-Wei Yu. « Superconducting cosmic string loops as sources for fast radio bursts ». In : *Phys. Rev. D* 97.2 (2018), p. 023022. doi : 10.1103/PhysRevD.97.023022 (cf. p. 38).

[124] Jiani Ye, Kai Wang et Yi-Fu Cai. « Superconducting cosmic strings as sources of cosmological fast radio bursts ». In : *Eur. Phys. J. C* 77.11 (2017), p. 720. doi : 10.1140/epjc/s10052-017-5319-2. arXiv : 1705.10956 [astro-ph.HE] (cf. p. 38).

[125] Sichun Sun et Yun-Long Zhang. « Gravitational Waves and Possible Fast Radio Bursts from Axion Clumps ». In : (mar. 2020). arXiv : 2003.10527 [hep-ph] (cf. p. 38).

[126] David F. Chernoff, Shing Yan Li et S.-H. Henry Tye. « Periodic Fast Radio Bursts from Axion Emission by Cosmic Superstrings ». In : (mar. 2020). arXiv : 2003.07275 [astro-ph.CO] (cf. p. 38).

[127] L.G. Spitler et al. « A Repeating Fast Radio Burst ». In : *Nature* 531 (2016), p. 202. doi : 10.1038/nature17168. arXiv : 1603.00581 [astro-ph.HE] (cf. p. 38).

[128] P. Scholz et al. « Simultaneous X-ray, gamma-ray, and Radio Observations of the repeating Fast Radio Burst FRB 121102 ». In : *Astrophys. J.* 846.1 (2017), p. 80. doi : 10.3847/1538-4357/aa8456. arXiv : 1705.07824 [astro-ph.HE] (cf. p. 38, 39).

[129] B. Marcote et al. « The Repeating Fast Radio Burst FRB 121102 as Seen on Milliarcsecond Angular Scales ». In : *Astrophys. J. Lett.* 834.2 (2017), p. L8. doi : 10.3847/2041-8213/834/2/L8. arXiv : 1701.01099 [astro-ph.HE] (cf. p. 38).

[130] S. Chatterjee et al. « The direct localization of a fast radio burst and its host ». In : *Nature* 541 (2017), p. 58. doi : 10.1038/nature20797. arXiv : 1701.01098 [astro-ph.HE] (cf. p. 38).

[131] Shriharsh P. Tendulkar et al. « The Host Galaxy and Redshift of the Repeating Fast Radio Burst FRB 121102 ». In : *Astrophys. J. Lett.* 834.2 (2017), p. L7. doi : 10.3847/2041-8213/834/2/L7. arXiv : 1701.01100 [astro-ph.HE] (cf. p. 38).

[132] M. Amiri et al. « A Second Source of Repeating Fast Radio Bursts ». In : *Nature* 566.7743 (2019), p. 235-238. doi : 10.1038/s41586-018-0864-x. arXiv : 1901.04525 [astro-ph.HE] (cf. p. 38).

[133] L.C. Oostrum et al. « Repeating fast radio bursts with WSRT/Apertif ». In : *Astron. Astrophys.* 635 (2020), A61. doi : 10.1051/0004-6361/201937422. arXiv : 1912.12217 [astro-ph.HE] (cf. p. 38).

[134] P. Scholz et al. « Simultaneous X-ray and Radio Observations of the Repeating Fast Radio Burst FRB 180916.J0158+65 ». In : (avr. 2020). arXiv : 2004.06082 [astro-ph.HE] (cf. p. 38).

[135] B. Marcote et al. « A repeating fast radio burst source localized to a nearby spiral galaxy ». In : *Nature* 577.7789 (2020), p. 190-194. doi : 10.1038/s41586-019-1866-z. arXiv : 2001.02222 [astro-ph.HE] (cf. p. 38, 49).

[136] E. Fonseca et al. « Nine New Repeating Fast Radio Burst Sources from CHIME/FRB ». In : *Astrophys. J. Lett.* 891.1 (2020), p. L6. doi : 10.3847/2041-8213/ab7208. arXiv : 2001.03595 [astro-ph.HE] (cf. p. 38).

[137] Amiri et al. « Periodic activity from a fast radio burst source ». In : (jan. 2020). arXiv : 2001.10275 [astro-ph.HE] (cf. p. 38).

[138] Ben Margalit, Paz Beniamini, Navin Sridhar et al. « Implications of a "Fast Radio Burst" from a Galactic Magnetar ». In : (mai 2020). arXiv : 2005.05283 [astro-ph.HE] (cf. p. 38, 49).

[139] Christopher D. Bochenek, Vikram Ravi, Konstantin V. Belov et al. « A fast radio burst associated with a Galactic magnetar ». In : (mai 2020). arXiv : 2005.10828 [astro-ph.HE] (cf. p. 38, 49).

[140] C.K. Li et al. « Identification of a non-thermal X-ray burst with the Galactic magnetar SGR 1935+2154 and a fast radio burst with Insight-HXMT ». In : (mai 2020). arXiv : 2005.11071 [astro-ph.HE] (cf. p. 38, 49).

[141] A. Ridnaia et al. « A peculiar hard X-ray counterpart of a Galactic fast radio burst ». In : (mai 2020). arXiv : 2005.11178 [astro-ph.HE] (cf. p. 38, 49).

[142] M. Tavani et al. « An X-Ray Burst from a Magnetar Enlightening the Mechanism of Fast Radio Bursts ». In : (mai 2020). arXiv : 2005.12164 [astro-ph.HE] (cf. p. 38, 49).

[143] D.J. Champion et al. « Five new fast radio bursts from the HTRU high-latitude survey at Parkes : first evidence for two-component bursts ». In : *Mon. Not. Roy. Astron. Soc.* 460.1 (2016), p. L30-L34. doi : 10.1093/mnrasl/slw069. arXiv : 1511.07746 [astro-ph.HE] (cf. p. 38, 48).

[144] A. Goldstein, R.D. Preece, R.S. Mallozzi et al. « The BATSE 5B Gamma-Ray Burst Spectral Catalog ». In : *Astrophys. J. Suppl.* 208 (2013), p. 21. doi : 10.1088/0067-0049/208/2/21. arXiv : 1311.7135 [astro-ph.HE] (cf. p. 38).

[145] E. Petroff et al. « A real-time fast radio burst : polarization detection and multiwavelength follow-up ». In : *Mon. Not. Roy. Astron. Soc.* 447.1 (2015), p. 246-255. doi : 10.1093/mnras/stu2419. arXiv : 1412.0342 [astro-ph.HE] (cf. p. 39).

[146] E. Petroff et al. « A survey of FRB fields : Limits on repeatability ». In : *Mon. Not. Roy. Astron. Soc.* 454.1 (2015), p. 457-462. doi : 10.1093/mnras/stv1953. arXiv : 1508.04884 [astro-ph.HE] (cf. p. 39).

[147] A. Albert et al. « A polarized fast radio burst at low Galactic latitude ». In : *Mon. Not. Roy. Astron. Soc.* 469.4 (2017), p. 4465-4482. doi : 10.1093/mnras/stx1098. arXiv : 1705.02911 [astro-ph.HE] (cf. p. 39).

[148] S. Bhandari et al. « The SUrvey for Pulsars and Extragalactic Radio Bursts – II. New FRB discoveries and their follow-up ». In : *Mon. Not. Roy. Astron. Soc.* 475.2 (2018), p. 1427-1446. doi : 10.1093/mnras/stx3074. arXiv : 1711.08110 [astro-ph.HE] (cf. p. 39, 48).

[149] Liam K Hardy et al. « A search for optical bursts from the repeating fast radio burst FRB 121102 ». In : *Mon. Not. Roy. Astron. Soc.* 472.3 (2017), p. 2800-2807. doi : 10.1093/mnras/stx2153. arXiv : 1708.06156 [astro-ph.IM] (cf. p. 39).

[150] J.J. DeLaunay, D.B. Fox, K. Murase et al. « Discovery of a transient gamma-ray counterpart to FRB 131104 ». In : *Astrophys. J. Lett.* 832.1 (2016), p. L1. doi : 10.3847/2041-8205/832/1/L1. arXiv : 1611.03139 [astro-ph.HE] (cf. p. 39).

[151] J.I. Katz. « Coherent Emission in Fast Radio Bursts ». In : *Phys. Rev. D* 89.10 (2014), p. 103009. doi : 10.1103/PhysRevD.89.103009. arXiv : 1309.3538 [astro-ph.HE] (cf. p. 39).

[152] Bing Zhang, Z.G. Dai et P. Meszaros. « High-energy neutrinos from magnetars ». In : *Astrophys. J.* 595 (2003), p. 346-351. doi : 10.1086/377192. arXiv : astro-ph/0210382 (cf. p. 39, 46, 47).

[153] Rajat K. Dey, Sabyasachi Ray et Sandip Dam. « Searching for PeV neutrinos from photomeson interactions in magnetars ». In : *EPL* 115.6 (2016), p. 69002. doi : 10.1209/0295-5075/115/69002. arXiv : 1603.07833 [astro-ph.HE] (cf. p. 39, 47).

[154] Ali Kheirandish, Alex Pizzuto et Justin Vandenbroucke. « Searches for neutrinos from fast radio bursts with IceCube ». In : *PoS* ICRC2019 (2020), p. 982. doi : 10.22323/1.358.0982. arXiv : 1909.00078 [astro-ph.HE] (cf. p. 39).

[155] M.G. Aartsen et al. « A Search for MeV to TeV Neutrinos from Fast Radio Bursts with IceCube ». In : (août 2019). doi : 10.3847/1538-4357/ab564b. arXiv : 1908.09997 [astro-ph.HE] (cf. p. 39).

[156] A. Albert et al. « The ANTARES Collaboration : Contributions to ICRC 2017 Part II : The multi-messenger program ». In : (nov. 2017). arXiv : 1711.01486 [astro-ph.HE] (cf. p. 39).

[157] A. Albert et al. « The search for high-energy neutrinos coincident with fast radio bursts with the ANTARES neutrino telescope ». In : *Mon. Not. Roy. Astron. Soc.* 482.1 (2019), p. 184-193. doi : 10.1093/mnras/sty2621. arXiv : 1807.04045 [astro-ph.HE] (cf. p. 39).

[158] Planck Collaboration, P. A. R. Ade, N. Aghanim et al. « Planck 2015 results. XIII. Cosmological parameters ». In : *A & A* 594, A13 (sept. 2016), A13. doi : 10.1051/0004-6361/201525830. arXiv : 1502.01589 [astro-ph.CO] (cf. p. 43).

[159] Bing Zhang. « A Possible Connection between Fast Radio Bursts and Gamma-Ray Bursts ». In : *Astrophys. J. Lett.* 780.2, L21 (jan. 2014), p. L21. doi : 10.1088/2041-8205/780/2/L21. arXiv : 1310.4893 [astro-ph.HE] (cf. p. 45).

[160] Eli Waxman et John N. Bahcall. « High-energy neutrinos from cosmological gamma-ray burst fireballs ». In : *Phys. Rev. Lett.* 78 (1997), p. 2292-2295. doi : 10.1103/PhysRevLett.78.2292. arXiv : astro-ph/9701231 (cf. p. 45).

[161] Kohta Murase et Shigehiro Nagataki. « High energy neutrino emission and neutrino background from gamma-ray bursts in the internal shock model ». In : *Phys. Rev. D* 73 (2006), p. 063002. doi : 10.1103/PhysRevD.73.063002. arXiv : astro-ph/0512275 (cf. p. 45, 47).

[162] Daniel Biehl, Jonas Heinze et Walter Winter. « Expected neutrino fluence from short Gamma-Ray Burst 170817A and off-axis angle constraints ». In : *Mon. Not. Roy. Astron. Soc.* 476.1 (2018), p. 1191-1197. doi : 10.1093/mnras/sty285. arXiv : 1712.00449 [astro-ph.HE] (cf. p. 45, 46).

[163] Svenja Hummer, Philipp Baerwald et Walter Winter. « Neutrino Emission from Gamma-Ray Burst Fireballs, Revised ». In : *Phys. Rev. Lett.* 108 (2012), p. 231101. doi : 10.1103/PhysRevLett.108.231101. arXiv : 1112.1076 [astro-ph.HE] (cf. p. 45).

[164] David M. Palmer et al. « Gamma-ray observations of a giant flare from the magnetar SGR 1806-20 ». In : *Nature* 434 (2005), p. 1107-1109. doi : 10.1038/nature03525. arXiv : astro-ph/0503030 (cf. p. 47).

[165] Bing Zhang, R.X. Xu et G.J. Qiao. « Nature and nurture : A Model for soft gamma-ray repeaters ». In : *Astrophys. J. Lett.* 545 (2000), p. L127-L130. doi : 10.1086/317889. arXiv : astro-ph/0010225 (cf. p. 47).

[166] Christopher Thompson. « Magnetars ». In : *IAU Colloq. 177 : Pulsar Astronomy - 2000 and Beyond*. Sous la dir. de M. Kramer, N. Wex et R. Wielebinski. T. 202. Astronomical Society of the Pacific Conference Series. Jan. 2000, p. 669 (cf. p. 47).

[167] M.G. Aartsen et al. « Search for Prompt Neutrino Emission from Gamma-Ray Bursts with IceCube ». In : *Astrophys. J. Lett.* 805.1 (2015), p. L5. doi : 10.1088/2041-8205/805/1/L5. arXiv : 1412.6510 [astro-ph.HE] (cf. p. 48).

[168] M. Caleb et al. « The first interferometric detections of Fast Radio Bursts ». In : *Mon. Not. Roy. Astron. Soc.* 468.3 (2017), p. 3746-3756. doi : 10.1093/mnras/stx638. arXiv : 1703.10173 [astro-ph.HE] (cf. p. 49).

[169] R. Shannon, J.-P Macquart, K. Bannister et al. « The dispersion–brightness relation for fast radio bursts from a wide-field survey ». In : *Nature* 562 (oct. 2018). doi : 10.1038/s41586-018-0588-y (cf. p. 49).

[170] CHIME/FRB Collaboration, B. C. Andersen, K. Bandura et al. « CHIME/FRB Discovery of Eight New Repeating Fast Radio Burst Sources ». In : *ApJ L* 885.1, L24 (nov. 2019), p. L24. doi : 10.3847/2041-8213/ab4a80. arXiv : 1908.03507 [astro-ph.HE] (cf. p. 49).

[171] Di Li, Rendong Nan et Zhichen Pan. « The Five-hundred-meter Aperture Spherical radio Telescope project and its early science opportunities ». In : *Neutron Stars and Pulsars : Challenges and Opportunities after 80 years*. Sous la dir. de Joeri van Leeuwen. T. 291. IAU Symposium. Mar. 2013, p. 325-330. doi : 10.1017/S1743921312024015. arXiv : 1210.5785 [astro-ph.IM] (cf. p. 49).

[172] V. Ravi et al. « A fast radio burst localized to a massive galaxy ». In : *Nature* 572.7769 (2019), p. 352-354. doi : 10.1038/s41586-019-1389-7. arXiv : 1907.01542 [astro-ph.HE] (cf. p. 49).

[173] K.W. Bannister et al. « A single fast radio burst localized to a massive galaxy at cosmological distance ». In : (juin 2019). doi : 10.1126/science.aaw5903. arXiv : 1906.11476 [astro-ph.HE] (cf. p. 49).

[174] Shivani Bhandari et al. « The host galaxies and progenitors of Fast Radio Bursts localized with the Australian Square Kilometre Array Pathfinder ». In : *Astrophys. J.* 895.2 (2020), p. L37. doi : 10.3847/2041-8213/ab672e. arXiv : 2005.13160 [astro-ph.GA] (cf. p. 49).

[175] M. Ageron et al. « The ANTARES Telescope Neutrino Alert System ». In : *Astropart. Phys.* 35 (2012), p. 530-536. doi : 10.1016/j.astropartphys.2011.11.011. arXiv : 1103.4477 [astro-ph.IM] (cf. p. 52-54).

[176] V.M. Lipunov et al. « Optical Observations Reveal Strong Evidence for High Energy Neutrino Progenitor ». In : (juin 2020). doi : 10.3847/2041-8213/ab96ba. arXiv : 2006.04918 [astro-ph.HE] (cf. p. 52).

[177] M.G. Aartsen et al. « The IceCube Realtime Alert System ». In : *Astropart. Phys.* 92 (2017), p. 30-41. doi : 10.1016/j.astropartphys.2017.05.002. arXiv : 1612.06028 [astro-ph.HE] (cf. p. 52).

[178] R. Abbasi et al. « Searching for soft relativistic jets in Core-collapse Supernovae with the IceCube Optical Follow-up Program ». In : *Astron. Astrophys.* 539 (2012), A60. doi : 10.1051/0004-6361/201118071. arXiv : 1111.7030 [astro-ph.HE] (cf. p. 52).

[179] A. Klotz, M. BoÃ« r, J. L. Atteia et al. « EARLY OPTICAL OBSERVATIONS OF GAMMA-RAY BURSTS BY THE TAROT TELESCOPES : PERIOD 2001-2008 ». In : *The Astronomical Journal* 137.5 (mar. 2009), p. 4100-4108. doi : 10.1088/0004-6256/137/5/4100 (cf. p. 52, 57).

[180] A. Klotz, M. BoÃ« r, J. L. Atteia et al. « The ROTSE-III Robotic Telescope System ». In : *Publications of the Astronomical Society of the Pacific* 115.803 (mar. 2003), p. 132-140. issn : 00046280, 15383873. doi : 10.1088/0004-6256/137/5/4100 (cf. p. 52, 57).

[181] D.M. Coward et al. « The Zadko Telescope : Exploring the transient Universe ». In : *Publ. Astron. Soc. Austral.* 34.803 (mar. 2017), e005. ISSN : 00046280, 15383873. DOI : 10.1017/pasa.2016.61. arXiv : 1609.06445 [astro-ph.HE] (cf. p. 52, 57).

[182] Nataly Tyurina et al. « MASTER prompt and follow-up GRB observations ». In : *Adv. Astron.* 2010.803 (mar. 2010), p. 763629. ISSN : 00046280, 15383873. DOI : 10.1155/2010/763629. arXiv : 0907.1036 [astro-ph.HE] (cf. p. 52, 57).

[183] J. Wei et B. Cordier. « The Deep and Transient Universe in the SVOM Era : New Challenges and Opportunities - Scientific prospects of the SVOM mission ». In : t. 115. 803. [The University of Chicago Press, Astronomical Society of the Pacific], oct. 2016, p. 132-140. DOI : 10.1088/0004-6256/137/5/4100. arXiv : 1610.06892 [astro-ph.IM] (cf. p. 52, 57, 112, 121).

[184] N. Gehrels et al. « The Swift Gamma-Ray Burst Mission ». In : *Astrophys. J.* 611.803 (mar. 2004). [Erratum : Astrophys.J. 621, 558 (2005)], p. 1005-1020. ISSN : 00046280, 15383873. DOI : 10.1086/422091. arXiv : astro-ph/0405233 (cf. p. 52).

[185] David N. Burrows et al. « The Swift X-Ray Telescope : Status and Performance ». In : *Proc. SPIE Int. Soc. Opt. Eng.* 6686.803 (mar. 2007), p. 668607. ISSN : 00046280, 15383873. DOI : 10.1117/12.735130. arXiv : 0803.1844 [astro-ph] (cf. p. 52, 57).

[186] C. Winkler et al. « The INTEGRAL mission ». In : *Astron. Astrophys.* 411.803 (mar. 2003), p. L1-L6. ISSN : 00046280, 15383873. DOI : 10.1051/0004-6361:20031288 (cf. p. 52, 58).

[187] C. J. Lonsdale, R. J. Cappallo, M. F. Morales et al. « The Murchison Widefield Array : Design Overview ». In : *IEEE Proceedings* 97.8 (août 2009), p. 1497-1506. ISSN : 00046280, 15383873. DOI : 10.1109/JPROC.2009.2017564. arXiv : 0903.1828 [astro-ph.IM] (cf. p. 52, 59).

[188] S. J. Tingay, R. Goeke, J. D. Bowman et al. « The Murchison Widefield Array : The Square Kilometre Array Precursor at Low Radio Frequencies ». In : *pasa* 30.803, e007 (jan. 2013), e007. ISSN : 00046280, 15383873. DOI : 10.1017/pasa.2012.007. arXiv : 1206.6945 [astro-ph.IM] (cf. p. 52, 59).

[189] F. Aharonian et al. « Observations of the Crab Nebula with H.E.S.S ». In : *Astron. Astrophys.* 457.803 (mar. 2006), p. 899-915. ISSN : 00046280, 15383873. DOI : 10.1051/0004-6361:20065351. arXiv : astro-ph/0607333 (cf. p. 52, 59).

[190] J.A. Aguilar et al. « A fast algorithm for muon track reconstruction and its application to the ANTARES neutrino telescope ». In : *Astropart. Phys.* 34.803 (mar. 2011), p. 652-662. ISSN : 00046280, 15383873. DOI : 10.1016/j.astropartphys.2011.01.003. arXiv : 1105.4116 [astro-ph.IM] (cf. p. 53).

[191] S. Adrián-Martínez et al. « Optical and X-ray early follow-up of ANTARES neutrino alerts ». In : *JCAP* 02.803 (mar. 2016), p. 062. ISSN : 00046280, 15383873. DOI : 10.1088/1475-7516/2016/02/062. arXiv : 1508.01180 [astro-ph.HE] (cf. p. 53, 57, 60, 62).

[192] Darren J. White, E.J. Daw et V.S. Dhillon. « A List of Galaxies for Gravitational Wave Searches ». In : *Class. Quant. Grav.* 28.803 (mar. 2011), p. 085016. ISSN : 00046280, 15383873. DOI : 10.1088/0264-9381/28/8/085016. arXiv : 1103.0695 [astro-ph.CO] (cf. p. 53).

[193] S. D. Barthelmy, T. L. Cline, P. Butterworth et al. « GRB Coordinates Network (GCN) : A status report ». In : *Gamma-ray Bursts, 5th Huntsville Symposium*. Sous la dir. de R. Marc Kippen, Robert S. Mallozzi et Gerald J. Fishman. T. 526. American Institute of Physics Conference Series 803. [The University of Chicago Press, Astronomical Society of the Pacific], sept. 2000, p. 731-735. DOI : 10.1063/1.1361631 (cf. p. 55).

[194] Rob Seaman, Roy Williams, Alasdair Allan et al. *Sky Event Reporting Metadata Version 2.0*. IVOA Recommendation 11 July 2011. Juil. 2011. DOI : 10.5479/ADS/bib/2011ivoa.spec.0711S. arXiv : 1110.0523 [astro-ph.IM] (cf. p. 55).

[195] P. A. Evans, J. P. Osborne, A. P. Beardmore et al. « 1SXPS : A DEEP SWIFT X-RAY TELESCOPE POINT SOURCE CATALOG WITH LIGHT CURVES AND SPECTRA ». In : *The Astrophysical Journal Supplement Series* 210.1 (mar. 2013), p. 8. ISSN : 00046280, 15383873. DOI : 10.1088/0067-0049/210/1/8 (cf. p. 57, 58).

[196] P. A. Evans, J. P. Osborne, J. A. Kennea et al. « Swift follow-up of IceCube triggers, and implications for the advanced-LIGO era ». In : *Monthly Notices of the Royal Astronomical Society* 448.3 (mar. 2015), p. 2210-2223. ISSN : 0035-8711. DOI : 10.1088/0004-6256/137/5/4100 (cf. p. 58).

[197] David J. Schlegel, Douglas P. Finkbeiner et Marc Davis. « Maps of dust IR emission for use in estimation of reddening and CMBR foregrounds ». In : *Astrophys. J.* 500.803 (mar. 1998), p. 525. ISSN : 00046280, 15383873. DOI : 10.1086/305772. arXiv : astro-ph/9710327 (cf. p. 61).

[198] P.A. Evans et al. « An online repository of Swift/XRT light curves of γ-ray bursts ». In : *Astron. Astrophys.* 469.803 (mar. 2007), p. 379-385. ISSN : 00046280, 15383873. DOI : 10.1051/0004-6361:20077530. arXiv : 0704.0128 [astro-ph] (cf. p. 64).

[199] Wolfgang VOGES et al. « The ROSAT all - sky survey bright source catalogue ». In : *Astron. Astrophys.* 349.803 (mar. 1999), p. 389. ISSN : 00046280, 15383873. DOI : 10.1088/0004-6256/137/5/4100. arXiv : astro-ph/9909315 (cf. p. 63).

[200] F. SCHÜSSLER. « H.E.S.S. multi-messenger observations ». In : *52nd Rencontres de Moriond on Very High Energy Phenomena in the Universe*. T. 115. 803. [The University of Chicago Press, Astronomical Society of the Pacific], mar. 2017, p. 167-174. DOI : 10.1088/0004-6256/137/5/4100. arXiv : 1705.08258 [astro-ph.HE] (cf. p. 66, 70).

[201] Klaus HODAPP, Rolf CHINI, Bo REIPURTH et al. « Commissioning of the Infrared Imaging Survey (IRIS) System ». In : *Proceedings of SPIE - The International Society for Optical Engineering* 7735.803 (juil. 2010), p. 132-140. ISSN : 00046280, 15383873. DOI : 10.1117/12.856288 (cf. p. 66).

[202] R. L. KURUCZ. « Model Atmospheres for Population Synthesis ». In : *The Stellar Populations of Galaxies*. Sous la dir. de Beatriz BARBUY et Alvio RENZINI. T. 149. IAU Symposium 803. [The University of Chicago Press, Astronomical Society of the Pacific], jan. 1992, p. 225. DOI : 10.1088/0004-6256/137/5/4100 (cf. p. 66).

[203] S. ABDOLLAHI et al. « *Fermi* Large Area Telescope Fourth Source Catalog ». In : *Astrophys. J. Suppl.* 247.1 (mar. 2020), p. 33. ISSN : 00046280, 15383873. DOI : 10.3847/1538-4365/ab6bcb. arXiv : 1902.10045 [astro-ph.HE] (cf. p. 68).

[204] S. ABDOLLAHI et al. « The second catalog of flaring gamma-ray sources from the Fermi All-sky Variability Analysis ». In : *Astrophys. J.* 846.1 (mar. 2017), p. 34. ISSN : 00046280, 15383873. DOI : 10.3847/1538-4357/aa8092. arXiv : 1612.03165 [astro-ph.HE] (cf. p. 68).

[205] P. PADOVANI, E. RESCONI, P. GIOMMI et al. « Extreme blazars as counterparts of IceCube astrophysical neutrinos ». In : *Mon. Not. Roy. Astron. Soc.* 457.4 (mar. 2016), p. 3582-3592. ISSN : 00046280, 15383873. DOI : 10.1093/mnras/stw228. arXiv : 1601.06550 [astro-ph.HE] (cf. p. 68).

[206] S. CROFT et al. « Murchison Widefield Array Limits on Radio Emission from ANTARES Neutrino Events ». In : *Astrophys. J. Lett.* 820.2 (mar. 2016), p. L24. ISSN : 00046280, 15383873. DOI : 10.3847/2041-8205/820/2/L24. arXiv : 1603.02271 [astro-ph.HE] (cf. p. 69).

[207] Fabian SCHÜSSLER et al. « H.E.S.S. observations following multi-messenger alerts in real-time ». In : *PoS* ICRC2017.803 (mar. 2018), p. 653. ISSN : 00046280, 15383873. DOI : 10.22323/1.301.0653. arXiv : 1708.00466 [astro-ph.HE] (cf. p. 71).

[208] M.W.E. Smith et al. « The Astrophysical Multimessenger Observatory Network (AMON) ». In : *Astropart. Phys.* 45.803 (mar. 2013), p. 56-70. ISSN : 00046280, 15383873. DOI : 10.1016/j.astropartphys.2013.03.003. arXiv : 1211.5602 [astro-ph.HE] (cf. p. 71, 76).

[209] H.A. Ayala Solares et al. « A Search for Cosmic Neutrino and Gamma-Ray Emitting Transients in 7.3 Years of ANTARES and Fermi LAT Data ». In : *Astrophys. J.* 886.803 (mar. 2019), p. 98. ISSN : 00046280, 15383873. DOI : 10.3847/1538-4357/ab4a74. arXiv : 1904.06420 [astro-ph.HE] (cf. p. 71).

[210] Soebur Razzaque, Peter Meszaros et Eli Waxman. « High energy neutrinos from gamma-ray bursts with precursor supernovae ». In : *Phys. Rev. Lett.* 90.803 (mar. 2003), p. 241103. ISSN : 00046280, 15383873. DOI : 10.1103/PhysRevLett.90.241103. arXiv : astro-ph/0212536 (cf. p. 73).

[211] Shiníchiro Ando et John F. Beacom. « Revealing the supernova-gamma-ray burst connection with TeV neutrinos ». In : *Phys. Rev. Lett.* 95.803 (mar. 2005), p. 061103. ISSN : 00046280, 15383873. DOI : 10.1103/PhysRevLett.95.061103. arXiv : astro-ph/0502521 (cf. p. 73).

[212] Nicholas Senno, Kohta Murase et Peter Meszaros. « Choked Jets and Low-Luminosity Gamma-Ray Bursts as Hidden Neutrino Sources ». In : *Phys. Rev. D* 93.8 (mar. 2016), p. 083003. ISSN : 00046280, 15383873. DOI : 10.1103/PhysRevD.93.083003. arXiv : 1512.08513 [astro-ph.HE] (cf. p. 73).

[213] Peter Meszaros. « Gamma-Ray Bursts ». In : *Rept. Prog. Phys.* 69.803 (mar. 2006), p. 2259-2322. ISSN : 00046280, 15383873. DOI : 10.1088/0034-4885/69/8/R01. arXiv : astro-ph/0605208 (cf. p. 77).

[214] Reetanjali Moharana, Soebur Razzaque, Nayantara Gupta et al. « High-energy neutrinos from the gravitational wave event GW150914 possibly associated with a short gamma-ray burst ». In : *prd* 93.12, 123011 (juin 2016), p. 123011. ISSN : 00046280, 15383873. DOI : 10.1103/PhysRevD.93.123011. arXiv : 1602.08436 [astro-ph.HE] (cf. p. 77).

[215] Kumiko Kotera et Joseph Silk. « Ultrahigh Energy Cosmic Rays and Black Hole Mergers ». In : *Astrophys. J. Lett.* 823.2 (mar. 2016), p. L29. ISSN : 00046280, 15383873. DOI : 10.3847/2041-8205/823/2/L29. arXiv : 1602.06961 [astro-ph.HE] (cf. p. 77).

[216] Rosalba Perna, Davide Lazzati et Bruno Giacomazzo. « Short Gamma-Ray Bursts from the Merger of Two Black Holes ». In : *Astrophys. J. Lett.* 821.1 (mar. 2016), p. L18. ISSN : 00046280, 15383873. DOI : 10.3847/2041-8205/821/1/L18. arXiv : 1602.05140 [astro-ph.HE] (cf. p. 77).

[217] Imre Bartos, Bence Kocsis, Zolt Haiman et al. « Rapid and Bright Stellar-mass Binary Black Hole Mergers in Active Galactic Nuclei ». In : *Astrophys. J.* 835.2 (mar. 2017), p. 165. issn : 00046280, 15383873. doi : 10.3847/1538-4357/835/2/165. arXiv : 1602.03831 [astro-ph.HE] (cf. p. 77).

[218] Nicholas C. Stone, Brian D. Metzger et Zoltán Haiman. « Assisted inspirals of stellar mass black holes embedded in AGN discs : solving the 'final au problem' ». In : *mnras* 464.1 (jan. 2017), p. 946-954. issn : 00046280, 15383873. doi : 10.1093/mnras/stw2260. arXiv : 1602.04226 [astro-ph.GA] (cf. p. 77).

[219] Kohta Murase, Kazumi Kashiyama, Peter Mészáros et al. « Ultrafast Outflows from Black Hole Mergers with a Minidisk ». In : *apjl* 822.1, L9 (mai 2016), p. L9. issn : 00046280, 15383873. doi : 10.3847/2041-8205/822/1/L9. arXiv : 1602.06938 [astro-ph.HE] (cf. p. 77).

[220] Shigeo S. Kimura, Kohta Murase, Imre Bartos et al. « Transejecta high-energy neutrino emission from binary neutron star mergers ». In : *Phys. Rev. D* 98.803 (4 août 2018), p. 043020. issn : 00046280, 15383873. doi : 10.1088/0004-6256/137/5/4100. url : https://link.aps.org/doi/10.1103/PhysRevD.98.043020 (cf. p. 78).

[221] Shigeo S. Kimura, Kohta Murase, Peter Mészáros et al. « High-energy Neutrino Emission from Short Gamma-Ray Bursts : Prospects for Coincident Detection with Gravitational Waves ». In : *apjl* 848.1, L4 (oct. 2017), p. L4. issn : 00046280, 15383873. doi : 10.3847/2041-8213/aa8d14. arXiv : 1708.07075 [astro-ph.HE] (cf. p. 78).

[222] Shigeo S. Kimura. « High-energy emissions from neutron star mergers ». In : *EPJ Web Conf.* 210.803 (mar. 2019). Sous la dir. d'I. Lhenry-Yvon, J. Biteau, O. Biteau et al., p. 03001. issn : 00046280, 15383873. doi : 10.1051/epjconf/201921003001. arXiv : 1903.06221 [astro-ph.HE] (cf. p. 78).

[223] Ke Fang et Brian D. Metzger. « High-Energy Neutrinos from Millisecond Magnetars formed from the Merger of Binary Neutron Stars ». In : *Astrophys. J.* 849.2 (mar. 2017), p. 153. issn : 00046280, 15383873. doi : 10.3847/1538-4357/aa8b6a. arXiv : 1707.04263 [astro-ph.HE] (cf. p. 78).

[224] B.P. Abbott et al. « Observation of Gravitational Waves from a Binary Black Hole Merger ». In : *Phys. Rev. Lett.* 116.6 (mar. 2016), p. 061102. issn : 00046280, 15383873. doi : 10.1103/PhysRevLett.116.061102. arXiv : 1602.03837 [gr-qc] (cf. p. 78).

[225] S. Adrian-Martinez et al. « High-energy Neutrino follow-up search of Gravitational Wave Event GW150914 with ANTARES and IceCube ». In : *Phys. Rev. D* 93.12 (mar. 2016), p. 122010. ISSN : 00046280, 15383873. DOI : 10.1103/PhysRevD.93.122010. arXiv : 1602.05411 [astro-ph.HE] (cf. p. 78).

[226] A. Albert et al. « Search for High-energy Neutrinos from Gravitational Wave Event GW151226 and Candidate LVT151012 with ANTARES and IceCube ». In : *Phys. Rev. D* 96.2 (mar. 2017), p. 022005. ISSN : 00046280, 15383873. DOI : 10.1103/PhysRevD.96.022005. arXiv : 1703.06298 [astro-ph.HE] (cf. p. 78).

[227] A. Albert et al. « Search for High-energy Neutrinos from Binary Neutron Star Merger GW170817 with ANTARES, IceCube, and the Pierre Auger Observatory ». In : *Astrophys. J. Lett.* 850.2 (mar. 2017), p. L35. ISSN : 00046280, 15383873. DOI : 10.3847/2041-8213/aa9aed. arXiv : 1710.05839 [astro-ph.HE] (cf. p. 79).

[228] Bruny Baret et al. « Bounding the Time Delay between High-energy Neutrinos and Gravitational-wave Transients from Gamma-ray Bursts ». In : *Astropart. Phys.* 35.803 (mar. 2011), p. 1-7. ISSN : 00046280, 15383873. DOI : 10.1016/j.astropartphys.2011.04.001. arXiv : 1101.4669 [astro-ph.HE] (cf. p. 79).

[229] A. Albert et al. « Search for neutrino counterparts of catalogued gravitational-wave events detected by Advanced-LIGO and Virgo during run O2 with ANTARES ». In : *Publications of the Astronomical Society of the Pacific* 115.803 (mar. 2020), p. 132-140. ISSN : 00046280, 15383873. DOI : 10.1088/0004-6256/137/5/4100. arXiv : 2003.04022 [astro-ph.HE] (cf. p. 79).

[230] B.P. Abbott et al. « GW190425 : Observation of a Compact Binary Coalescence with Total Mass $\sim$3.4 $M_\odot$. » In : *Astrophys. J. Lett.* 892.803 (mar. 2020), p. L3. ISSN : 00046280, 15383873. DOI : 10.3847/2041-8213/ab75f5. arXiv : 2001.01761 [astro-ph.HE] (cf. p. 81).

[231] R. Abbott et al. « GW190412 : Observation of a Binary-Black-Hole Coalescence with Asymmetric Masses ». In : *Publications of the Astronomical Society of the Pacific* 115.803 (avr. 2020), p. 132-140. ISSN : 00046280, 15383873. DOI : 10.1088/0004-6256/137/5/4100. arXiv : 2004.08342 [astro-ph.HE] (cf. p. 81).

[232] Marta Colomer Molla, Bruny Baret, Alexis Coleiro et al. « Search for neutrino counterparts of cataloged gravitational-wave events detected by Advanced-LIGO and Virgo during run O2 with ANTARES ». In : *PoS* ICRC2019.803 (mar. 2020), p. 856. ISSN : 00046280, 15383873. DOI : 10.1088/0004-6256/137/5/4100 (cf. p. 81).

[233] S. Adrián-Martínez et al. « Stacked search for time shifted high energy neutrinos from gamma ray bursts with the ANTARES neutrino telescope ». In : *Eur. Phys. J. C* 77.1 (mar. 2017), p. 20. ISSN : 00046280, 15383873. DOI : 10.1140/epjc/s10052-016-4496-8. arXiv : 1608.08840 [astro-ph.HE] (cf. p. 86).

[234] A. Albert et al. « Search for high-energy neutrinos from bright GRBs with ANTARES ». In : *Mon. Not. Roy. Astron. Soc.* 469.803 (mar. 2017), p. 906. ISSN : 00046280, 15383873. DOI : 10.1093/mnras/stx902. arXiv : 1612.08589 [astro-ph.HE] (cf. p. 86).

[235] B.Cameron Reed. « New estimates of the solar-neighborhood massive-stars birthrate and the Galactic supernova rate ». In : *Astron. J.* 130.803 (mar. 2005), p. 1652-1657. ISSN : 00046280, 15383873. DOI : 10.1086/444474. arXiv : astro-ph/0506708 (cf. p. 100).

[236] Weidong Li, Ryan Chornock, Jesse Leaman et al. « Nearby Supernova Rates from the Lick Observatory Supernova Search. III. The Rate-Size Relation, and the Rates as a Function of Galaxy Hubble Type and Colour ». In : *Mon. Not. Roy. Astron. Soc.* 412.803 (mar. 2011), p. 1473. ISSN : 00046280, 15383873. DOI : 10.1111/j.1365-2966.2011.18162.x. arXiv : 1006.4613 [astro-ph.SR] (cf. p. 100).

[237] Roland Diehl et al. « Radioactive Al-26 and massive stars in the galaxy ». In : *Nature* 439.803 (mar. 2006), p. 45-47. ISSN : 00046280, 15383873. DOI : 10.1038/nature04364. arXiv : astro-ph/0601015 (cf. p. 100).

[238] E.F. Keane et M. Kramer. « On the birthrates of Galactic neutron stars ». In : *Mon. Not. Roy. Astron. Soc.* 391.803 (mar. 2008), p. 2009. ISSN : 00046280, 15383873. DOI : 10.1111/j.1365-2966.2008.14045.x. arXiv : 0810.1512 [astro-ph] (cf. p. 100).

[239] D.A. Leahy, S. Ranasinghe et M. Gelowitz. « Evolutionary Models for 43 Galactic Supernova Remnants with Distances and X-ray Spectra ». In : *Astrophys. J. Suppl.* 248.1 (mar. 2020), p. 16. ISSN : 00046280, 15383873. DOI : 10.3847/1538-4365/ab8bd9. arXiv : 2003.08998 [astro-ph.HE] (cf. p. 100).

[240] Karolina Rozwadowska, Francesco Vissani et Enrico Cappellaro. « On the rate of core collapse supernovae in the milky way ». In : *New Astron.* 83.803 (mar. 2021), p. 101498. ISSN : 00046280, 15383873. DOI : 10.1016/j.newast.2020.101498. arXiv : 2009.03438 [astro-ph.HE] (cf. p. 100).

[241] Irene Tamborra, Florian Hanke, Bernhard Müller et al. « Neutrino signature of supernova hydrodynamical instabilities in three dimensions ». In : *Phys. Rev. Lett.* 111.12 (mar. 2013), p. 121104. ISSN : 00046280, 15383873. DOI : 10.1103/PhysRevLett.111.121104. arXiv : 1307.7936 [astro-ph.SR] (cf. p. 101, 106).

[242] Irene Tamborra, Georg Raffelt, Florian Hanke et al. « Neutrino emission characteristics and detection opportunities based on three-dimensional supernova simulations ». In : *Phys. Rev.* D90.4 (mar. 2014), p. 045032. ISSN : 00046280, 15383873. DOI : 10.1103/PhysRevD.90.045032. arXiv : 1406.0006 [astro-ph.SR] (cf. p. 101, 107).

[243] Laurie Walk, Irene Tamborra, Hans-Thomas Janka et al. « Neutrino emission characteristics of black hole formation in three-dimensional simulations of stellar collapse ». In : *Publications of the Astronomical Society of the Pacific* 115.803 (mar. 2019), p. 132-140. ISSN : 00046280, 15383873. DOI : 10.1088/0004-6256/137/5/4100. arXiv : 1910.12971 [astro-ph.HE] (cf. p. 101).

[244] Scott M. Adams, C. S. Kochanek, John F. Beacom et al. « Observing the Next Galactic Supernova ». In : *Astrophys. J.* 778.803 (mar. 2013), p. 164. ISSN : 00046280, 15383873. DOI : 10.1088/0004-637X/778/2/164. arXiv : 1306.0559 [astro-ph.HE] (cf. p. 103).

[245] K. Scholberg. « The SuperNova Early Warning System ». In : *Astron. Nachr.* 329.803 (mar. 2008), p. 337-339. ISSN : 00046280, 15383873. DOI : 10.1002/asna.200710934. arXiv : 0803.0531 [astro-ph] (cf. p. 104).

[246] Adam Burrows, Klein Klein et Raj Gandhi. « The future of supernova neutrino detection ». In : *Phys. Rev. D* 45.803 (10 mai 1992), p. 3361-3385. ISSN : 00046280, 15383873. DOI : 10.1103/PhysRevD.45.3361. URL : https://link.aps.org/doi/10.1103/PhysRevD.45.3361 (cf. p. 105).

[247] A. Coleiro, M. Colomer Molla, D. Dornic et al. « Combining neutrino experimental light-curves for pointing to the next Galactic Core-Collapse Supernova ». In : *Eur. Phys. J. C* 80.9 (mar. 2020), p. 856. ISSN : 00046280, 15383873. DOI : 10.1140/epjc/s10052-020-8407-7. arXiv : 2003.04864 [astro-ph.HE] (cf. p. 105, 106, 109).

[248] David Corre et al. « End-to-end simulations for COLIBRI, ground follow-up telescope for the SVOM mission ». In : *Proc. SPIE Int. Soc. Opt. Eng.* 10705.803 (mar. 2018). Sous la dir. de George Z. Angeli et Philippe Dierickx, p. 10705. ISSN : 00046280, 15383873. DOI : 10.1117/12.2313127 (cf. p. 117, 119).

[249] B.S. Acharya et al. *Science with the Cherenkov Telescope Array*. T. 115. 803. WSP, nov. 2018, p. 132-140. ISBN : 978-981-327-008-4. DOI : 10.1142/10986. arXiv : 1709.07997 [astro-ph.IM] (cf. p. 120).

[250] Ignacio Taboada et Rudy C. Gilmore. « Prospects for the detection of GRBs with HAWC ». In : *Nucl. Instrum. Meth. A* 742.803 (mar. 2014). Sous la dir. d'Antonio Capone, Giulia De Bonis, Mario De Vincenzi et al., p. 276-277. ISSN : 00046280, 15383873. DOI : 10.1016/j.nima.2013.09.013. arXiv : 1306.1127 [astro-ph.HE] (cf. p. 120).

[251] X. Bai et al. « The Large High Altitude Air Shower Observatory (LHAASO) Science White Paper ». In : *Publications of the Astronomical Society of the Pacific* 115.803 (mai 2019), p. 132-140. ISSN : 00046280, 15383873. DOI : 10.1088/0004-6256/137/5/4100. arXiv : 1905.02773 [astro-ph.HE] (cf. p. 120).

[252] A. Albert et al. « Science Case for a Wide Field-of-View Very-High-Energy Gamma-Ray Observatory in the Southern Hemisphere ». In : *Publications of the Astronomical Society of the Pacific* 115.803 (fév. 2019), p. 132-140. ISSN : 00046280, 15383873. DOI : 10.1088/0004-6256/137/5/4100. arXiv : 1902.08429 [astro-ph.HE] (cf. p. 120).